DEVELOPMENT OF ANTIFOULING NANOFILTRATION AND ANTIBIOFOULING ULTRAFILTRATION POLYMERIC MEMBRANES USING FACILE PROTOCOLS

A Thesis Submitted to
the Graduate School of Engineering and Sciences of
İzmir Institute of Technology
in Partial Fulfillment of the Requirements for the Degree of

DOCTOR OF PHILOSOPHY

in Chemical Engineering

by
Aydın CİHANOĞLU

July 2021
İZMİR

ACKNOWLEDGMENTS

Firstly, I would like to express my deepest and sincere gratitude to my advisor Prof. Dr. Sacide ALSOY ALTINKAYA, and my co-advisor Prof. Dr. Erol ŞEKER for their support, encouragement, guidance, and patience throughout the thesis.

I would like to thank my sincere gratitude to my PhD Thesis Committee and Jury Members, Prof. Dr. Mustafa M. DEMİR, Assoc. Prof. Dr. Ayben TOP, Prof. Dr. Nalan KABAY and Prof. Dr. Şerife Birgül TANTEKİN ERSOLMAZ for sharing their valuable knowledge to improve the quality of my thesis.

I would like to special thanks to all my dear close friends and lab mates for supporting me during this journey. I appreciate knowing each of them. Their valuable support and understanding always helped me to overcome problems in the way.

I would like to thank the valuable specialists working in Biotechnology and Bioengineering Application and Research Center, Center for Materials Research, and Environmental Development Application and Research Center at İzmir Institute of Technology, and Central Research Test and Analysis Laboratory Application and Research Center at Ege University for their kind help and technical support.

I would like to thank Assoc. Prof. Dr. Jessica Schiffman for accepting me to her laboratory as an international scholar and each of my lab mates at Chemical Engineering at UMass for the hospitality they showed me.

I especially want to thank Linda and Nico, who host in the USA. They always made me feel like I was a member of their family. I appreciate to know them.

I would like to thank TÜBİTAK for financially supporting me with the 2211-E and 2214-A scholarship programs through my PhD.

Lastly, I would like to thank my dear wife and family for their endless support, understanding, and love.

ABSTRACT

DEVELOPMENT OF ANTIFOULING NANOFILTRATION AND ANTIBIOFOULING ULTRAFILTRATION POLYMERIC MEMBRANES USING FACILE PROTOCOLS

One of the major goals in membrane separation technology is to develop fouling-resistant membranes that can provide a long operating time and low operation costs. This thesis aims to manufacture fouling and biofouling-resistant polymeric nanofiltration (NF) and ultrafiltration (UF) membranes using unique approaches. The first approach was to change coagulation bath composition in the phase inversion technique for manufacturing fouling-resistant polyamide-imide (PAI) based NF and biofouling-resistant polysulfone (PSF)/sulfonated polyethersulfone (PSF-SPES) based UF membranes. To this end, hydrophilic branched polyethyleneimine (PEI) dissolved in the coagulation bath allowed the preparation of a positively charged PAI based NF membrane by forming a covalent bond with the imide group in the PAI. To manufacture antibacterial UF membranes, a strong antibacterial surfactant, cetyltrimethylammonium bromide (CTAB), was dissolved in the coagulation bath and made an electrostatic interaction with SPES at the polymer/bath interface during phase inversion. Both membranes were prepared in a one-step process without using any pore formers in the casting solution. The second approach used in the thesis focused on modification of commercial polyethersulfone (PES) UF membranes with co-deposition of dopamine and CTAB molecules to impart antibiofouling behavior without compromising the pore size and pure water flux of the support. To achieve this task, during modification, an inert physical barrier was created inside the membrane pores by continuously feeding nitrogen gas (N_2) from the backside of the support to prevent pore penetration. In the last approach, ultrasound as a green, controllable trigger was used for modifying PSF and PSF-SPES UF membranes with dopamine. The main purpose of using ultrasound was to accelerate the polymerization kinetics of dopamine, hence shortening the modification time.

ÖZET

KOLAY PROTOKOLLER KULLANILARAK KİRLENME DİRENÇLİ NANOFİLTRASYON VE BİYOLOJİK KİRLİLİK ÖNLEYİCİ ULTRAFİLTRASYON POLİMERİK MEMBRANLARIN GELİŞTİRİLMESİ

Membran ayırma teknolojisindeki ana hedeflerden biri, uzun çalışma süresi ve düşük işletme maliyeti sağlayabilen kirlenmeye dayanıklı membranlar geliştirmektir. Bu tezin amacı, özgün yaklaşımlar kullanarak kirlenmeye ve biyolojik kirlenmeye dayanıklı polimerik nanofiltrasyon (NF) ve ultrafiltrasyon (UF) membranları üretmektir. İlk yaklaşımda, kirlenmeye dirençli poliamid-imid (PAI) bazlı NF ve biyolojik kirlenmeye dirençli polisülfon (PSF)/sülfonlanmış polietersülfon (PSF-SPES) bazlı UF membranlarının üretimi için faz değişim yönteminde koagülasyon banyosunun bileşimi değiştirilmiştir. Bu amaçla, koagülasyon banyosunda çözünen hidrofilik dallanmış polietilenimin (PEI), PAI'nın yapısındaki imid grubu ile kovalent bir bağ oluşturarak pozitif yüklü bir NF membranının hazırlanmasına olanak sağlamıştır. Antibakteriyel UF membranları üretmek için, güçlü bir antibakteriyel yüzey aktif madde olan setiltrimetilamonyum bromür (CTAB), koagülasyon banyosunda çözdürülmüş ve faz değişimi sırasında polimer/banyo ara yüzünde SPES ile elektrostatik bir bağ oluşturmuştur. Her iki membran da döküm çözeltisinde herhangi bir gözenek oluşturucu ajan kullanmadan, tek aşamalı bir protokolle hazırlanmıştır. Tezde kullanılan ikinci yaklaşımda, ticari polietersülfon (PES) UF membranının yüzeyi, membranın gözenek boyutu ve saf su akısını değiştirmeksizin dopamin ve CTAB moleküllerinin aynı anda kaplanması ile modifiye edilerek biyolojik kirliliğe karşı dirençli hale getirilmiştir. Modifikasyon sırasında, gözeneklerin içinde kaplamayı engellemek için destek membranının arkasından sürekli olarak azot gazı (N_2) beslenerek membranın gözenekleri içinde inert bir fiziksel bariyer oluşturulmuştur. Tezde kullanılan son yaklaşımda, PSF ve PSF-SPES UF membranlarını dopamin ile modifiye etmek için ultrason uygulanmıştır. Ultrason kullanmanın temel amacı, dopaminin polimerizasyon kinetiğini hızlandırmak, dolayısıyla modifikasyon süresini kısaltmaktı.

TABLE OF CONTENTS

LIST OF FIGURES

Figure **Page**

Figure **Page**

Figure **Page**

LIST OF TABLES

Table **Page**

CHAPTER 1

INTRODUCTION

Water is an indispensable source of life. Although it is an abundant resource, only 1% of the total water on Earth is accessible as freshwater (Oki et al., 2006). Both inadequate water quality and water quantity are important critical challenges for the 21st century. Since 1980, the global water consumption has been increasing by almost 1% due to the rapid growth of population and unsustainable industrial production. The rate of water demand is expected to increase at a similar rate until 2050 (Oki et al., 2006).

The United Nations World Water Development Report (UN-Water) published in 2019 revealed that over 2 billion people live-in high-water stress areas, and around 4 billion people face severe water scarcity for at least one month of the year (UN-Water, 2019). Furthermore, the World Health Organization (WHO) announced that around 30% of the world population does not have access to safely managed drinking water and sanitation services. Especially, access to water contaminated with living microorganisms causes serious diseases such as cholera, diarrhoea, dysentery, hepatitis A, typhoid, polio, and the WHO estimates that around half a million people die each year from diarrhoea due to lack of safe drinking water (UNICEF and WHO, 2015).

Membrane-based separation technologies are considered accessible, relatively green, and energy-efficient to meet the clean water demand. Alternative processes such as adsorption, distillation, flocculation, advanced oxidation require complex equipment, high energy and chemical consumption and may produce by products and sludge making water treatment more complicated. The bottleneck for the membrane based treatment technologies is the membrane fouling reducing flux, deteriorating product water quality, and increasing energy consumption (Zhang et al., 2016a). Many research efforts have focused on developing foulant resistant membranes. The aim of this thesis is also to develop membranes with antifouling/antibiofouling properties. While developing these membranes, the scalability of the protocol for large scale applications was always considered as a criterion.

1.1. Membrane Separation Processes and Membrane Manufacturing Methods

Membrane-based separation processes operating under the pressure difference as a driving force are classified as microfiltration (MF), ultrafiltration (UF), nanofiltration (NF), and reverse osmosis (RO) (Mulder, 1996). MF membranes have the largest pore size and are located between UF membranes and conventional filters. MF membranes are typically used for water clarification, pre-treatment processes, and bacteria removal. MF membrane process removes impurities based on the sieving rejection mechanism and operates at low pressure (less than 2 bar). UF membranes have a smaller pore size than MF membranes and fall between MF and NF membranes. UF membranes are basically used for pre-treatment processes and the removal of bacteria and viruses. They operate through the same sieving rejection mechanism as MF membranes. UF membranes are operated at relatively high pressure (less than 10 bar). NF is the newest classified membrane process, and its pore size lies between UF and RO membranes. NF membranes are used for multivalent ions rejection and to remove small organics that cannot be eliminated by MF and UF membranes. The rejection mechanism of NF membranes is based on both sieving effect and Donnan exclusion (charge effect), and the separation process is carried out at high working pressure (less than 40 bar). RO membranes have the smallest pore size and operate via the solution-diffusion mechanism. RO membranes are commonly used for desalination process and very high pressures (60 bar - 70 bar) are required (Mulder, 1996; Baker, 2012).

The most common technique used for manufacturing polymeric MF and UF membranes is phase inversion (Mulder, 1996). In this technique, first, a polymer is dissolved in a suitable organic solvent. Then, the polymer solution is cast on a solid surface in the absence or presence of support material by adjusting its thickness with a blade. Next, the polymer solution is immersed into a coagulation bath including non-solvent, and the solid membrane is obtained in less than a few seconds. During the formation of a solid membrane, non-solvent diffuses into the polymer solution, while organic solvent in the polymer solution diffuses into the non-solvent in the coagulation bath (Figure 1.1). At one point, phase separation takes place forming polymer-rich and polymer-poor phases, representing the membrane backbone and pores, respectively.

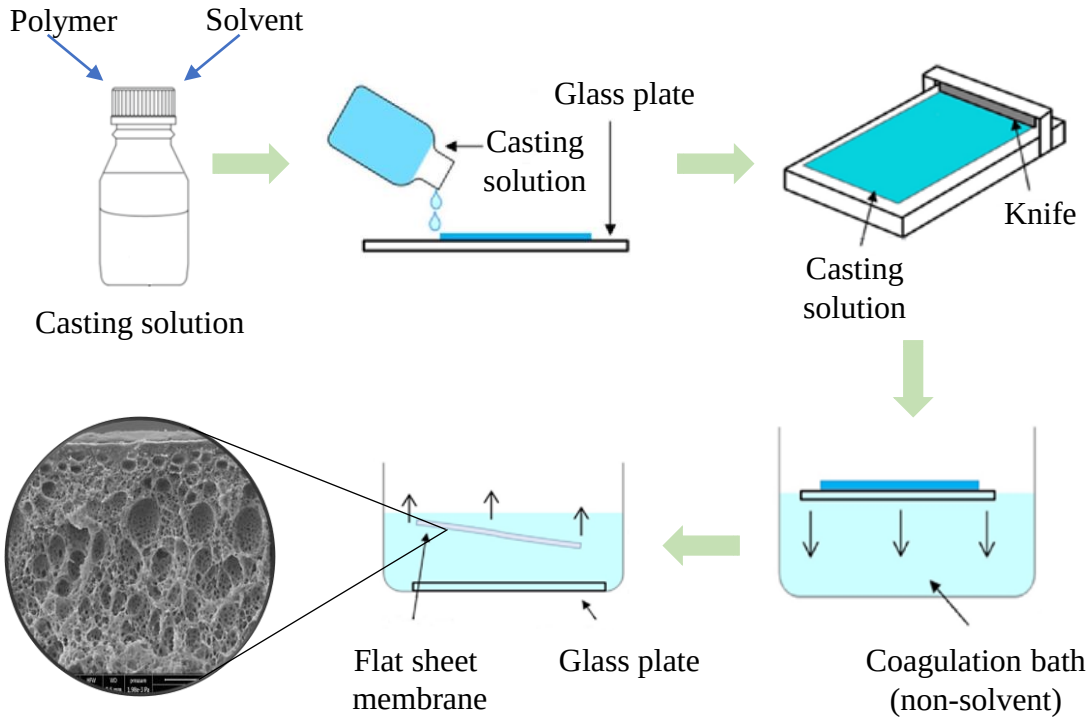

Figure 1.1. Membrane preparation by non-solvent induced phase separation technique.

In this technique, many parameters including the coagulation bath composition and temperature, casting solution composition and temperature and pre-evaporation step before coagulation affect the final structure of the membranes (Guillen et al., 2011). Depending on the casting and coagulation conditions determining the phase separation time, spongy or finger like porous structures are obtained (Figure 1.2).

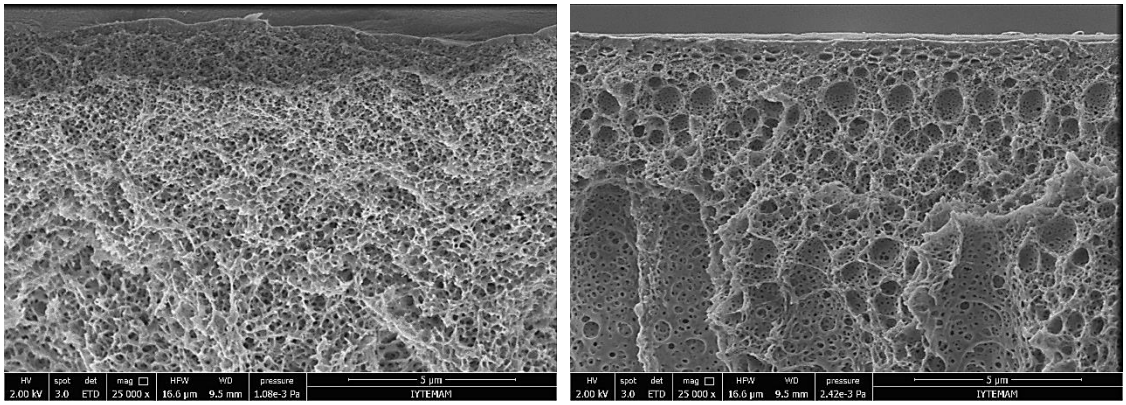

a) b)

Figure 1.2. Membrane porous structures a) spongy like b) finger like.

NF and RO membranes are generally manufactured in the form of thin-film composite (TFC) membranes (Figure 1.3). First, UF membranes are prepared by phase inversion technique to be used as a support layer. Next, the selective layer is formed through grafting, layer by layer deposition of polyelectrolytes and interfacial polymerization. It is desired that the support layer should only provide mechanical strength but not add significant mass transfer resistance. The selective layer should be formed defect free, as thin as possible with the desired pore size. Also, to prevent detachment of the selective layer, the protocol should ensure strong binding between the selective layer and the support (Mulder, 1996).

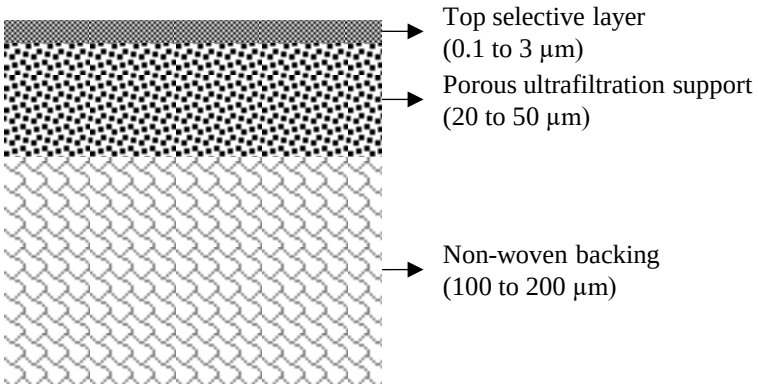

Figure 1.3. The components of thin-film composite membranes.

1.2. The Design Strategies Applied for Developing Fouling-Resistant Membranes

The physical and chemical properties of membranes are considered the most important design parameters to fabricate fouling-resistant membranes. The physical properties include surface roughness, pore size distribution, and the architecture of membranes, whereas chemical properties include hydrophilicity, hydrophobicity, and surface charge (Zhang et al., 2016a; Hong and Elimelech, 1997). The surface roughness triggers the fouling propensity of the membrane since rough surfaces increase the surface area in contact with foulants and free space between ridge and valley structures hosts foulants accumulation (Myint et al., 2010; Hoek et al., 2001, 2003; Elimelech et al., 1997). In addition, the pore size distribution of porous membranes affects the fouling tendency because the large pores create a relatively high flux, and foulants can penetrate the inside the pores (Belfort et al., 1994). It is known that commercial polymeric

membranes, such as polyethersulfone (PES), polysulfone (PSF), polyacrylonitrile (PAN), and polyvinylidene fluoride (PVDF) are quite hydrophobic, and strong hydrophobic-hydrophobic interactions occur during the filtration between the membranes and foulants. Whitesides and coworkers (2001) investigated 60 different surface chemistries related to the protein fouling behavior, and they found that the surface should include four molecular characteristics: Hydrophilicity, hydrogen-bond acceptor, not hydrogen-bond donor and overall neutral electrical charge (Ostuni et al., 2001; Wei et al., 2014). Water quickly forms strong hydration layers on hydrophilic surfaces and this layer prevents the foulant's contact with the membranes. Most organic, inorganic, and biological foulants have a negative surface charge at neutral pH. To mitigate the fouling tendency of the membrane, the surface should be designed to use the electrostatic repulsion between the foulants and surfaces (Rana and Matsuura, 2010).

In the literature, various chemicals have been used to impart the hydrophilic character to the membrane surfaces. For instance, polyethylene glycol (PEG) and PEG-based polymers (Banerjee et al., 2011; Castrillón et al., 2014), polyelectrolytes (Tekinalp and Altinkaya, 2019; Cihanoğlu and Altinkaya, 2018), inorganic nanoparticles such as metal (Ag) (Hoek et al., 2011), metal oxide (TiO_2, Al_2O_3, ZrO_2) (Arsuaga et al., 2013), carbon nanotubes (Vatanpour et al., 2011), graphene oxide (Zinadini et al., 2014) are commonly used. Recently, dopamine (Lee et al., 2007), and chitosan-based coatings (Zhang et al., 2013a; Boributh et al., 2009) with bio-inspired chemistry have been used frequently to mitigate fouling.

Zwitterionic molecules containing almost equal positively and negatively charged groups have also been used to make membrane surface neutral and increase the hydrophilicity of the surface (Hadidi and Zydney, 2014; Li et al., 2015a; Jiang and Cao, 2010). There are three well-known zwitterionic molecules: i) carboxybetaine methacrylate (Tada et al., 2009), ii) sulfobetaine methacrylate (Birkner and Ulbricht, 2015), iii) phosphobetaine (Razi et al., 2012). All the above-mentioned zwitterionic molecules have quaternary amine as positively charged groups. The quaternary amine is located in the inner groups of the carboxy-betaine methacrylate and sulfobetaine methacrylate, while it is located in the head group of the phospho-betaine. Also, negatively charged groups, carboxylic acid and sulfonate, are located in the head groups of the carboxy-betaine methacrylate and sulfobetaine methacrylate, respectively, while phosphate is in the inner group of the phospho-betaine.

1.3. The Design Strategies Applied for Developing Biofouling-Resistant Membranes

It is well known that the design strategies used to obtain fouling-resistant membranes are not very effective to create membrane surfaces that are resistant to bacteria and viruses. In addition to the anti-adhesion properties, the surface should also contain bactericidal particles or molecules to obtain excellent biofouling-resistance. Bactericidal particles inactivate bacteria through release-killing mode or contact-killing mode. In release-killing approach, bactericidal agents release from the surface and kill bacteria or viruses in the bulk phase. Inorganic particles such as silver (Cao et al., 2010), silver-based (Mauter et al., 2011), or copper-based (Gilbertson et al., 2016) nanoparticles, or carbon-based materials such as graphene oxide (Perreault et al., 2015), and carbon nanotubes (Tiraferri et al., 2011) are commonly used to produce biofouling-resistant membranes. Continuous release nanoparticles shorten the service life of membranes and cause serious environmental risks. In contact-killing approach, bactericidal agents are permanently fixed on the surface, and inactivate bacteria or viruses through contact. To this end, quaternary ammonium containing molecules (Tiller et al., 2001; Thorsteinsson et al., 2003) or quaternary ammonium-based surfactants (Cihanoğlu and Altinkaya, 2020) are frequently preferred to fabricate biofouling-resistant membranes.

Recently, studies focused on developing dual functional membranes through combining “defensive” and “offensive” strategies (Liu et al., 2017; Zhu et al., 2021; Yang et al., 2021; Zhao et al., 2020; Xu et al., 2019; Yang et al., 2020a; Yang et al., 2020b). Defensive strategy is based on creating an antiadhesive surface defined with its hydrophilic, smooth, and neutral characteristics. Offensive strategies rely on using biocidal agents to create antibacterial surfaces that can inactivate bacteria (Figure 1.4).

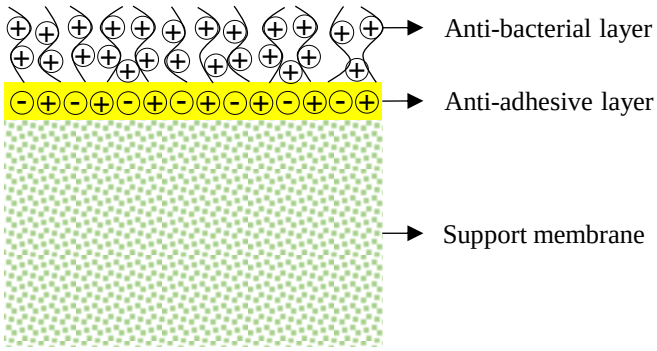

Figure 1.4. The components of dual functional membranes.

1.4. Motivation

All membrane processes used for water treatment suffer from fouling due to direct contact with foulants in water such as living microorganisms, natural organic matter, colloidal particles, oil, and salt. Although pre-treatment of feed, optimization of operating conditions, and biocide dosing are applied as fouling control strategies, new membrane development and modification of existing membranes to make them less prone to fouling offer long-term solution for the fouling control. While developing/modifying the membranes, many constraints should be considered including hydraulic resistance, separation performance, mechanical stability, chemical stability, and the cost of the assembly. Sustainable water treatment technologies are needed to solve the water crisis problem. In addition, green engineering principles should not be overlooked during membrane development. Green membrane production is achieved not only with the sustainable materials and green solvents but also with reducing the energy consumption and number of steps for the preparation. The main motivation in this thesis study was to contribute to the efforts in the development of antifouling/antibiofouling membranes using scalable protocols. To make the protocols adaptable for large scale applications, lengthy procedures, unnecessary post treatment/pre-treatment steps were avoided. Furthermore, the constraints listed above regarding the permeabilities, and long-term stabilities of the membranes were also considered.

1.5. Thesis Overview

The main objective of this PhD thesis was to develop fouling and biofouling resistant polymeric nanofiltration (NF) and ultrafiltration (UF) membranes.

The details of each chapter were described below:

i. In Chapter 2, polyamide-imide (PAI) based positively charged NF membranes were prepared in a single step by dissolving PEI in a coagulation bath at ambient temperature. The pH value was the driving force for the chemical crosslinking between PAI and PEI. To obtain long term stable NF membranes, no pore forming agent was used in the casting solution to obtain long term stable NF membranes.

ii. In Chapter 3, a facile approach was proposed for preparing cetyltrimethylammonium bromide (CTAB) containing polysulfone-sulfonated polyethersulfone (PSF-SPES) based ultrafiltration membranes with antibacterial properties. The membranes were prepared in a single step by adding CTAB into the coagulation bath. The effects of CTAB concentration on the membrane structure and performance were investigated in detail.

iii. In Chapter 4, dopamine and CTAB were co-deposited to impart the antibiofouling behaviour to commercial polyethersulfone (PES) UF membranes using a unique coating approach. The main aim was to improve the antibiofouling resistance without compromising the transport properties of the bare PES membrane. The effects of the CTAB concentration on the biofouling resistance of the membranes was investigated in detail through characterization and bacteria filtration studies.

iv. In Chapter 5, the ultrasound assisted polymerization technique was suggested to improve the fouling resistance of the PSF and PSF-SPES blend membranes. The effect of ultrasound on the structure and oily water filtration performance of the membranes was investigated.

1.6. Contributions to the Literature

The contributions of this PhD thesis to the literature are listed below:

i. Chapter 2: Positively charged NF membranes are usually manufactured in the form of thin film composite (TFC) membrane through interfacial polymerization. It is difficult to control the uniform deposition of selective layer without changing the structure of the support. The selective layer of TFC membranes prepared with coating techniques may detach from the surface. In Chapter 2, for the first time a positively charged NF membrane with a molecular weight cut-off (MWCO) value less than 1 kDa was prepared using a single step phase inversion technique without using any pore former. This protocol is less complicated and requires fewer steps than the other existing techniques. In addition, the membrane does not contain any compound with a leaching risk.

ii. Chapter 3: Various bactericidal components such as antimicrobial polymers (Munoz-Bonilla and Fernandez-Garcia, 2012) and carbon nanotube (Kang et al.,

2007) are used to manufacture antibacterial membranes killing bacteria upon contact. In Chapter 3, the use quaternary ammonium surfactant instead of specially produced bactericidal molecules was proposed due to its low cost, strong antibacterial efficiency, and non-toxic behaviour. In literature, few studies utilize quaternary ammonium surfactants, but they follow complex manufacturing protocols to build antibacterial membranes (Hu et al., 2016; Zhang et al., 2018a). Herein, a novel approach that was not used before was proposed to incorporate quaternary ammonium surfactant into polymer membranes. This approach offers a simple route to prepare antibiofouling membranes and can be easily scaled up for industrial production.

iii. Chapter 4: In recent years, dopamine has been used to improve hydrophilicity, which in turn enhances the fouling resistance of the membranes. A trade-off was usually observed between the improved fouling resistance and reduction in the flux. In Chapter 4, a new co-deposition strategy was proposed to impart antibiofouling behavior to commercial PES membranes without compromising their flux values.

iv. Chapter 5: The most important challenge for the surface modification of membranes with dopamine is the long polymerization time ranging from several hours to a few days. Different strategies utilizing UV (Du et al., 2014), microwave (Lee et al., 2017), microplasma (Wang et al., 2017a), and chemical oxidizing agents (Wang et al., 2018; Zhang et al., 2016b) have accelerated the polymerization rate to overcome this drawback. However, the first three techniques are not suitable for the polymeric membrane surfaces, and the last one contaminates the surface with the inorganic particles used in this technique. In Chapter 5, for the first time in the literature ultrasound has been used as a trigger for PDA coating on polymeric membrane surfaces.

CHAPTER 2

DEVELOPMENT OF POSITIVELY CHARGED FOULING-RESISTANT NANOFILTRATION MEMBRANES USING A FACILE APPROACH

2.1. Introduction

Nanofiltration (NF) membranes fill the gap between ultrafiltration (UF) and reverse osmosis (RO) membranes and are used for separation of neutral and charged molecules in the range of 0.5-2 nm in diameter (Bowen et al., 1997; Lin et al., 2016a; Lin et al., 2015a; Ye et al., 2018; Lin et al, 2015b; Zhu et al., 2016a). Positively charged NF membranes can exhibit high rejections for multivalent cations depending on their pore size and charge densities, hence, they can be used for recovery of valuable cationic macromolecules in the biotechnology and pharmaceutical industries or removal of multivalent cations such as dyes and heavy metals from effluents in the paper and pulp, textile, nuclear, and automotive industries (Zhao et al., 2018; Cheng et al., 2012).

Positively charged NF membranes are usually manufactured in the form of thin film composite (TFC) membrane through interfacial polymerization (Zhang et al., 2017a; Pal et al., 2016; Wang et al., 2013; Li et al., 2017a; Wang et al., 2011; Bai et al., 2013;Wu et al., 2014; Zhao et al., 2016; Fang et al., 2013; Wei et al., 2014; Chiang et al., 2009). The main disadvantages of this method are the difficulty in controlling uniform growth of the selective layer over the surface and the possibility of changing the bulk structure of the support due to penetration of monomers. The second commonly used approach to prepare TFC NF membranes is to coat preformed polymer on the surface of a UF membrane by physical adsorption, electrostatic interactions or in some cases through a chemical reaction (Wang et al., 2017b; Yao et al., 2009; Zheng et al., 2013; Zhu et al., 2016b; Ji et al., 2011; Li et al., 2017b; Goh et al., 2015; Gao et al., 2014; Zhang et al., 2014).

This chapter has been published as:
A. Cihanoğlu, S. A. Altinkaya, A Facile Approach for Preparation of Positively Charged Nanofiltration Membranes by In-Situ Crosslinking between Polyamide-imide and Polyethylenimine, Separation and Purification Technology 207 (2018) 353-362.

In both methods, the challenge is to obtain a very thin and stable selective layer in order to minimize the mass transfer resistance and maintain selectivity for a long period of time. NF membranes have also been manufactured by chemical or thermal post treatment of the integrally skinned asymmetric membranes. Economy's group designed positively charged flat sheet NF membranes by chemical post treatment of P84 copolyimide asymmetric membrane using branched polyethylenimine (PEI) (Ba et al., 2009). Cui et al. (2015) blended polyvinyl chloride with an amphiphilic copolymer of poly (methyl methacrylate-co-dimethyl aminoethyl methacrylate) (P(MMA-co-DMA)) and at the end of phase inversion, the membranes were immersed into p-xylene dichloride (XDC) solution to achieve crosslinking between XDC and tertiary amine units in the membrane.

To obtain positively charged NF membranes in a single step without using any post treatment process, casting formulation has usually been adjusted to change the kinetics and thermodynamics of phase inversion. Yu et al. (2016) mixed modified Mg/Al hydrotalcite (mHT) with poly(ether sulfone) (PES) and pore former polyvinylpyrrolidone to fabricate loose NF membrane through nonsolvent induced phase separation (NIPS) method. The membrane showed high retention for dyes, reactive black 5 and reactive red 49 and low rejections for salts. Zhang et al. (2011) used a positively charged polymer-cardo poly(arylene ether sulfone) with pendant tertiary amine groups (PES-TA) to prepare positively charged loose NF membrane in a single step. By changing the ratio of solvent (DMF) to co-solvent (THF) in the casting solution, the MWCO value of the membranes changed from 5555 to 1360. Yu et al. (2015) blended modified silica spheres with polyethersulfone and pore former polyvinylpyrrolidone and tested the membranes for the dye/salt separation. The review of literature studies indicates that the positively charged NF membranes prepared in a single step with phase inversion are all in loose nanofiltration category with a MWCO greater than 1 kDa. The positive charge in the membranes was achieved either with fillers or a polymer modified with tertiary amine groups. In both approaches lengthy and complex procedures are applied which limit the scalability of the membrane production. On the other hand, the lack of a chemical bond between the filler and matrix polymer may cause a change in the long-term performance of the membranes due to leaching of the filler. These drawbacks indicate that there is still a need for simple protocols for an economical full-scale production of positively charged NF membranes.

Polyamide-imide (PAI), commercially known as Torlon, is a good candidate for membrane fabrication due to its superior mechanical properties, high thermal and also

good chemical stability over a wide pH range. In literature, PAI was used for preparing positively charged NF membranes at least in two steps (Sun et al., 2011; Qiu et al., 2012). First, bare PAI membrane was formed using phase inversion process and then chemical post-treatment was applied on the prepared support layer at high temperature. In addition, various pore forming agents such as ethylene glycol (EG) (Sun et al., 2011), polyethylene glycol (PEG) with different molecular weights, polyvinylpyrrolidone (PVP) and LiCl (Qiu et al., 2012) were added into the casting solution. Due to uncontrolled leaching of these agents, it is not easy to obtain long term stable NF membranes when used a pore former.

In the present work, PAI based positively charged NF membranes were prepared in a single step by dissolving PEI in the coagulation bath at ambient temperature. During the phase inversion process, chemical crosslinking occurs between amide group in the PAI and amine group of the PEI preventing back diffusion of PEI into water. The surface tension of the coagulation bath decreases in the presence of PEI, causing delayed demixing, hence, providing the dense skin layer production on the membrane surface. To obtain long term stable membranes, no pore forming agent was used in the casting solution. It has been hypothesized that the pH value is the driving force for the chemical crosslinking between PAI and PEI. To prove that pH of the coagulation bath was adjusted to three different values. The membrane prepared at optimum pH was tested for its salt rejection performance and characterized in terms of its MWCO, morphology, elemental composition of the surface, surface charge, surface roughness, hydrophilicity, chemical stability and its antifouling behaviour. To the best of our knowledge, we report for the first time single step preparation of positively charged NF membranes with a MWCO less than 1 kDa without using any pore former. This one-step preparation is less complicated and requires fewer steps than either interfacial polymerization or surface coating without any leaching risk.

2.2. Materials and Methods

2.2.1 Materials

Polyamide-imide (PAI) (Trade name Torlon®, 4000T-LV) kindly supplied by Solvay Advanced Polymers, was used to obtain flat sheet substrates. N-methyl-2-

pyrrolidone (NMP, anhydrous, >99.5%) was provided by Merck and was used to dissolve PAI. Branched polyethyleneimine (PEI) a with molecular weight 25 kg/mol (kDa) was purchased from Sigma-Aldrich. Neutral solutes of glucose (Merck), sucrose (Sigma-Aldrich), PEG 1000 (Sigma-Aldrich) and PEG 600 (Fluka) were utilized to determine molecular weight cut-off (MWCO). $MgCl_2$ (VWR), $CaCl_2$ (Merck), NaCl (Sigma-Aldrich) and Na_2SO_4 (Merck) were used for determining the ion rejection capacity of the membrane. HCl with 37% purity (Sigma-Aldrich) was used to determine the chemical stability of the membrane. All the reagents were used without further purification.

2.2.2 Preparation of the Positively Charged Flat Sheet Membranes

The positively charged flat sheet membranes were prepared by phase inversion method. PAI was first dried in a vacuum oven according to the Solvay drying procedure (177 ^{o}C, 3 h) to remove moisture. Dried polymer (20 wt.%) was dissolved in NMP (80 wt.%) solvent in a schott bottle. The mixture was stirred (100 rpm) in an oil bath at 70 ^{o}C for 18 h to obtain a homogeneous casting solution. Resulting solution was viscous and in order to eliminate air bubbles, solution was waited for 24 h without stirring. Then, the solution was cast on a clean glass plate with the help of an automated film applicator (Sheen Instrument Ltd., model number: 1133N). The initial thickness of the cast membrane was adjusted by a four-sided applicator with a gap size of 200 μm. Following casting, the glass plate was immediately immersed into the coagulation bath including 0.5 wt.% PEI and kept in the bath for 18 h. The pH of the coagulation bath was adjusted to three different values, acidic (pH=4), neutral (pH=7) and basic (pH=10). The membranes prepared in acidic, neutral and basic coagulation bath were coded as PAI-PEI_pH 4, PAI-PEI_pH 7, PAI-PEI_pH 10, respectively. The prepared membranes were then rinsed several times using deionised (DI) water to remove loosely bound crosslinking agent (PEI), and finally stored in DI water at 4 ^{o}C (refrigerator) until further tests.

2.2.3 Nanofiltration Experiments

The filtration performance of the membranes was carried out using a dead-end cell filtration system with a cell volume of 10 mL and an effective surface area of 4.1 cm^2 (Millipore, Amicon Stirred Cell 8010). Each membrane was compacted at a pressure of

2.5 bar for 1 h prior to any filtration test to ensure steady state conditions. Then, water was filtered at 2 bar and the volume of collected permeate was recorded for specific time intervals by reading weight of water from digital balance. The volumetric flux of water was calculated from the slope of the permeate volume vs. time graph and converted to hydraulic permeability (PWP) using following equation:

$$PWP = \frac{\Delta V}{A \Delta t \Delta P} \tag{2.1}$$

where ΔV is the volume of permeated water (L), A (m^2) is the membrane area, Δt (h) is the permeation time and ΔP (bar) is the transmembrane pressure difference applied through the membrane.

In rejection experiments, 1 g/L aqueous solution of each neutral molecule was used instead of pure water. The solutes were filtered under the transmembrane pressure of 2 bar and the concentrations of permeate, retentate and feed solutions were measured by Rudolph - J357 Automatic Refractometer. To determine the monovalent and divalent ion rejection capacity of the membrane, 1 g/L salt solutions were filtered at pH 3 under the transmembrane pressure of 2 bar. The concentration of permeate, retentate and feed solutions were measured by Dionex ICS-5000^+ Ion Chromatography (IC). The solute rejection (%) was calculated using the equation:

$$R(\%) = \left[1 - \frac{C_P}{\frac{C_f + C_r}{2}}\right] x100 \tag{2.2}$$

where C_p, C_r and C_f are the concentrations of permeate, retentate and feed solution, respectively.

To determine the fouling behaviour of the membrane, bovine serum albumin (BSA) was used as a foulant. The concentration of the BSA solution was fixed at 1.0 g/L. The antifouling experiment was carried out at pH 4.8 (isoelectric point). Firstly, pure water flux (J_W) of the clean membrane was measured with DI-water at 1 bar for 30 min and then BSA solution used as feed solution. The flux of BSA solution (J_P) passing through the membrane was measured at 1 bar for 1 h. At the end of the 1 h BSA filtration, the fouled membrane was washed with DI-water in static condition for 15 min. After that, pure water

flux (J_R) of the washed membrane was measured again using DI-water. Such a cycle of filtration was repeated for 3 times. The flux recovery ratio (FRR) was calculated using the equation:

$$FRR(\%) = \frac{J_R}{J_W} x100 \tag{2.3}$$

In order to investigate the fouling behaviour of the membrane in detail, fouling resistance parameters which are total fouling ratio (R_t), reversible fouling ratio (R_r) and irreversible fouling ratio (R_{ir}) were calculated. The fouling resistance parameters were calculated using following equations:

$$R_t(\%) = \left(1 - \frac{J_P}{J_W}\right) x100 \tag{2.4}$$

$$R_r(\%) = \left(\frac{J_R - J_P}{J_W}\right) x100 \tag{2.5}$$

$$R_{ir}(\%) = \left(\frac{J_W - J_R}{J_W}\right) x100 \tag{2.6}$$

The magnetic stirrer was used to reduce the concentration polarization occurred on the membrane surface during the solute filtration. The experiments were carried out at room temperature.

2.2.4 Stability of the Membranes

The structural stability of the membrane was examined by storing in HCl aqueous solution at pH 3 up to 7 days under static condition in refrigerator. The PEG 1000 rejection of the membrane was measured before and after exposure to the HCl acid.

2.2.5 Characterization of Membranes

The cross-section and surface of the membranes were characterized using a scanning electron microscope (SEM) (FEI Quanta 250 FEG). In order to obtain a cross-sectional view, the membrane was first immersed in liquid nitrogen, and then cut with a clean razor blade. Also, energy dispersive x-ray analysis (EDX) was performed using the same SEM device to determine the elemental composition of the membrane surface. Before imaging and analysis, all membrane samples were coated with gold nanoparticles to increase the conductivity of the surface using Magnetron Sputter Coating Instrument. Surface roughness of the membranes was examined using atomic force microscopy (AFM) (MMSPM Nanoscope 8, Bruker). Membrane samples with an area of 2 μm x 2 μm were scanned at a rate of 1 Hz using tapping mode in air at ambient temperature by using NCHV model tip (Bruker). Mean roughness (R_a) and root mean square Z values (R_{ms}) were measured to obtain the information about the surface topology in detail. The chemical crosslinking between imide group in PAI and amine group of the PEI was confirmed by Attenuated Total Reflectance Fourier Transformed Infrared Spectrometer (ATR-FTIR), (Perkin Elmer). ATR-FTIR spectra were collected at ambient temperature over a scanning range of 2000-650 cm^{-1} with a resolution of 4.0 cm^{-1}. The flat sheet membranes were dried in a vacuum oven (Memmert) at 25 ^{o}C prior to analysis. The surface charge of the pristine and modified membranes (zeta potential) was determined using streaming potential measurements with NanoPlus Micromeritics Instrument. The measurements were carried out in the presence of 10^{-3} M KCl electrolyte solution. To determine the isoelectric point (IEP) of the membranes, the measurements were performed at different pH values. The pH value of the electrolyte solution was adjusted using 0.5 M hydrochloric acid (HCl) (Sigma-Aldrich) for acidic pH and 0.5 M sodium hydroxide (NaOH) (Sigma-Aldrich) for basic pH. The Helmholtz-Smoluchowski equation was used to calculate the apparent zeta potential of membrane surface (Kim et al., 1996). Contact angle of the pristine and crosslinked membranes was measured using Attension Optical tensiometer. Before measurement, membranes were dried in a vacuum oven (Memmert) at 25 ^{o}C. The dried membranes were fixed to a glass surface using double-sided tape. All measurements were carried out for each membrane with 5 μl volume of deionized water droplet.

2.3. Results and Discussion

2.3.1 Characterization of Membranes

The PAI based positively charged flat sheet NF membranes were prepared in a single step by using a new approach. In this approach, positively charged polyelectrolyte PEI is dissolved in the coagulation bath and diffuses into PAI solution during immersion step of the phase inversion process. As shown in Figure 2.1, chemical crosslinking occurs between imide groups in PAI and amine groups of PEI. The degree of crosslinking can be easily adjusted with the immersion time in the coagulation bath without any need for high temperature. It is hypothesized that the pH of the coagulation bath determines the degree of crosslinking and to prove this hypothesis, three different membranes were prepared by adjusting the pH to 4, 7 and 10.

The chemical crosslinking between imide groups in PAI and amine groups of PEI was confirmed by ATR-FTIR measurement (Figure 2.2). The pristine PAI membrane can be identified by the characteristic peaks belonging to imide groups at wavenumbers of 1777 and 1716 cm^{-1} (symmetric and asymmetric C=O stretching, respectively), 1382 cm^{-1} (C-N-C stretching), 1108 and 722 cm^{-1} (imide ring) and the amide groups at wavenumbers of 1643 cm^{-1} (C=O stretching) and 1542 cm^{-1} (C-N stretching of the C-N-H group). Figure 2.2 demonstrates that as the pH of the coagulation bath was changed from 4 to 10, the characteristic peaks for the imide group slowly decreased while the peaks for the amide group increased progressively. This result indicates more imide ring opening and higher degree of chemical crosslinking formed between amine and imide groups with the increased pH in the coagulation bath.

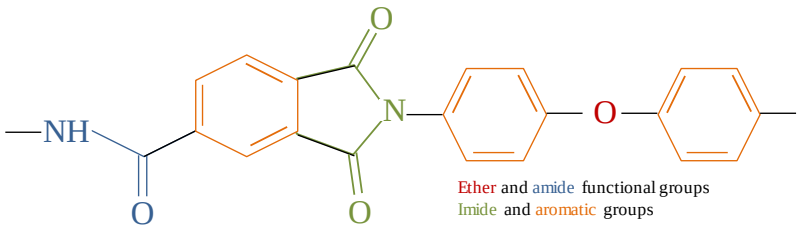

a) PAI

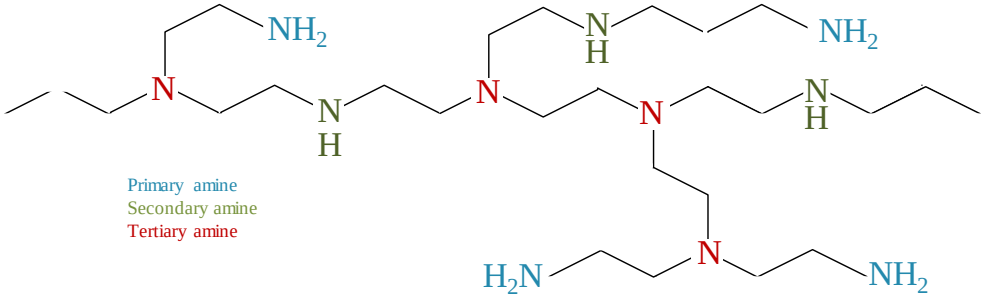

b) PEI

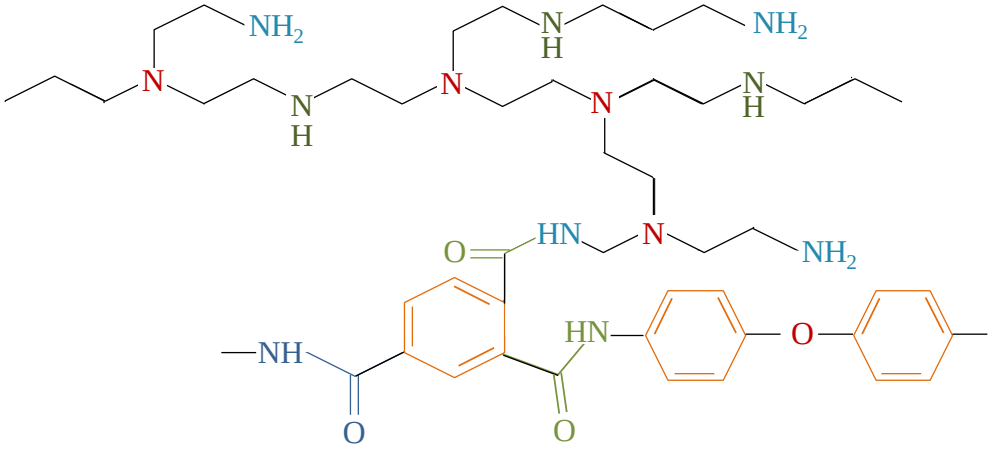

c) PAI-PEI crosslinking

Figure 2.1. The chemical structures of PAI and PEI and the crosslinking reaction between PAI and PEI.

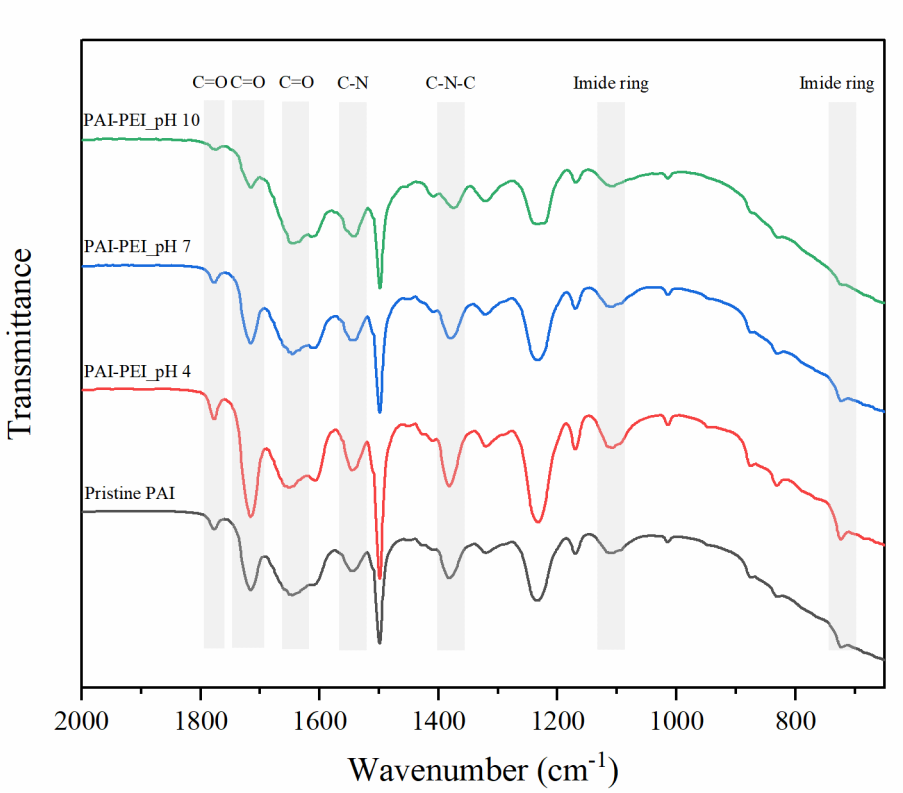

Figure 2.2. ATR-FTIR spectra of uncrosslinked (pristine PAI) and crosslinked PAI membranes (PAI_PEI) at acidic, neutral and alkaline pH values.

The surface charges of pristine and crosslinked membranes were determined by zeta potential measurement. As shown in Figure 2.3, the pristine membrane (PAI) has a negative charge within the pH range of 3-11 due to deprotonation of the carboxyl groups. After chemical crosslinking with PEI, the surface charge of the PAI membranes gradually directed towards the positive values as a result of protonation of the amine groups in the PEI. Also, isoelectric point (IEP) (embedded in Figure 2.3) of the membranes shifted to higher pH values because of the amine groups attached to the membrane surface. The membrane formed at alkaline pH, PAI-PEI_pH 10, has the highest positively charged group which indicated the highest degree of crosslinking achieved at this pH. As the pH of the PEI solution shifted towards neutral and acidic values (pH 7 and pH 4), the amount of positive charge dramatically decreased. This simply proved our hypothesis about the pH dependent degree of crosslinking. From the zeta potential and ATR FTIR data, it can be concluded that the tendency of the imide ring opening is low in acidic and neutral pH values and the chemical crosslinking is favoured in alkaline rather than in acidic pH.

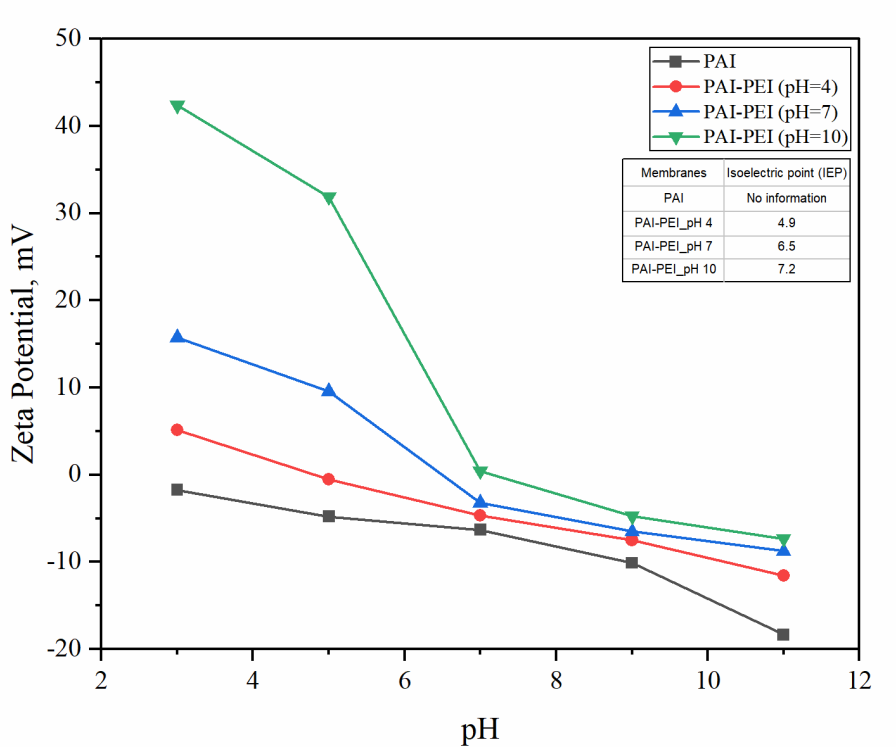

Figure 2.3. Zeta potential as a function of pH for uncrosslinked (pristine PAI) and crosslinked PAI membranes (PAI_PEI) at acidic, neutral and alkaline pH values.

The cross-section and surface morphologies of the membranes were characterized using SEM pictures. As shown in Figures 2.4 and 2.5, the change in the pH of the coagulation bath did not cause a difference in the structure of the membranes. Instead, a thin dense skin layer and finger like pores in the sublayer were observed for all the membranes.

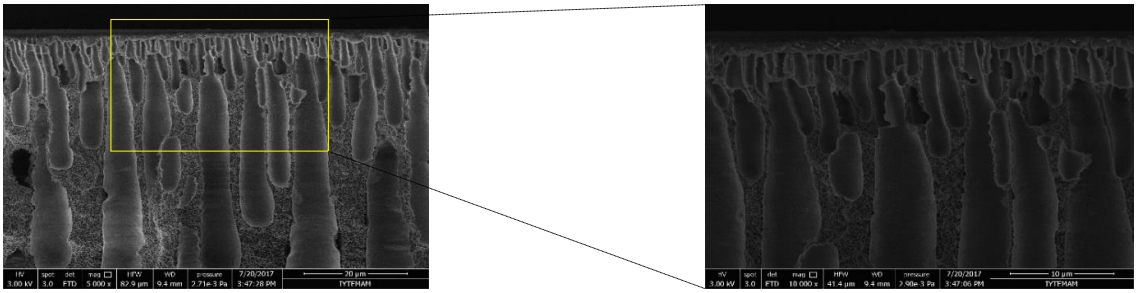

a) PAI

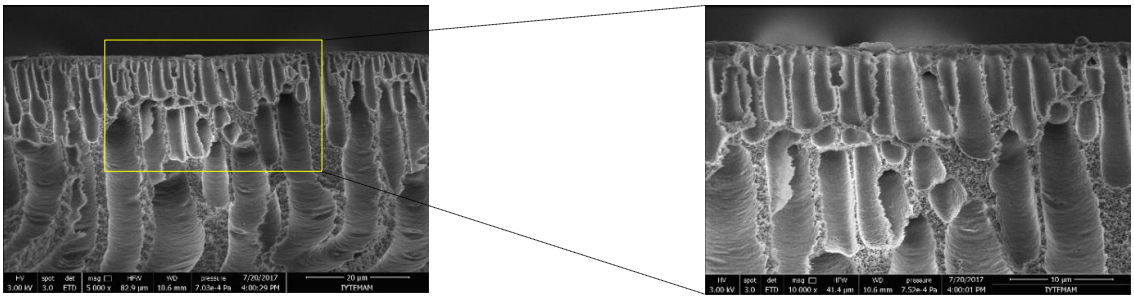

b) PAI-PEI_pH 4

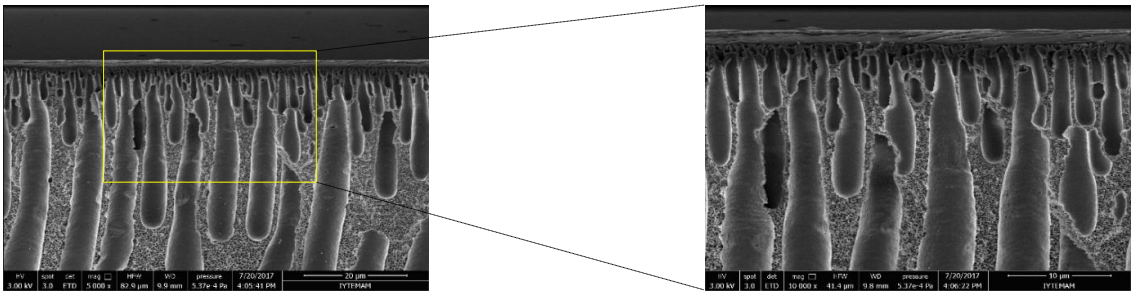

c) PAI-PEI_pH 7

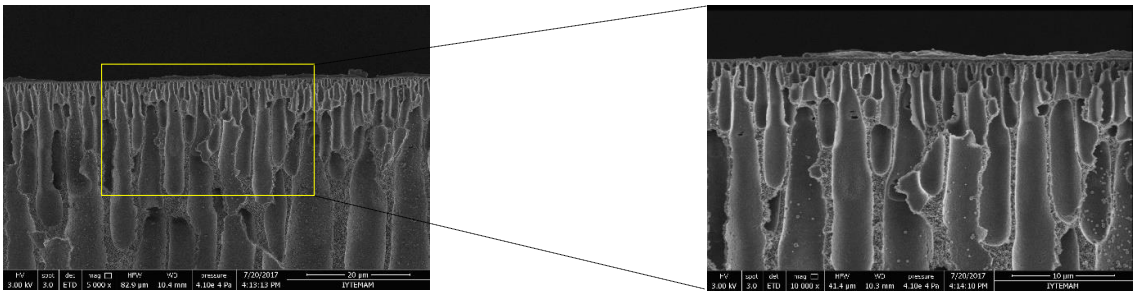

d) PAI-PEI_pH 10

Figure 2.4. Cross-sectional SEM images of uncrosslinked (pristine PAI) and crosslinked PAI membranes (PAI_PEI) at acidic, neutral and alkaline pH values.

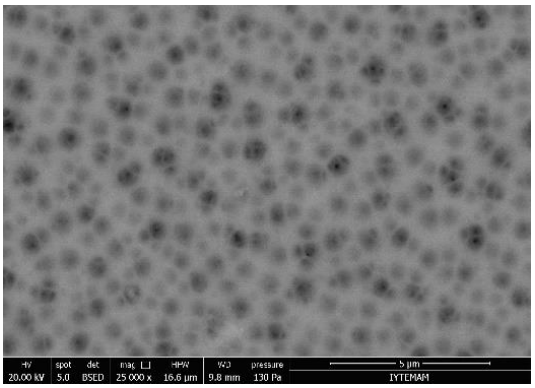

PAI

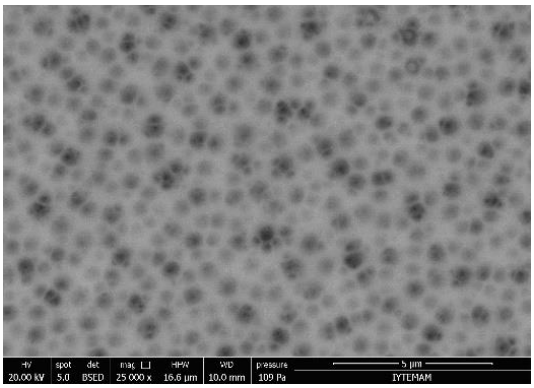

PAI_PEI_pH 4

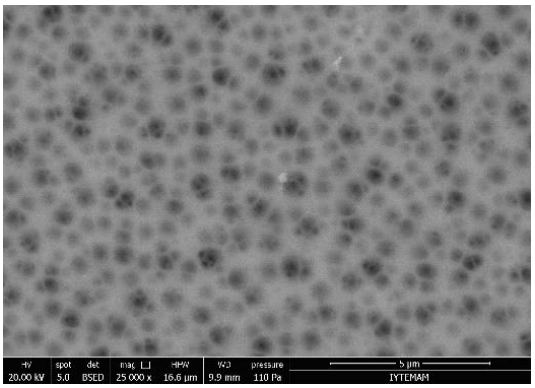

PAI_PEI_pH 7

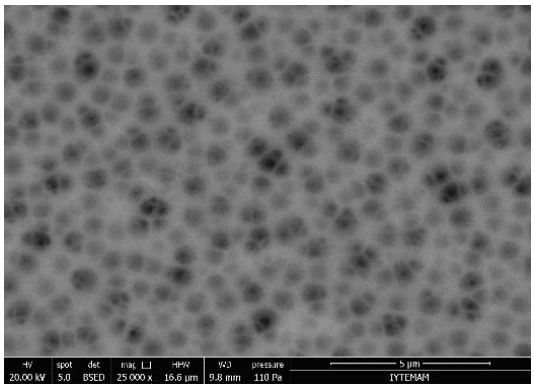

PAI_PEI_pH 10

Figure 2.5. Surface SEM images of uncrosslinked (pristine PAI) and crosslinked PAI membranes (PAI_PEI) at acidic, neutral and alkaline pH values.

Based on the results in Figures 2.2 through 2.5, we have selected the membrane carrying the highest positive charge density, PAI-PEI_pH 10, as the optimum membrane. EDX analysis of the uncrosslinked and crosslinked membranes were done to show the amount of increased nitrogen. After crosslinking of PAI with PEI, the amount of nitrogen increased almost 60% due to the high amount of nitrogen present in the structure of PEI. This result clearly shows that the occurrence of the ionic crosslinking between PAI and PEI. Also, we have characterized this membrane in terms of its surface properties, average pore size and salt rejection performance.

Table 2.1. EDX analysis of the uncrosslinked (pristine PAI) and crosslinked PAI membranes with PEI at pH 10.

Membranes	C (wt.%)	N (wt.%)	O (wt.%)	C/N
PAI	67.11	10.19	22.70	6.59
PAI-PEI_pH 10	61.16	16.31	22.54	3.75

Figure 2.6 shows surface topology of the membranes. The surface roughness of the pristine PAI membrane was found to be nearly 50% higher than the PAI-PEI_pH10 membrane in terms of arithmetic and root mean square average roughness values.

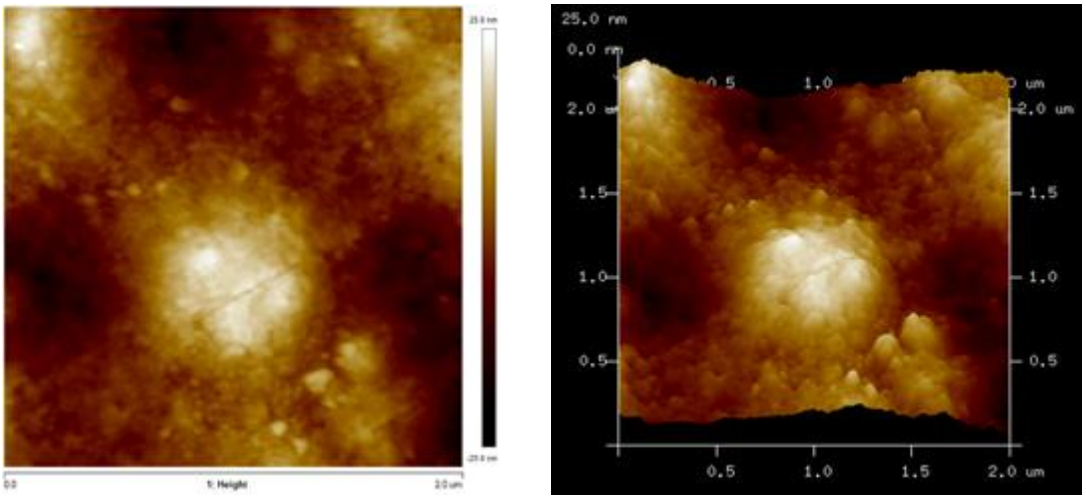

a) PAI

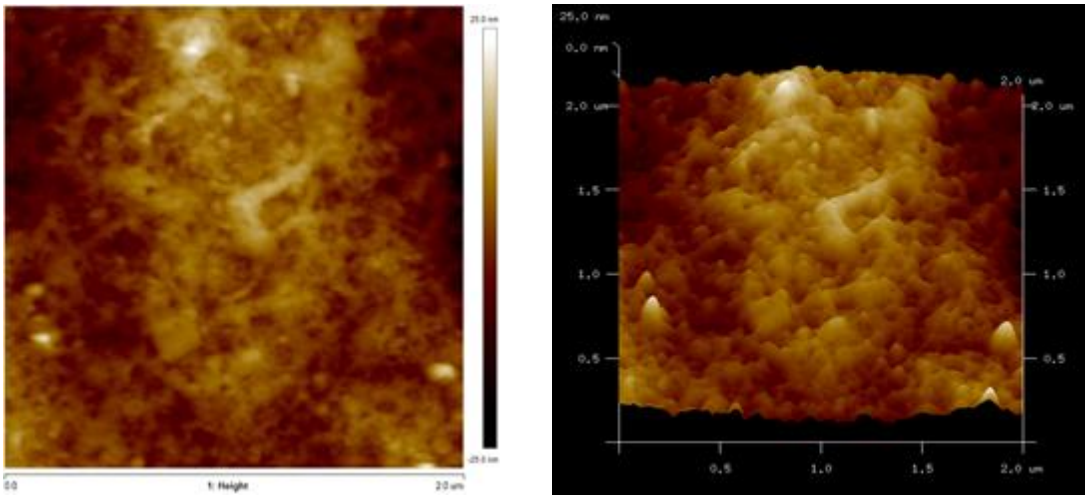

b) PAI-PEI_pH 10

Figure 2.6. AFM images of uncrosslinked (pristine PAI) and crosslinked PAI membranes with PEI at pH 10.

Table 2.2. Surface roughness values of uncrosslinked and crosslinked PAI membranes with PEI at pH 10.

Membranes	R_a (nm)	R_q (nm)
PAI	3.35	4.17
PAI-PEI_pH 10	1.76	2.33

The change in water contact angles of the pristine and crosslinked membranes is shown in Figure 2.7. The PAI membrane is slightly hydrophilic displaying the initial and final contact angle values of 92°-89°. On the other hand, after chemical crosslinking with PEI, the contact angle decreased by almost 20° and the pristine membrane became more hydrophilic due to the presence of the amine group. The lower surface roughness and higher hydrophilic nature of PAI_PEI membrane compared to the unmodified PAI membrane are other evidence of successful crosslinking between amine and imide groups.

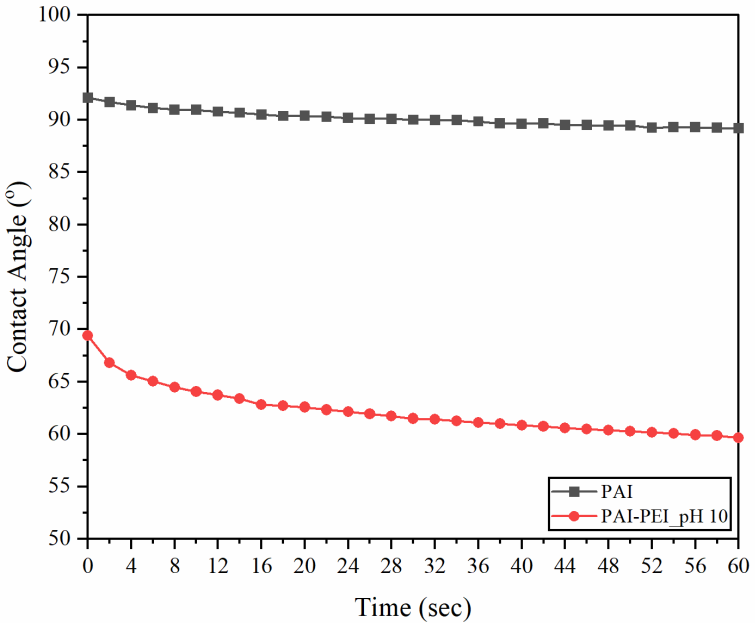

Figure 2.7. Water contact angle of uncrosslinked and crosslinked PAI membranes with PEI at pH 10.

2.3.2 Molecular weight cut-off (MWCO) and pure water permeability (PWP) of membranes

Four different neutral organic molecules glucose, sucrose, PEG 600 and PEG 1000 (embedded in Figure 2.8) were used to determine MWCO of the PAI-PEI_pH 10 membrane. Figure 2.8 shows the rejection of solutes as a function of their molecular weights. The MWCO and pore radius of the PAI-PEI_pH 10 membrane were determined to be 560 Da and 0.568 nm, respectively while its PWP was found as 4.77±0.45 L/m^{2}hbar. The uncrosslinked pristine PAI membrane completely (100%) rejected PEG 600, however, the PWP of this membrane was found very low (0.35±0.05 L/m^{2}hbar) due to its hydrophobic nature and lack of pore forming agent in the casting solution. The result demonstrates significant contribution of adding PEI into the coagulation bath not only for

obtaining a positively charged membrane but also for increasing the PWP of the membrane to an acceptable level.

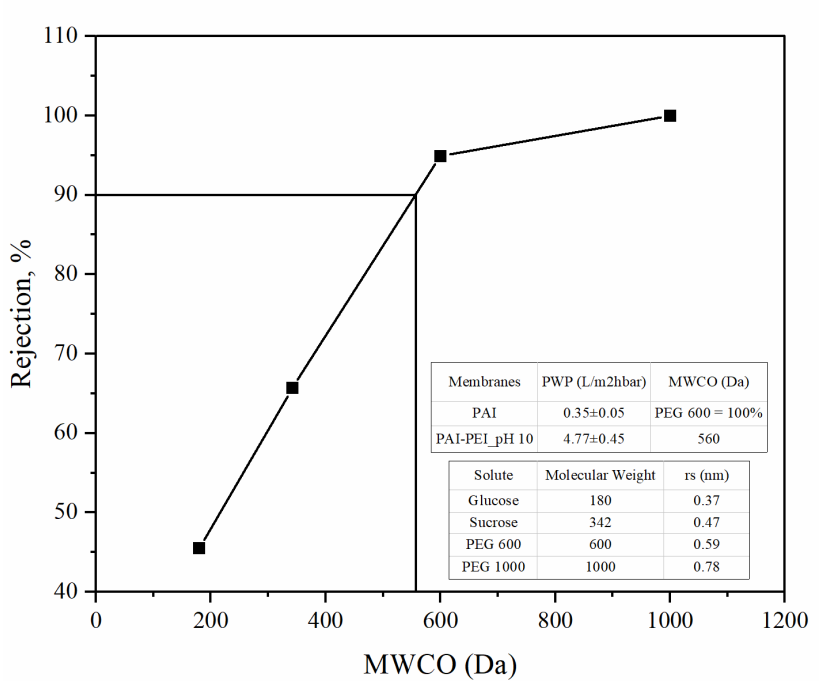

Figure 2.8. The MWCO curve of the PAI membrane crosslinked with PEI at pH 10.

2.3.3 Monovalent and Multivalent Ions Separation Performance of the Membrane

To show the salt separation efficiency of the PAI-PEI_pH 10 flat sheet NF membrane, four different salts ($MgCl_2$, $CaCl_2$, Na_2SO_4, NaCl) were used at the same concentration (1000 ppm) and pH (pH=3). The permeation flux of the PAI-PEI_pH 10 membrane was measured as 4.21±0.17 L/m^2hbar. The experiments were carried out in acidic condition because protonation capacity of the membrane in acid medium is higher than in neutral condition as illustrated with zeta potential measurements. Thus, we wanted to benefit from Donnan exclusion (electrostatic repulsion) mechanism effectively in addition to size exclusion for rejection of ions. Figure 2.9 shows that the salt retention order is $MgCl_2 > CaCl_2 > NaCl > Na_2SO_4$. This order is consistent with Donnan exclusion theory and supports the zeta potential measurement that the membrane surface is the positively charged (Peeters et al., 1998). The PAI-PEI_pH 10 membrane displayed excellent rejection for positively charged multivalent ions (95.6% Mg^{2+} and 90.2% Ca^{2+}) and moderate rejection for monovalent ions.

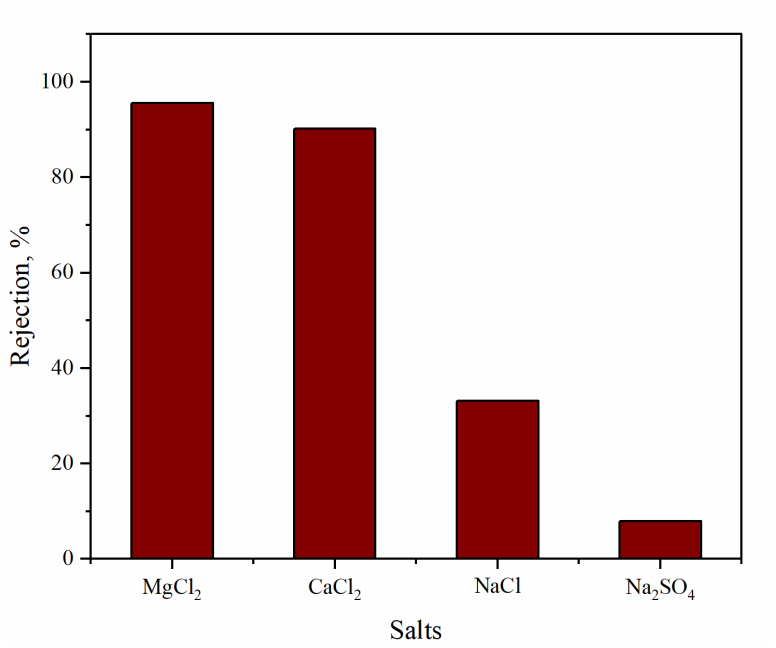

Figure 2.9. Salt rejection performance of the PAI membrane crosslinked with PEI at pH 10.

The application of positively charged NF membranes in acidic environment for the rejection of monovalent and divalent ions is limited. On the other hand, such an application may offer a solution in metal recovery from mine waste streams. Typical mine wastewater contains both divalent and monovalent ions, Ca^{2+}, SO_4^{2-}, K^+, Na^+ and Cl^- (Mullett et al., 2014) in addition to metal ions, thus, high selectivity for the separation of metals from salts is necessary to make NF an alternative separation process. Table 3 lists the selectivities of commercial and custom-made NF membranes for the separation of monovalent and divalent ions. Among the membranes listed in Table 3, our membrane has the highest selectivity in the recovery of Mg^{2+} ions from divalent salt Na_2SO_4. Although selectivity of the commercial membrane NTR-729HF for separating NaCl from $MgCl_2$ is slightly higher than our membrane, their feed concentrations are much lower (293 and 238 ppm for NaCl and $MgCl_2$, respectively). If these low feed concentrations are used, we expect higher Na^+/Mg^{2+} ($NaCl/MgCl_2$) selectivities for our membrane than the commercial NTR-729HF since the Donnan exclusion is much more effective when the ion concentration in feed is low. It should also be noted that all salt rejection data reported by other groups was obtained at pressures higher than the pressure used in our study. Achieving high selectivity at low pressures is important to perform energy efficient separation, thus, to propose NF as an alternative process in the recovery of metals from salt containing acidic solutions.

Table 2.3. The ion selectivities of various positively charged NF membranes at pH 3.

Membrane	Applied Pressure (bar)	Feed Concentration (ppm)	Selectivity					Ref
			Na^+/Mg^{2+} ($Na_2SO_4/MgCl_2$)	Na^+/Mg^{2+} ($NaCl/MgCl_2$)	Na^+/Ca^{2+} (Na_2SO_4/ $CaCl_2$)	Na^+/Ca^{2+} ($NaCl/CaCl_2$)	SO_4^{2-}/Cl^- (Na_2SO_4/ $NaCl$)	
PEI/TMC	4	1000	3.4	3.1	-	-	1.1	Chiang et al., 2009
PEI/TPC			6.3	4.7	-	-	1.4	
UTC-60	3	NaCl (293 ppm) Na_2SO_4 (710 ppm) $CaCl_2$ (277 ppm) $MgCl_2$ (238 ppm)	10	11	13.3	14.7	0.9	Kim et al., 2006
NTR-729HF			-	18.7	-	9.3	-	
NF-255	5	NaCl (500 ppm) Na_2SO_4 (500 ppm) $CaCl_2$ (620 ppm)	-	-	2.7	2.8	0.98	Szoke et al., 2003
NF-45	2.4		-	-	26	25	1.0	
NF-45	NaCl (10 bar) Na_2SO_4 (14 bar) $MgCl_2$ (14 bar)	NaCl (257 ppm) Na_2SO_4 (2750 ppm) $MgCl_2$ (1850 ppm)	1.1	1.9	-	-	0.6	Xu and Lebrun, 1999
PAI-PEI_pH 10	2	1000	20.9	15.2	9.4	6.8	1.3	This work

In Table 2.4, the pure water permeabilities and MWCO values of different PAI based hollow fiber and flat sheet membranes are listed. Although our membrane was prepared in a single step, its MWCO is half of the PAI_PEI hollow fiber membranes prepared in two steps (Sun et al., 2011) while the PWP values are similar. Thus, with our membrane it is possible to recover smaller molecular weight valuable neutral compounds. Gherasim et al. (2016) manufactured their hollow fiber membranes in a single step, however, the PWP of these membranes are lower and MWCO values are higher than our membrane.

Table 2.4. Comparison of the performances of different PAI based NF membranes.

NF membrane	Preparation procedure	MWCO (Da)	PWP (L/m^2hbar)	Ref
PAI-PEI hollow fiber (PEI_2K)	Chemical modification	1278	6.37	Sun et al., 2011
PAI-PEI hollow fiber (PEI_20K)		1278	4.85	
PAI-PEI hollow fiber (PEI_60K)		912	3.58	
PAI-PEI hollow fiber (PEI_800)	Chemical modification	-	2.25	Setiawan et al., 2011
P84-PEI hollow fiber (PEI_60K)	Chemical modification	-	0.98	Gao et al., 2014
P84-PEI flat sheet (PEI_25K)	Chemical modification	-	3.6	Ba et al., 2009
PAI-PEI flat sheet (PEI_800)	Chemical modification	-	4.58	Qiu et al., 2012
PES-$PEI_{5\%}$ hollow fiber (PEI_750K)	Single step preparation	700	0.4	Gherasim et al., 2016
PES-$PEI_{10\%}$ hollow fiber (PEI_750K)		1040	2.0	
PAI-PEI flat sheet (PEI_25K)	Single step preparation	560	4.77	This work

2.3.4 Chemical Stability and Antifouling Property of the Membrane

Industrial applications of nanofiltration in acidic environment are still limited due to insufficient acid resistance of commercial membranes. To evaluate the potential of the PAI_PEI NF membrane for the treatment of acidic solutions, the membrane was exposed to HCl acid solution at pH 3 up to 7 days. The change in the structure of the membrane was checked by measuring its PEG 1000 rejection. Figure 2.10 shows the rejection data normalized with respect to the PEG 1000 rejection value of fresh membrane not treated with HCl solution. As seen from the data, there is no significant change in the rejection values which demonstrated that our membrane was not affected from highly acidic condition. Although transport and rejection properties of the PAI based flat sheet NF membrane were measured in previous studies, its chemical stability was not tested.

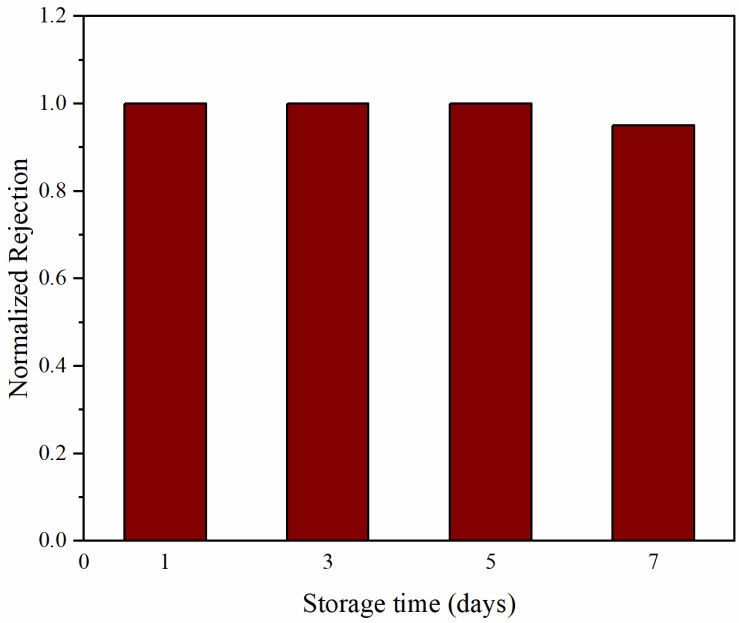

Figure 2.10. Chemical stability performance of the PAI membrane crosslinked with PEI at pH 10.

In the study, antifouling performance of the optimized membrane was tested using 1 g/L BSA solution which represents the protein type of foulant. Figures 2.11 shows the change of normalized BSA flux up to 3 hours through PEI crosslinked membrane. In fouling phenomena, hydrophobic-hydrophobic interaction between the foulant and membrane surface or inside the pores is one of the most significant interaction that reduces the permeate flux. Due to the presence of PEI known as hydrophilic polyelectrolyte in the membrane structure, this interaction was reduced. Flux recovery

ratio (FRR) and resistances of the membrane were given in Figure 2.12. In the fouling experiment, FRR values of the membrane at the end of first, second and third cycle respectively were obtained as 96.4%, 94.1% and 92.2% and total fouling ratio (R_t) values of the membrane for each cycle was found to be as 10.5%, 14.4% and 15.7%, respectively.

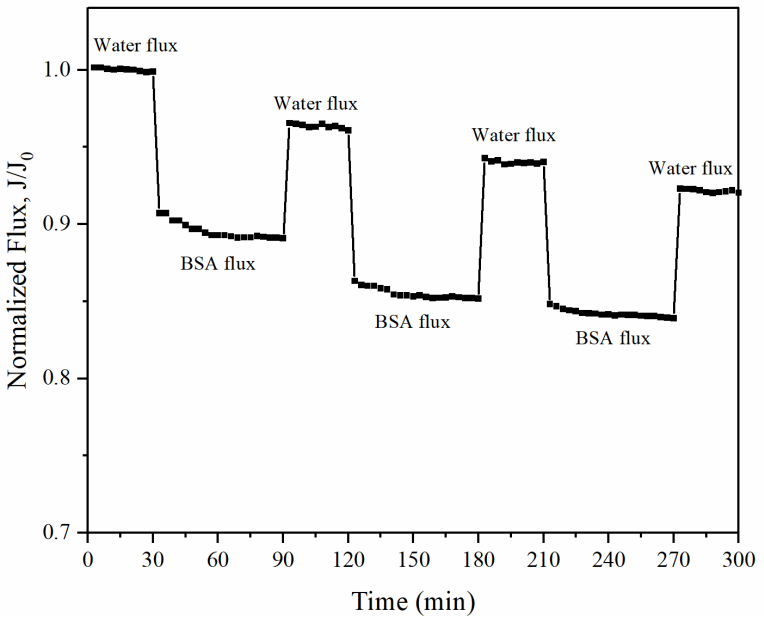

Figure 2.11. Antifouling performance of the PAI membrane crosslinked with PEI at pH 10.

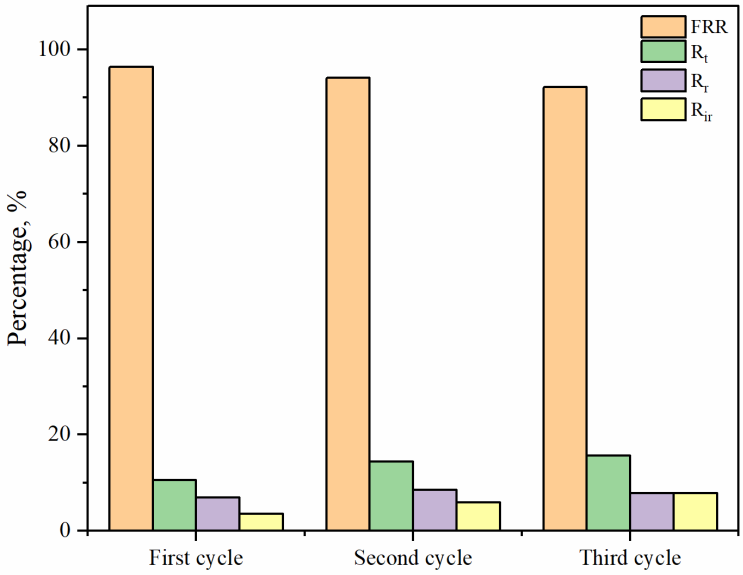

Figure 2.12. Fouling resistances and flux recovery ratio of the PAI membrane crosslinked with PEI at pH 10.

2.4. Conclusion

In this study, a facile approach is proposed for the fabrication of PAI based positively charged flat sheet NF membranes. In this approach, PEI dissolved in the coagulation bath makes in situ chemical crosslinking with PAI during the phase inversion. Alkaline pH in the coagulation bath enhanced the positive charge density of the membrane when compared to acidic and neutral conditions. Although not investigated in this study, the positive charge density of the membrane can be further adjusted by changing the concentration of PEI and immersion time in the PEI containing coagulation bath. The obtained membrane showed good performance in terms of pure water permeability (PWP) and removal of multivalent ions such as Ca^{2+} and Mg^{2+} and displayed higher selectivity in the recovery of magnesium from salt containing acidic solution than commercial membranes. In addition, the membrane has shown no significant change in its stability when stored in acidic solution. Thus, we can conclude that the membrane has a great potential in the treatment of acidic mine wastewater and in the recovery of valuable cationic metals without any need for pH adjustment. Furthermore, due to its chemical stability, it could also be used for treating acidic wastewater generated e.g., from pharmaceutical industry. Also, optimized membrane carried out good performance in terms of fouling resistance and flux recovery ratio after 3 hours filtration of BSA. The facile approach proposed in this study can be used for fabricating positively charged PAI based NF membranes due to its various advantageous such as single step preparation without need for any pore former, use of commercially available polymers and easy scalability.

CHAPTER 3

DEVELOPMENT OF POLYSULFONE-SULFONATED POLYETHERSULFONE BASED ANTIBACTERIAL ULTRAFILTRATION MEMBRANES

3.1. Introduction

Biofouling due to attachment of living microorganisms and subsequent cohesive biofilm formation on membrane surfaces is a serious problem limiting the cost effectiveness of membrane technology. Various approaches have been developed to suppress biofouling including pre-treatment of feed solution, optimization of operating conditions, periodically cleaning membrane and using antibiofouling membranes (Mansouri et al., 2010; Khan et al., 2015; Matin et al., 2011; Prihasto et al., 2009; Cornelissen et al., 2007). Among these strategies, fabricating antibiofouling membranes is an attractive alternative since other solutions require high cost, delicate operation and use of toxic chemicals. Antibiofouling membranes are developed by introducing antibacterial agents on the surface or in the bulk structure of membranes (Zhu et al., 2018). These types of membranes kill bacteria through release of active agents (release-killing) or direct contact of active agents with bacteria (contact-killing). In release-killing approach, continuous release of antibacterial agent results in a shorter lasting period of the membrane and causes an environmental risk. Therefore, recent studies focused on developing membranes with stable and long-lasting antibacterial activities through contact-killing properties.

This chapter has been published as:
A. Cihanoğlu, S. A. Altinkaya, A Facile Route to the Preparation of Antibacterial Polysulfone-Sulfonated Polyethersulfone Ultrafiltration Membranes Using a Cationic Surfactant Cetyltrimethylammonium Bromide, Journal of Membrane Science 594 (2020) 117438.

Various bactericidal components such as graphene oxide (Perreault et al., 2014), carbon nanotube (Kang et al., 2007; Kang et al., 2008) antimicrobial polymers (Munoz-Bonilla and Fernandez-Garcia, 2012) and quaternary ammonium compounds (QACs) (Kaur and Liu, 2016) have been used to develop antibacterial membranes capable of inactivating microorganisms upon contact. Among these agents, QACs are promising candidates due to their high antibacterial efficiency, lack of skin irritation, non-toxic behaviour and low cost. In literature different QACs have been integrated into membranes through in-situ membrane modification during preparation (Zhang et al., 2016c; Zhang et al., 2017b), coating (Wu et al., 2018; Xu et al., 2015) and grafting (Fei et al., 20218; Zhang et al., 2018a; Hu et al., 2016) on the membrane surface or quaternized polymers have been used for membrane preparation (Kakihana et al., 2017; Ma et al., 2017). Quaternization of poly(vinyl chloride) ultrafiltration membranes through post treatment by soaking commercial PVC hollow fiber membranes in trimethylamine solution changed the bulk structure of the membrane by blocking the pores (Wu et al., 2018). Covalent immobilization of 3-chloro-2-hydroxypropyl-trimethyl ammonium chloride (CHPTAC) onto partially hydrolysed cellulose triacetate reverse osmosis membranes had an etching effect on the surface of the membrane resulting in a decrease in the thickness of dense top layer (Fei et al., 2018). Other than causing changes in the bulk and surface structure, coating and grafting techniques require abundant chemical usage and utilize a lengthy procedure for preparing the membranes. The QAC was blended into the casting solution without any modification (Kakihana et al., 2017) or after being immobilized on a support (Zhang et al., 2017b; Kakihani et al., 2017; Ma et al., 2017). The major drawback of the physical blending technique is considered to be distribution of contact-killing antibacterial compound through the membrane cross section, hence, its insufficient concentration on the surface. To overcome this disadvantage, Zhang et al. (2017b) proposed triggering surface segregation of the QAC. For this purpose, they first produced a carbon support by ultrasonic spray pyrolysis, modified the support by oxidizing in $KMnO_4$ and $NaNO_3$ in concentrated H_2SO_4 and then immobilized the QAC on this support. Finally, the membrane was prepared by mixing this QAC@Carbon composite into polyvinylidene fluoride (PVDF). Although physical blending is a simple technique, the substantial pre-treatment steps for the preparation of the QAC or the polymer including QACs hamper simplicity of the method. The current state of the art indicates that to commercialize antibacterial membranes with contact-killing properties there is still a need for new manufacturing protocols which can easily be scaled up without any change

in production lines and significant increase in the production time. Pre-treatment or post treatment of the antibacterial agent and/or membrane increases manufacturing cost, as a result reduces the possibility of scale up and commercialization.

In this study we report a facile approach for developing stable antibiofouling membranes in a single step. Prior studies added QACs into casting solution, instead, we dissolved cetyltrimethylammonium bromide (CTAB) in the coagulation bath. We hypothesize that when the casting solution prepared from polysulfone (PSF) and sulfonated polyethersulfone (SPES) is immersed into the coagulation bath, hydrophilic polymer SPES diffuses towards coagulation bath/polymer solution interface faster than hydrophobic PSF. This allows electrostatic interaction between positively charged quaternary ammonium group (NR_4^+) in CTAB and negatively charged sulfonic acid (SO_3^-) group in SPES to occur mostly at the interface which in turn lead to accumulation of CTAB on the surface. With our approach the CTAB-containing antibacterial membrane is prepared in a single step through classical phase inversion process and the leakage of CTAB is prevented through its electrostatic attachment to the SPES. Compared to prior studies, our strategy does not require pre-treatment or grafting of QAC on a support to maintain stability and high antibacterial activity at the surface. We added CTAB in the coagulation bath at its critical micelle concentration (CMC) and significantly below (LCMC) and above the CMC (HCMC). The resulting membranes were characterized in terms of their fluxes, molecular weight cut-off values, morphology and surface properties. Based on flux data and static antibacterial activities against Gram-positive (*Staphylococcus aureus*) and Gram-negative (*Escherichia coli*) bacteria, optimum CTAB concentration was determined. The membrane prepared at the optimum concentration was further characterized to evaluate its antibiofouling performance and stability. To the best of our knowledge, the facile approach proposed in this study has been applied for the first time to incorporate QAC into polymer membranes. This approach offers a simple route to prepare antibiofouling membranes and can be easily scaled up for industrial production.

3.2. Materials and Methods

3.2.1. Materials

PSF (Mw = 35 kDa) purchased from Sigma-Aldrich and SPES (Mw = 80 kDa, Sulfonation degree (SD)<30%) kindly donated by Konishi Chemicals, Japan were used to prepare flat sheet ultrafiltration membrane. 1-methyl-2- pyrrolidone (NMP, 99.5%) and N, N-Dimethylacetamide (DMAc, 99%) purchased from Fluka and Sigma-Aldrich, respectively were used to dissolve PSF and SPES. CTAB was used as an antibacterial agent and supplied by Alfa Aesar. Polyethylene glycols (PEGs) with different molecular weights (1 kDa (Sigma-Aldrich), 4 kDa (Merck), 6 kDa (Merck), 10 kDa (Sigma-Aldrich), 20 kDa (Sigma-Aldrich), and 35 kDa (Sigma-Aldrich)) and Polyethylene oxide (PEO) (100 kDa (Sigma-Aldrich)) were used for determining molecular weight cut-off of the prepared membranes. NaCl and Phosphate Buffered Saline (PBS) were obtained from Sigma-Aldrich and used for testing the stability of the CTAB and for rinsing the membrane after bacteria filtration, respectively. Gram-negative (*Escherichia coli*, ATCC 25922) and Gram-positive (*Staphylococcus aureus*, RSKK 1009) bacteria used as model microorganisms for antibacterial tests were received from Biotechnology Research Center (BIOMER) of İzmir Institute of Technology.

3.2.2. Preparation of CTAB-Containing Ultrafiltration Membranes

Membranes were prepared from a blend of PSF and SPES by non-solvent phase inversion technique. The PSF:SPES blending ratio was adjusted to 3:1. Polymers were first dried in a vacuum oven at 80 ^{o}C for 24 h to remove moisture and dissolved (25 wt.%) in DMAc and NMP (DMAc:NMP ratio of 2:1) by stirring at 100 rpm for 24 h. In order to eliminate air bubbles in the casting solution, the solution was held for 24 h without stirring. Next, the solution was cast on a clean glass plate using automated film applicator (Sheen Instrument Ltd., model number: 1133N) and the casting thickness was adjusted to 250 μm by a four-sided applicator. Following casting, the glass plate was immediately immersed into the coagulation bath containing CTAB dissolved in water and kept in the bath for 24 h. The CTAB concentration was adjusted to 10^{-4} M, 10^{-3} M and 10^{-2} M and the resulting membranes were coded as MQ_{LCMC}, MQ_{CMC}, MQ_{HCMC}, respectively. The

pristine membrane coagulated in the absence of the CTAB just in deionised (DI) water was denoted as M0. The obtained membranes were rinsed several times with DI water to remove loosely bound CTAB molecules and stored in DI water at 4 ^{o}C (refrigerator) until further tests. A facile route to the preparation of antibacterial PSF-SPES ultrafiltration membranes using CTAB is shown in Scheme 3.1.

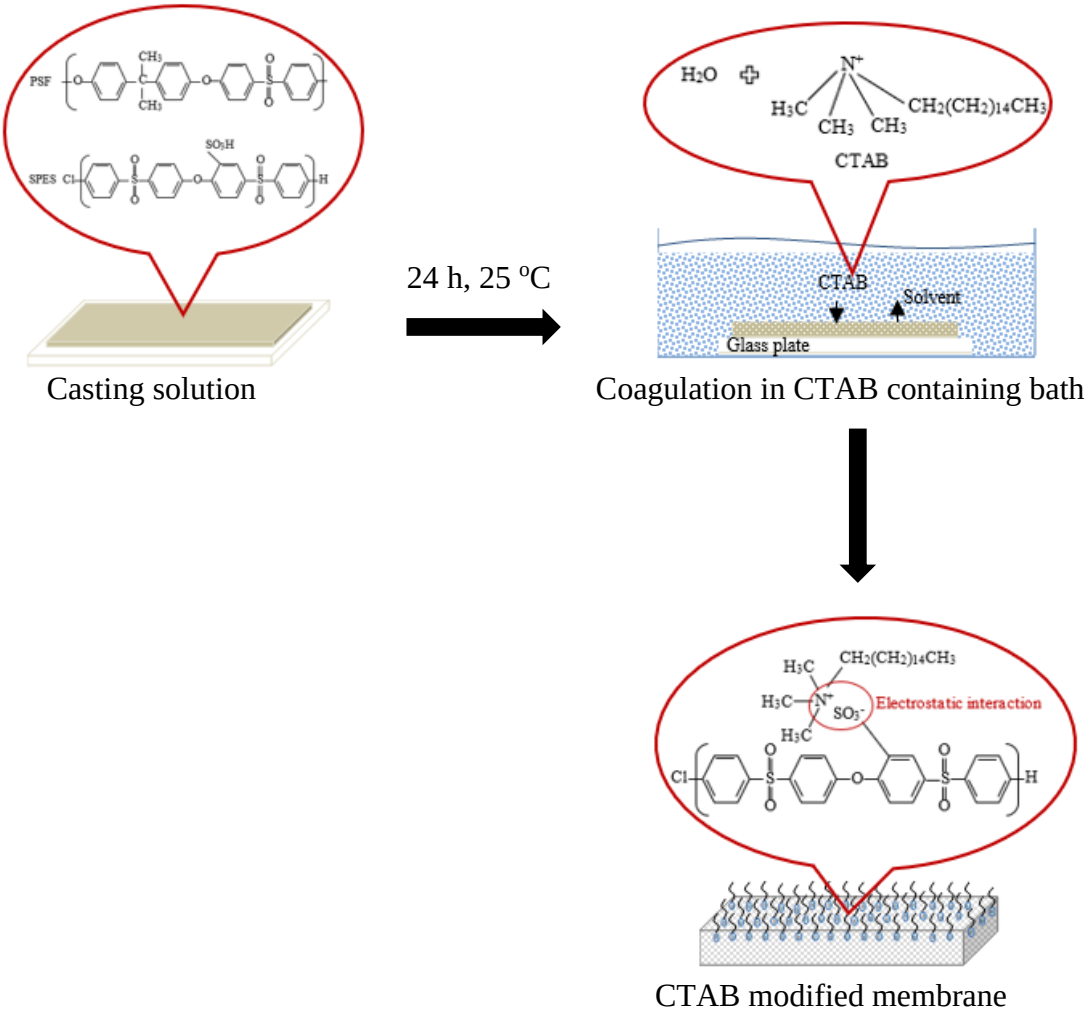

Scheme 3.1. The protocol used for preparing CTAB containing membranes.

3.2.3. Membrane Filtration Performance

The filtration performance of the pristine and modified membranes was carried out using a dead-end cell filtration system (Millipore, Amicon Stirred Cell 8010). Each membrane was compacted to reach steady state conditions prior to any filtration test. Then, pure water was filtered at 1 bar and collected permeate volume was recorded for specific time intervals. The volumetric flux was calculated from the slope of the permeate

volume vs. time graph and converted to hydraulic pure water permeability (PWP) using following equation:

$$PWP = \frac{\Delta V}{A\Delta t\Delta P} \tag{3.1}$$

where ΔV is the volume of permeated water (L), A (m^2) is the membrane area, Δt (h) is the permeation time and ΔP (bar) is the transmembrane pressure difference applied through the membrane (n=3 where n is the number of repeated experiments). To determine molecular weight cut-off (MWCO) of the membranes, 10 mL of 1 g/L aqueous solutions of neutral PEG molecules with different molecular weights were filtered at 1 bar until 5 mL of permeate was collected (n=3). To ensure that the membrane was fully conditioned with PEG 1000, fresh solution was filtered three times. The concentrations of permeate, retentate and feed solutions were measured by Rudolph-J357 Automatic Refractometer. The solute rejection (%) was calculated using the equation:

$$R(\%) = \left(1 - \frac{C_p}{\frac{C_f + C_r}{2}}\right) x100 \tag{3.2}$$

where C_p, C_r and C_f are the concentrations of permeate, retentate and feed solution, respectively. To eliminate concentration polarization, the solution was stirred at 300 rpm. The pore radius distribution of the membranes was calculated using the probability density function based on the assumption of no interaction (steric and hydrodynamic) between the neutral PEG molecules and pores of the membranes (Lin et al., 2016b).

$$\frac{dR(r_p)}{dr_p} = \frac{1}{r_p x ln\sigma_p x\sqrt{2\pi}} exp\left[-\frac{\left(lnr_p - ln\mu_p\right)^2}{2x\left(ln\sigma_p\right)^2}\right] \tag{3.3}$$

where μ_p is the mean effective pore radius determined at the PEG rejection coefficient of 50% and σ_p is the geometric standard deviation defined as the ratio of radius r_p at the PEG rejection of 83.14% over that at 50%.

The stokes radius of the neutral PEG molecules can be calculated through the following equation:

$$r_p = 16.73x10^{-12}xMW^{0.557}, (MW \leq 35000) \quad (3.4)$$

The porosity of the membranes (ε) was calculated from weight and thickness measurements as follows (Yang et al., 2007):

$$\varepsilon = \frac{W_w - W_d}{S \times d \times \rho_w} \quad (3.5)$$

where W_w and W_d are the weights of the wet and dry membranes, respectively, S is the area of the membranes, d is the average thickness of the membranes and ρ_w is the density of water (0.998 g/cm^3).

3.2.4. Membrane Characterization

The chemical structure of the pristine and modified membranes was determined by Attenuated Total Reflectance Fourier Transformed Infrared Spectrometer (ATR-FTIR), (Perkin Elmer). The spectrums of the membranes were collected at ambient temperature over a scanning range of 4000-650 cm^{-1} with a resolution of 4.0 cm^{-1}. Prior to analysis, all the membranes were dried in a vacuum oven (Memmert) at 25 ^{o}C. The surface charge of the membranes was determined by streaming potential measurements (NanoPlus Micromeritics Instrument) using 10^{-2} M NaCl (pH 7.4) as an electrolyte solution (n=3). Water contact angle of the membranes was measured (Attension Optical tensiometer) with 5 μL water droplet after drying the membranes in a vacuum oven at 25 ^{o}C (n=5). The surface and cross-section morphology of the membranes were characterized using a scanning electron microscope (SEM) (FEI Quanta 250 FEG). Before imaging, dried membranes were coated with gold using a Magnetron Sputter Coating Instrument. The surface roughness (R_a = arithmetic mean roughness, R_q = root-mean-square roughness) of the membranes was determined for a 5x5 μm^2 surface using atomic force microscopy (AFM) (MMSPM Nanoscope 8, Bruker) (n=3). The elemental composition of the membrane prepared at the CMC (MQ_{CMC}) was determined using X-ray photoelectron spectra (XPS) (Thermo Scientific) at the emission angles of 0^{o}, 15^{o}, 30^{o} and 45^{o}. The amount of CTAB loaded into the membrane was determined using TGA

analysis (Setaram, Labsys, TG-DTA/DSC). The heating rate was adjusted to 10 ^{o}C/min between 25 ^{o}C to 800 ^{o}C.

3.2.5. Antibacterial Activity Assessment of Membranes

The antibacterial activities of the membranes were determined with colony-counting method according to ASTM E2180 standard protocol. Briefly, *E. coli* (Gram negative) and *S. aureus* (Gram positive) were inoculated in Mueller-Hinton agar at 37 ^{o}C. After incubation, bacteria colonies were picked off with a swab and mixed with 0.1% (w) peptone water to adjust concentration to the value of 0.5 in the McFarland standards scale. Then, bacteria suspensions were serially diluted with Mueller-Hinton broth to obtain final concentrations of $3.5x10^{6}$ and $4.2x10^{6}$ CFU/mL for *E. coli* and *S. aureus*, respectively.

Membrane coupons (effective area 3 cm *x* 3 cm) were first sterilized with UV light for 30 min and placed on agar plates. Next, the active side of the coupons were contacted with 300 µL of bacteria suspension for 24 h at 37 ^{o}C. Following incubation, the membranes were transferred into Erlenmeyer flasks containing 50 mL phosphate buffered saline solution (PBS, pH = 7.4) and sonication was applied for 10 min to remove deposited bacteria from the membrane surface. Finally, the bacteria suspension was spread on a LB plate, incubated for 24 h at 37 ^{o}C and the colonies were counted. The bactericidal rate was calculated using the following equation:

$$Antibacterial\ rate\ (\%) = (\frac{N_P - N_M}{N_P})x100 \tag{3.6}$$

where N_P and N_M are the number of visual bacterial colonies on the agar plate after contacting with the pristine and modified membranes, respectively (n=3).

3.2.6. Stability of the CTAB-Containing Membranes

The long-term stability of the CTAB-containing membrane was determined by measuring the CTAB released from the membrane. After storing membrane coupons in DI water for 1, 3, 7 and 30 days, the leached CTAB in water was measured with Total Organic Carbon (TOC) analyser. In addition, the membrane was stored in 1 M NaCl for 15 days at 4 ^{o}C and 30 days at 25 ^{o}C in a refrigerator and 1 M NaCl solution (1 L) was

filtered through the membrane at 25 ºC. At the end of static storage and dynamic salt filtration, the antibacterial activities of the used membrane against *E. coli* and *S. aureus* were measured. The amount of CTAB loaded into the membrane was calculated from the weight loss determined by TGA analysis.

3.2.7. Analysis of Antibiofouling Performance

The dynamic biofouling potentials of the M0 and MQ_{CMC} membranes were evaluated in a dead-end cell filtration system with a cell volume of 50 mL and an effective surface area of 13.4 cm^2 (Millipore, Amicon Stirred Cell 8050). Prior to experiments, membrane coupons were sterilized with UV light for 20 min. *E. coli* and *S. aureus* bacteria suspensions were prepared in PBS (pH 7.4) to reach concentrations of $1.75x10^8$ and $2.1x10^8$ CFU/mL, respectively. The biofouling experiment was carried out using 250 mL bacteria suspensions under similar initial fluxes for the pristine and the CTAB-containing membranes. Following filtration, the membrane coupons were rinsed with PBS for 10 min and water flux was re-measured to calculate the flux recovery ratio (FRR). Total fouling (R_{total}), reversible fouling (R_{rev}), irreversible fouling (R_{irrev}) and flux recovery ratios (FRR) were calculated using Eqs. (7)-(10).

$$R_{total}(\%) = \left(1 - \frac{J_P}{J_W}\right) x100 \tag{3.7}$$

$$R_{rev}(\%) = \left(\frac{J_R - J_P}{J_W}\right) x100 \tag{3.8}$$

$$R_{irrev}(\%) = \left(\frac{J_W - J_R}{J_W}\right) x100 \tag{3.9}$$

$$FRR(\%) = \left(\frac{J_R}{J_W}\right) x100 \tag{3.10}$$

where J_W is the pure water flux of the clean membrane, J_P is the flux of the bacteria suspensions passing through the membrane and J_R is the pure water flux of the washed membrane. The experiments were carried out at ambient temperature.

3.3. Results and Discussion

3.3.1. Characterization of Membranes

Figure 3.1 shows the ATR-FTIR spectra for the pristine (M0) and CTAB-containing membranes. The peaks appeared at around 2925 cm^{-1} and 2853 cm^{-1}, assigned to the C-H symmetric and asymmetric stretching present in CH_2 group, confirmed the presence of CTAB in the membranes. The intensity of these peaks depends on the amount of CTAB added into the coagulation bath. As shown in Table 3.1, the higher CTAB concentration in the coagulation bath (< CMC, =CMC and > CMC) the larger the peak areas for both the C-H symmetric and asymmetric stretching. The increase in peak areas can be attributed to more electrostatic interaction formed between positively charged quaternary ammonium group in the CTAB (NR_4^+) and negatively charged sulfonic acid group in the PSF-SPES (SO_3^-) (Scheme 3.1).

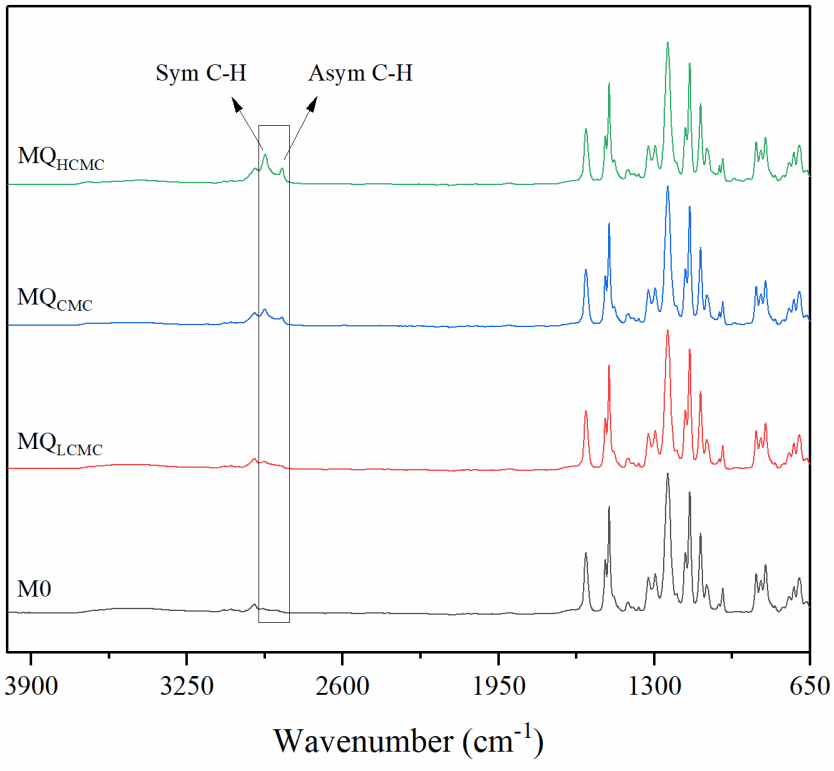

a)

Figure 3.1. ATR-FTIR spectra of the pristine and CTAB modified membranes.

(Cont. on next page)

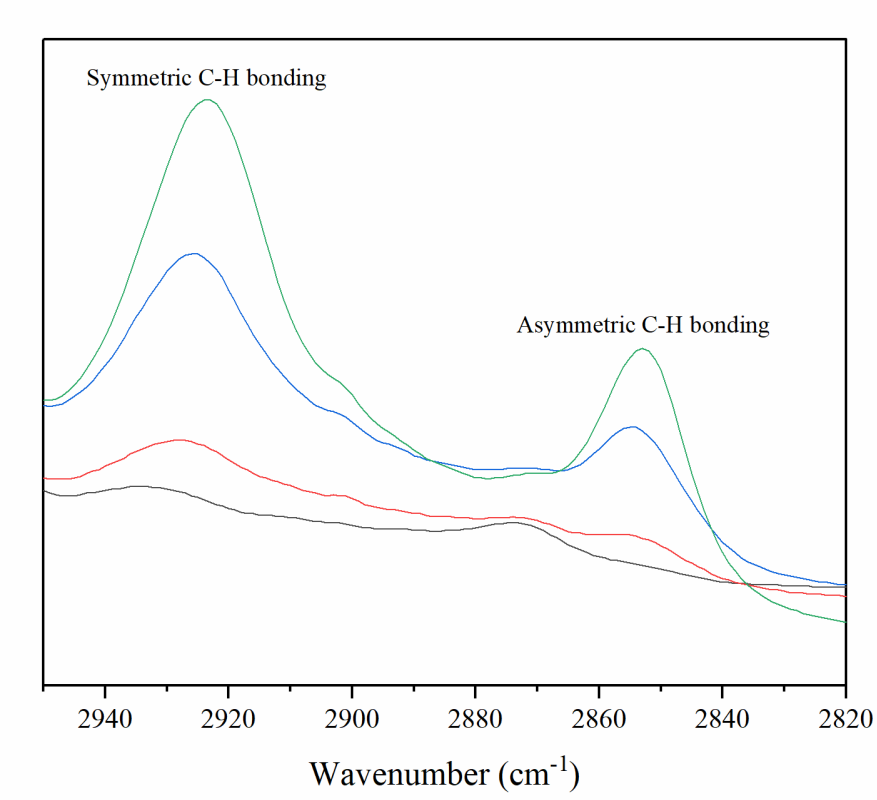

b)

Figure 3.1. Cont.

Table 3.1. Peak areas for the pristine and CTAB-containing membranes.

Membranes	Peak Area	
	Sym C-H stretching (2925 cm^{-1})	Asym C-H stretching (2853 cm^{-1})
M0	-	-
MQ_{LCMC}	0.10	0.01
MQ_{CMC}	0.33	0.13
MQ_{HCMC}	0.64	0.23

The surface charge of the membranes determined at pH 7.4 is shown in Figure 3.2. The pristine membrane (M0) has a negative charge (-22.21±0.77 mV) due to deprotonation of the sulfonic acid group in SPES. Coagulation in the presence of CTAB allows obtaining membranes with an active layer formed via an electrostatic interaction between CTAB and SPES. Consequently, the surface charge of the CTAB-containing membranes shifted towards positive values.

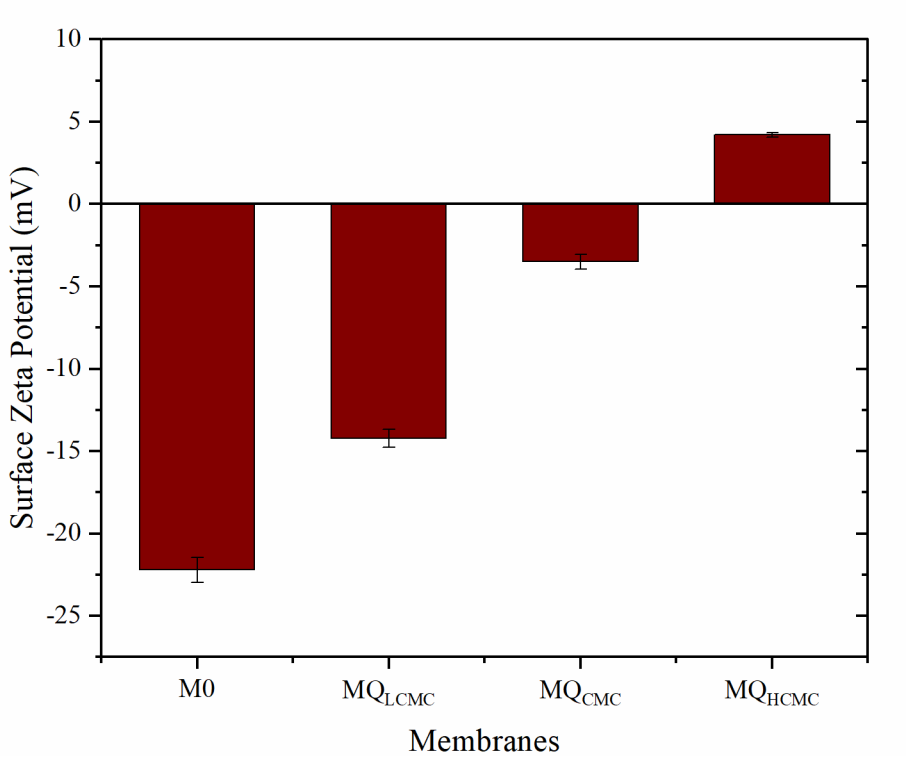

Figure 3.2. Zeta potential of the pristine and CTAB modified membranes at pH 7.4.

The hydrophilicity of the membranes decreased in the presence of CTAB as demonstrated by the increased contact angle values (62.6±3.9, 69.4±1.1, 72.6±1.3, 80.2±1.5 for M0, MQ_{LCMC}, MQ_{CMC}, MQ_{HCMC} membranes, respectively) in Figure 3.3. Hydrophilic quaternary ammonium head in the structure of the CTAB interacts with sulfonic acid group on the membrane surface and hydrophobic tail becomes free. This free tail makes the surface of the CTAB-containing membranes more hydrophobic than the pristine membrane.

The cross-section and surface morphologies of the membranes are shown in Figures 3.4 and 3.5. For all membranes, a typical dense skin layer on the top surface and finger like structure in the sublayer were observed. A closer look at the structure nearby the surface with the higher magnification SEM images (x20000) showed the influence of the coagulation bath composition. With the increased CTAB concentration, the density of spongy pores increased, in addition, the small pores located in the macrovoids decreased. As shown in red frame in Figure 3.4, almost all the pores in the finger like structure of the membrane prepared with the highest CTAB concentration (MQ_{HCMC}) disappeared compared to the pristine membrane (M0).

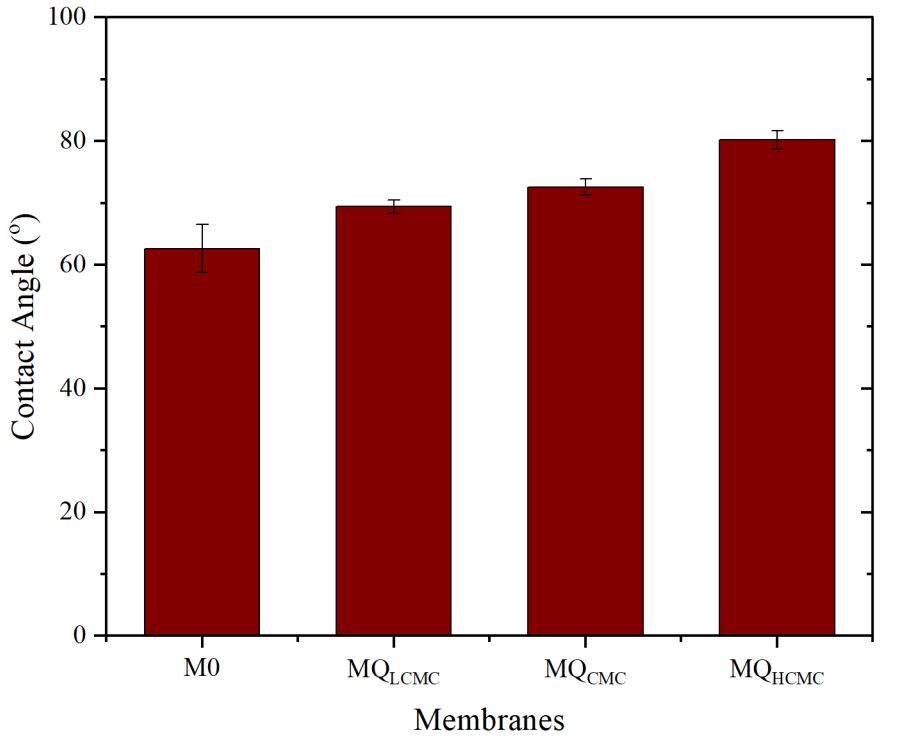

Figure 3.3. Water contact angle of the pristine and CTAB modified membranes.

The disappearance of finger-like pores in the sublayer of the CTAB-containing membranes is related with the decrease in the surface tension of the coagulation bath. It was reported that the surface tension of water is reduced from 72.8 dyne/cm to 37 dyne/cm by adding 10^{-2} M CTAB into water (Olcay et al., 2016). As discussed by Matz (1972), the finger like pores and large macro void formation in the membrane structure occur due to hydrodynamic interfacial instabilities. In the presence of CTAB, such interfacial instabilities, as a result, tendency of finger like-cavity formation are reduced. Adding CTAB into the coagulation bath also changes the kinetics of phase inversion. The CTAB in gelation medium makes electrostatic interaction with the SPES at the interface, hence, forms a barrier layer and slows down the exchange of solvent/nonsolvent (Scheme 3.2). This delays the precipitation and as shown in Table 3.2 causes the pore size of the skin layer to become smaller and porosity of the membrane to decrease. Surface SEM images in Figure 3.5 demonstrate that the pristine (M0) membrane has the largest pore size. Compared to most of the Loeb-Sourirajan phase separation membranes often having an average porosity of 0.7-0.8 (Baker, 2012), the overall porosities of the pristine and CTAB containing membranes are lower since no pore formers were used in the casting solution.

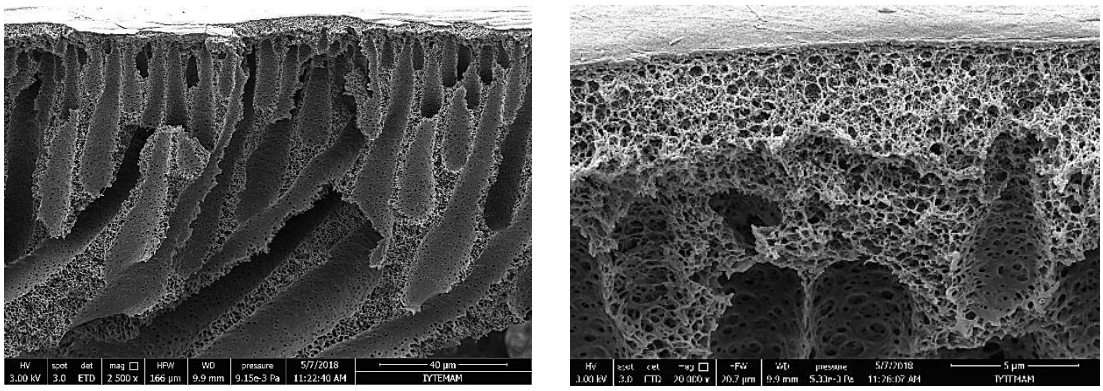

M0

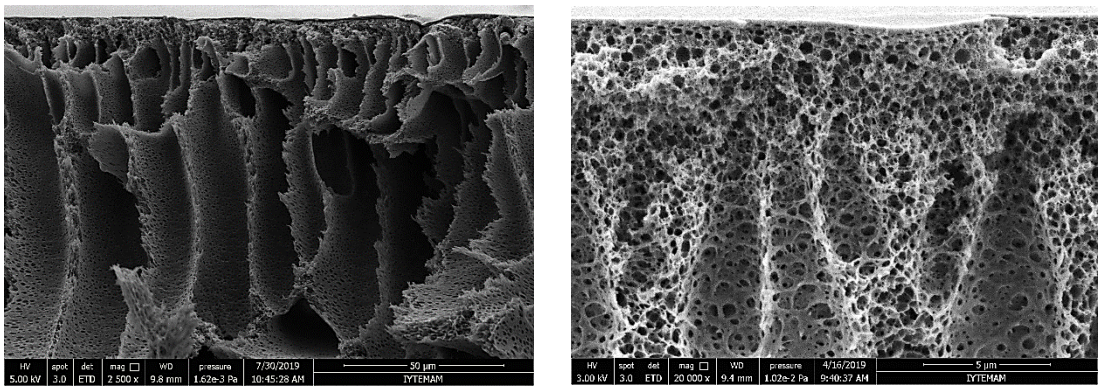

MQ_{LCMC}

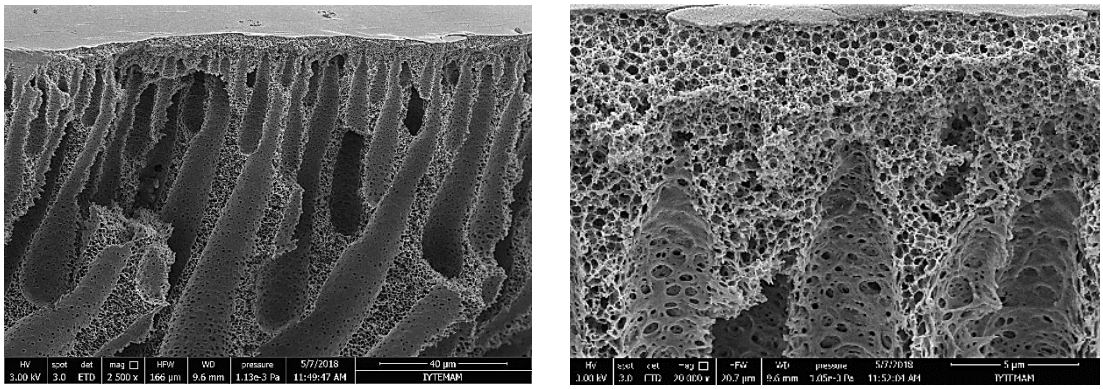

MQ_{CMC}

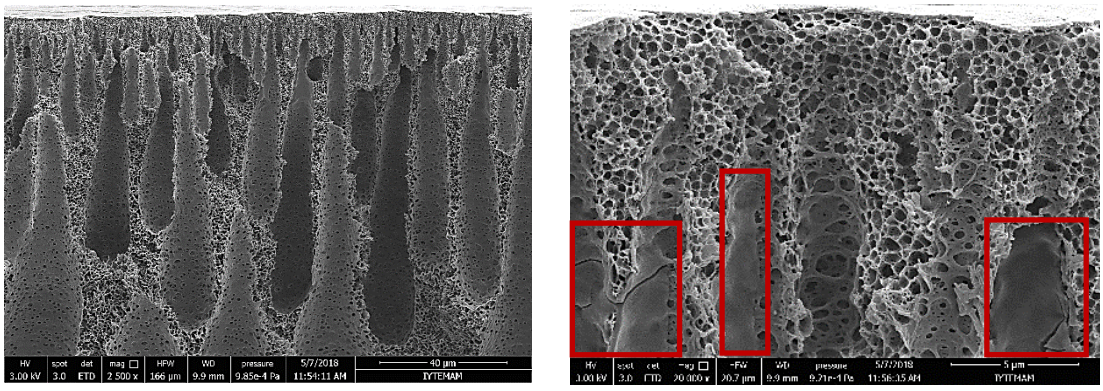

MQ_{HCMC}

Figure 3.4. Cross-sectional SEM images of the pristine and CTAB modified membranes.

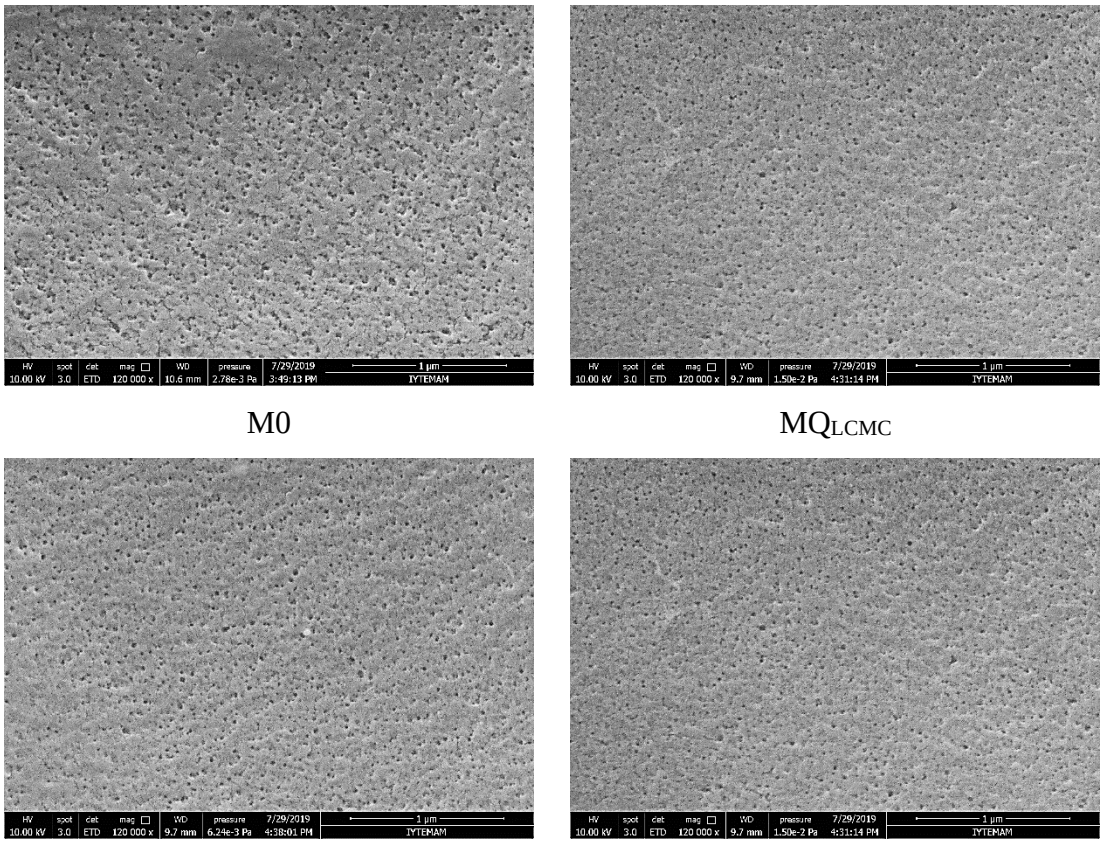

Figure 3.5. Surface SEM images of the pristine and CTAB modified membranes.

AFM images of the membranes are shown in Figure 3.6. The roughness parameters listed in Table 3.2 for the CTAB modified membranes were found lower compared to that of the pristine membrane which confirms strong interaction between the CTAB and SPES at the surface.

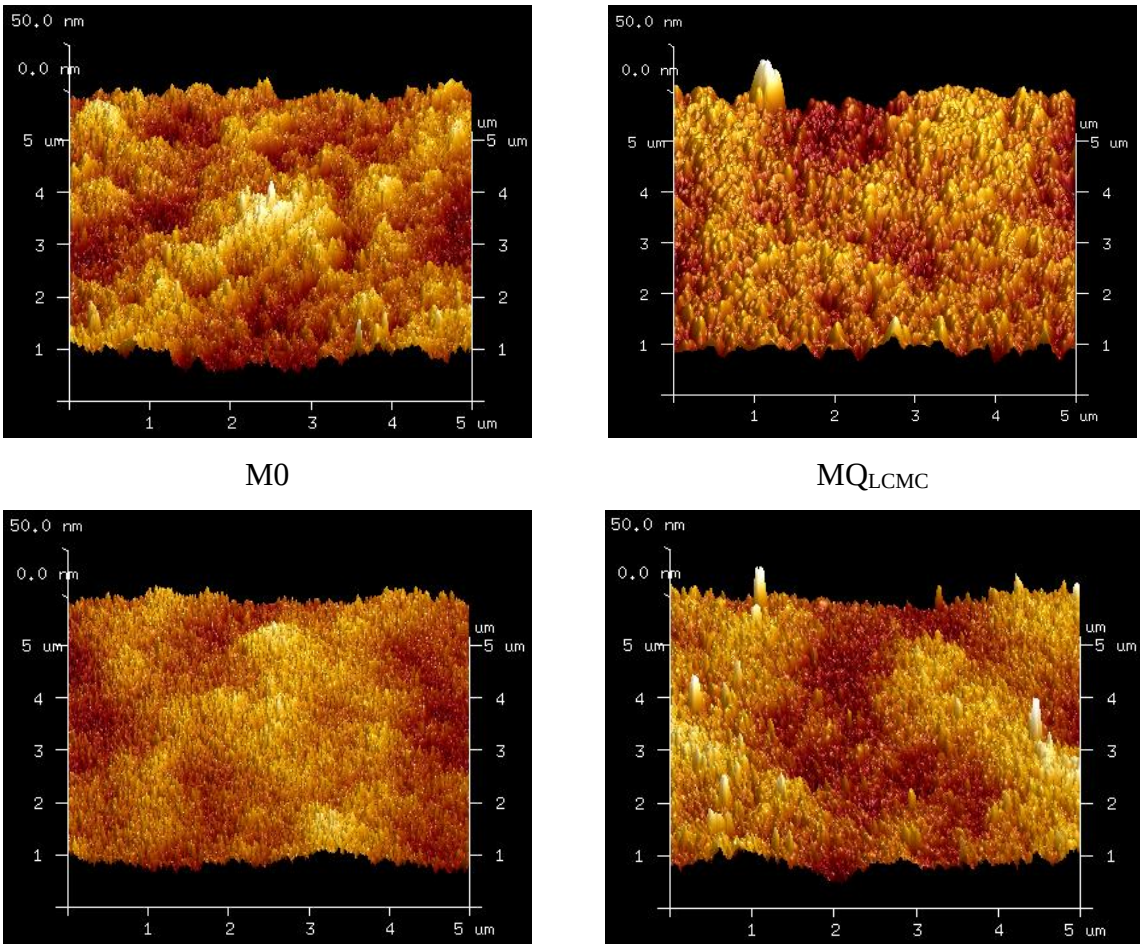

M0 MQ_{LCMC}

MQ_{CMC} MQ_{HCMC}

Figure 3.6. AFM images of the pristine and CTAB modified membranes.

3.3.2. Pure Water Permeability (PWP) and Molecular Weight Cut-Off (MWCO) of Membranes

The pure water permeability of the pristine membrane was found to be 182.4±8.3 L/m^2hbar. As shown in Figure 3.7, the permeability decreased to 127.4±3.2, 93.2±1.6 and 39.3±3.2 L/m^2hbar for the membranes coagulated in CTAB-containing bath at concentrations below (MQ_{LCMC}), at (MQ_{CMC}) and above (MQ_{HCMC}) the critical micelle concentration of the CTAB, respectively. The decline in permeability can be mainly explained by the increase in hydrophobicity of the membranes as confirmed by an increase in the contact angle of the membranes (Figure 3.3). In addition, the disappearance of small pores in the sublayer of the membranes can also account for the dramatic flux decline. Figure 3.8 illustrates the rejection of six different PEGs (molecular weights 1, 4, 6, 10, 20, 35 kDa) and PEO (100 kDa) by the pristine and modified

membranes. The MWCO of the membranes, defined as the molecular weight at which 90% of the solute is rejected by the membrane (Hoek and Tarabara, 2013) were determined to be 30.5 kDa, 27.1 kDa, 27.4 kDa and 21.4 kDa for the M0, MQ_{LCMC}, MQ_{CMC} and MQ_{HCMC}, respectively. As expected, smaller pore size and lower porosity of the CTAB containing membranes resulted in lower MWCO values as compared to that of the pristine membrane. In the presence of CTAB at the CMC (the CTAB is in spherical shape in the bulk phase) or below the CMC (the CTAB has a rod like shape in the bulk phase) in the coagulation medium, its barrier effect on the exchange of solvent/nonsolvent is similar. Consequently, the MWCO values of the membranes prepared under these conditions (MQ_{LCMC}, MQ_{CMC}) were found the same. On the other hand, above the CMC, the shape of CTAB molecules changes from spherical to cylindrical (Coppola et al., 2004), they form micelles in gelation medium and rate of exchange of solvent and nonsolvent, is significantly hindered due to thicker adsorbed CTAB layer (Scheme 3.2c). As a result, the MQ_{HCMC} has a smaller MWCO value than the other CTAB-containing membranes. In the presence of highest CTAB concentration (10*x*CMC) in gelation medium, the mean effective pore radius of the membranes decreased from 3.21 nm to 2.79 nm. On the other hand, the pore size distributions of the membranes were found similar regardless of the coagulation condition (Figure 3.8).

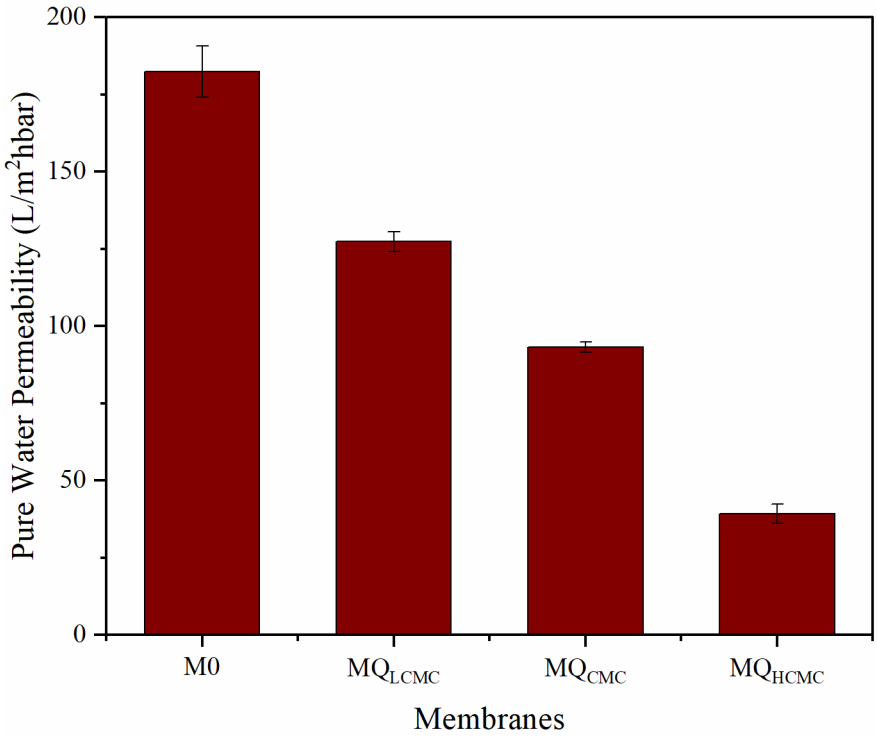

Figure 3.7. PWP of the pristine and CTAB modified membranes.

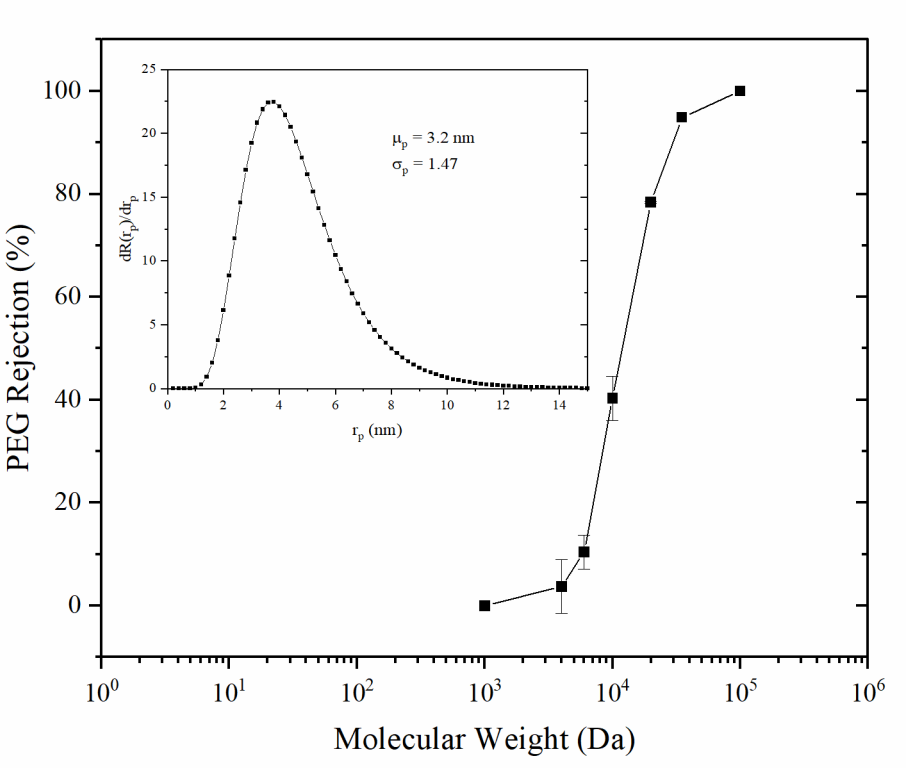

a) M0

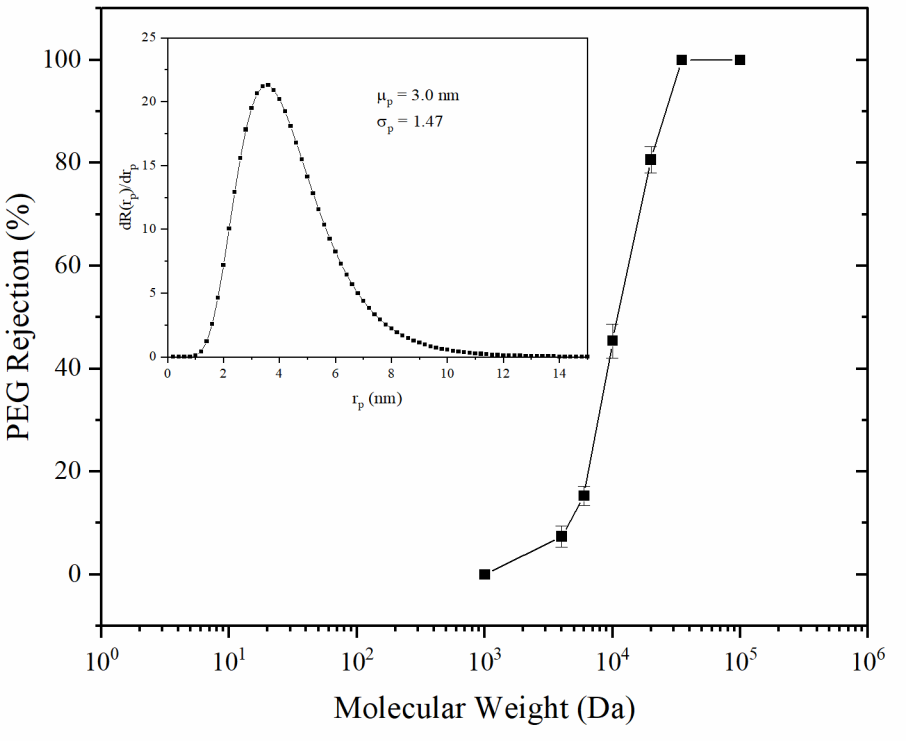

b) MQ_{LCMC}

Figure 3.8. MWCO of the pristine and CTAB modified membranes.

(Cont. on next page)

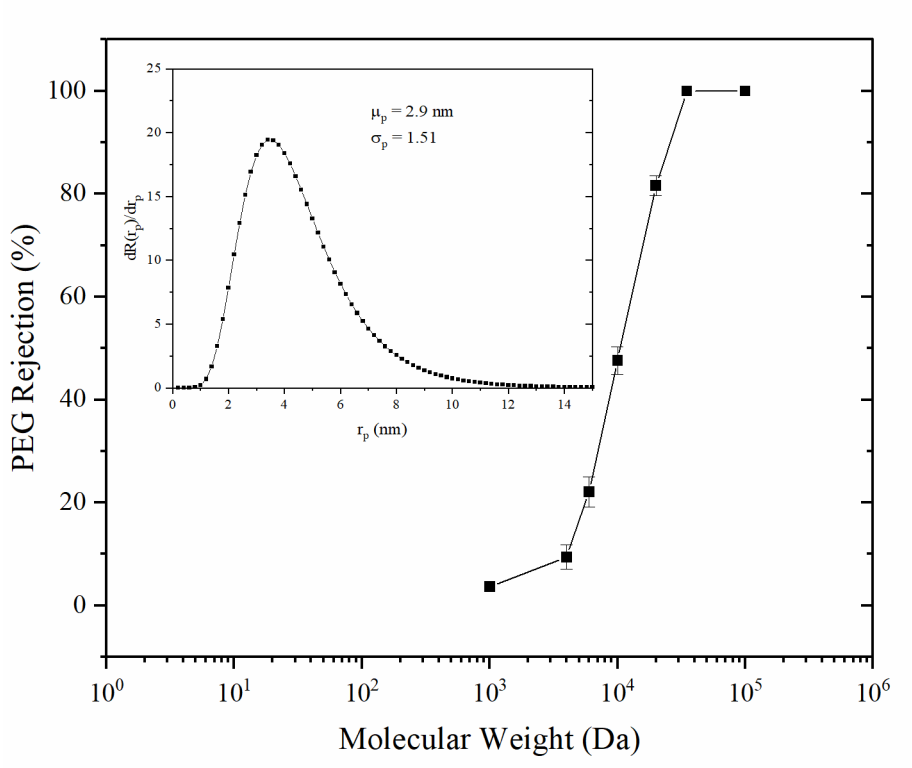

c) MQ_{CMC}

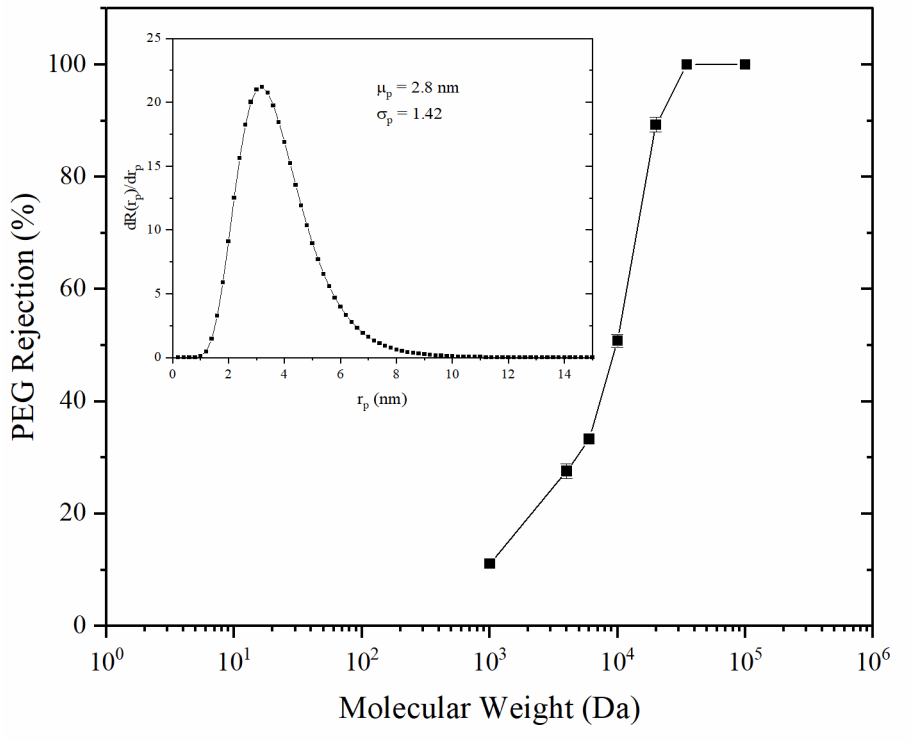

d) MQ_{HCMC}

Figure 3.8. Cont.

Table 3.2. Porosity, pore size and roughness of the pristine and CTAB modified membranes.

Membranes	Porosity, ε %	Pore radius (nm)	Ra (nm)	Rq (nm)
M0	43.1	3.21	4.99±0.17	6.35±0.29
MQ_{LCMC}	41.8	3.04	3.81±0.18	4.93±0.33
MQ_{CMC}	38.1	2.94	3.80±0.08	4.69±0.07
MQ_{HCMC}	35.8	2.79	4.40±0.72	5.43±0.96

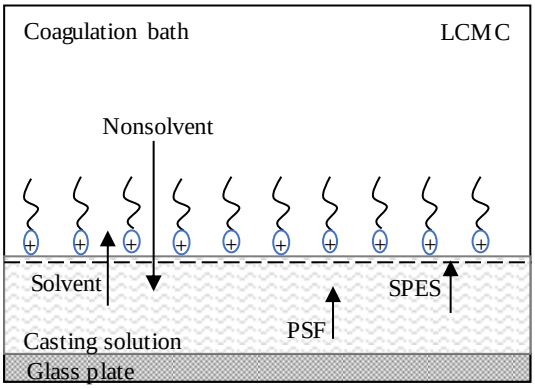

a) MQ_{LCMC}

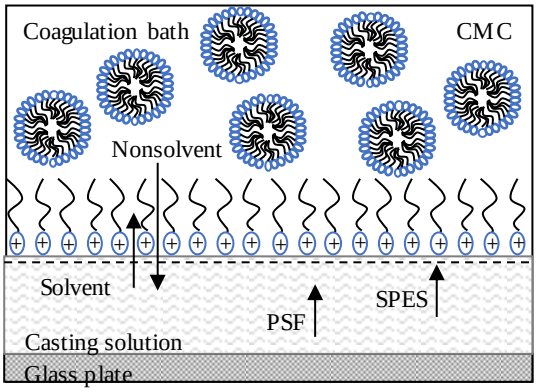

b) MQ_{CMC}

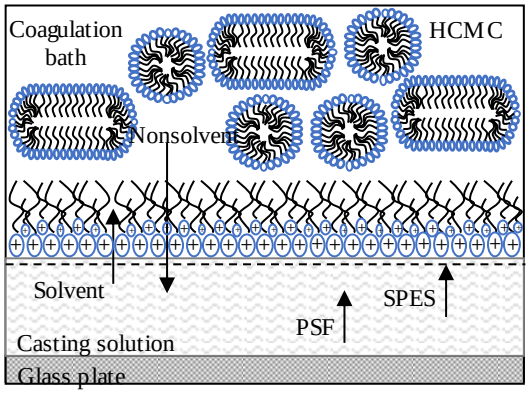

c) MQ_{HCMC}

Scheme 3.2. The effect of CTAB concentration in coagulation bath on the rate of exchange solvent/nonsolvent and accumulation of CTAB on the surface.

3.3.3. Antibacterial Activity Assessment of the Membranes

The antibacterial activities of the pristine and CTAB modified membranes were tested using Gram-negative (*E. coli*) and Gram-positive (*S. aureus*) bacteria. The pristine membrane did not inhibit the growth of bacteria. As shown in Table 3.3, the CTAB concentration below the CMC was insufficient to create a fully antibacterial surface (inhibition rate for *E coli* and *S. aureus* are 87.35% and 27.5%, respectively). On the other hand, the membranes prepared at (MQ_{CMC}) and above the CMC (MQ_{HCMC}) showed excellent growth inhibition both on *E. coli* and *S. aureus*. compared to the inhibition values reported in literature (Table 3.3).

The difference in the performance of the membranes listed in Table 3.3 can be explained by the method used for incorporating antibacterial agents. In previous studies, antibacterial agents were blended with polymers and distributed through the cross section (Yu et al., 2013a; Yu et al., 2013b; Wang et al., 2014), hence their surface concentration becomes insufficient. In our study, the active agent CTAB was added into the coagulation bath. During the coagulation step, the SPES selectively migrates to the interface due to its low surface energy. On the other hand, prior to phase inversion it is transported more slowly from the surface into the casting solution than the hydrophobic PSF (Hester et al., 1999). This results in surface enrichment of the hydrophilic SPES, hence, the accumulation of the CTAB at the surface due to electrostatic interaction between the CTAB and SPES (Scheme 3.1). To prove our hypothesis, XPS analysis was carried out at four different angles (0^o, 15^o, 30^o and 45^o) (Figure 3.9) to determine the near-surface composition of the membrane MQ_{CMC}. As illustrated in Table 3.4, % of nitrogen element which comes from the CTAB was found highest at 45^o. The analysis of the data collected at 45^o demonstrated that near-surface coverage of 68.7 wt.% is achieved with a very low CTAB concentration of 0.036 wt.% in the coagulation bath. The fraction of the CTAB at the surface is expected to be even higher, since the 45° take off angle used in the experiment takes into account contributions from a depth of 50 Å (Hester et al., 1999).

Table 3.3. Static antibacterial activity of the ultrafiltration membranes in the literature.

Membranes	Antibacterial agent / Polymer (wt/wt, %)	Bacteria concentration (CFU/mL)		Antibacterial rate (%)		Refs.
		E. coli	S. aureus	E. coli	S. aureus	
SiO_2@N-Halamine/PES	7.5	10^6	-	60.22	-	Yu et al., 2013a
HPEI-GO/PES	16.7	10^6	-	74.88	-	Yu et al., 2013b
PES/TPQP-Cl	25.0	-	-	76.00	-	Wang et al., 2014
Chitosan/BPPO	-	-	-	70.00	-	Feng et al., 2014
PDA-b-PBA	-	10^6	10^6	92.70	81.30	Wang et al., 2017c
PSF/P(H-M-A)	16.7	-	-	89.20	-	Xu et al., 2013
PVDF/N-Si-MWNTs	1.875	10^4	10^5	95.60	98.00	Huang et al., 2017
QPVC	-	-	-	74.20	-	Wu et al., 2018
GO-p-PES	-	10^5	-	80.00	-	Zhang et al., 2018b
PVDF/MWNTs-g-CDDAC	4.17	10^6	10^6	92.70	95.20	Kang et al., 2016
HNTs-CS@Ag/PES	3.0	10^6	10^6	94.00	92.60	Chen et al.,2013
MQ_{LCMC}	-			87.35	27.50	
MQ_{CMC}	3.1	10^6	10^6	95.78	100	This work
MQ_{HCMC}	-			99.84	100	

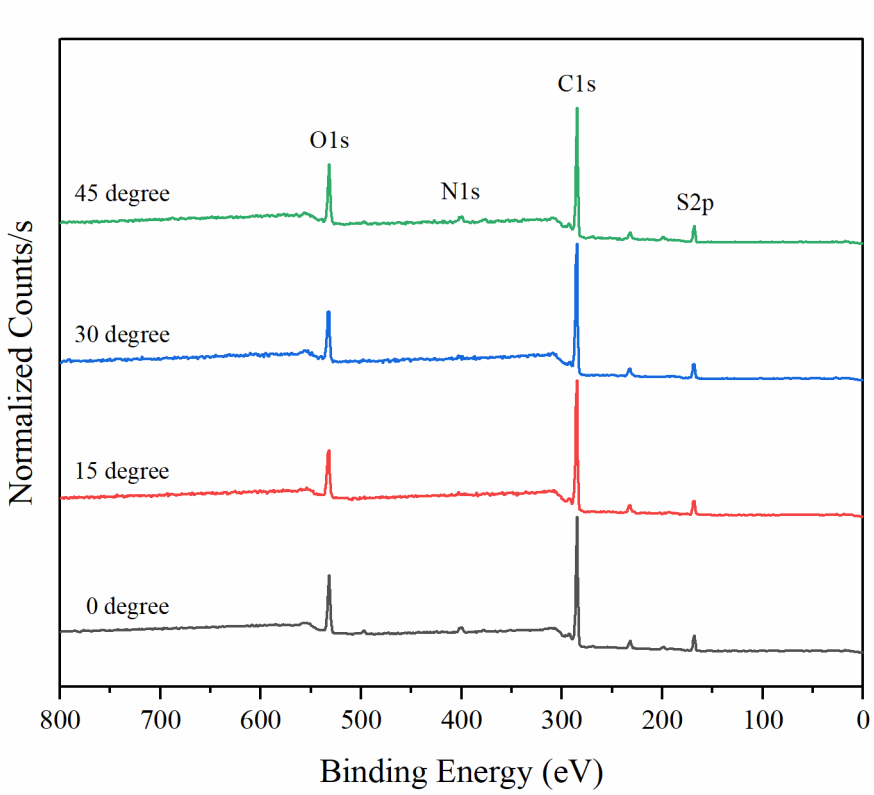

Figure 3.9. General XPS survey of the MQ_{CMC} membrane.

Table 3.4. Surface elemental composition (wt %) of the MQ_{CMC} membrane.

Angle (°)	Surface elemental composition (wt.%)				
	C1s	O1s	S2p	N1s	N/C
0	74.62	16.52	5.28	3.58	0.048
15	74.83	16.37	5.02	3.78	0.051
30	74.44	16.52	5.13	3.91	0.053
45	74.60	16.22	5.21	3.97	0.053

Based on XPS data Zhang et al. (2017b) reported QAC/PVDF ratio at the surface as 6.8% when QAC was blended into PVDF. They demonstrated that the rate of segregation of QAC to the surface can be increased by immobilizing it on a hydrophilic carbon material (QAC@Carbon). In this case QAC@Carbon/Polymer ratio was determined as 15.1% while in our case CTAB/Polymer ratio is 24.3%. These results clearly indicate the advantage of our approach in incorporating the QAC into the membranes. It should be noted that even though our membranes were prepared in a single step, they exhibited higher antibacterial performance than the thin film composite membranes (Feng et al., 2014; Wang et al., 2017c) where the antibacterial agent is located

on the surface in direct contact with the bacteria (Table 3.3). The superior performance can be attributed to both strong antibacterial activity of the CTAB and its sufficiently high concentration at the surface. Complexity of synthesis method used in previous studies for preparing the antibacterial agents renders these agents non-competitive candidates for manufacturing antibacterial membranes (Xu et al., 2015; Fei et al., 2018; Zhang et al., 2018a; Hu et al., 2016; Yu et al., 2013a; Yu et al., 2013b; Wang et al., 2014; Feng et al., 2014; Wu et al., 2018; Zhang et al., 2018b). In contrast, commercially available CTAB can be used without any need for modification leading to reduction in the cost of fabrication and the difficulty of scale up.

3.3.4. The Stability of the CTAB-Containing Membrane

The membrane prepared at the CMC showed the meaningful flux and antibacterial activity at the same time, consequently, was chosen as the optimum membrane. Leaching experiment was conducted to evaluate the stability of this membrane. For this purpose, first the incorporated CTAB concentration was determined using TGA analysis. As seen in Figure 3.10, single stage decomposition was observed for the CTAB below 400 ^{o}C (Zhang et al., 2017b) and the pristine membrane (M0) between 480 ^{o}C and 560 ^{o}C. On the other hand, the MQ_{CMC} membrane decomposed in two stages due to the loss of CTAB below 400 ^{o}C and the loss of the polymers, PSF and SPES, between 480 ^{o}C and 560 ^{o}C. Using the weight loss data for the CTAB and the MQ_{CMC}, the loading of CTAB to the membrane was determined as 3.1%. Figure 3.11 shows that the release of CTAB continued up to 7 days. At the end of 30 days of storage, a small amount of the CTAB around 4.2% leached from the membrane. This amount corresponds to the free CTAB which did not involve in electrostatic interaction. Zhang et al. (2017b) reported 30% and 2% losses for the CTAB and CTAB@Carbon composites, respectively from polyvinylidene fluoride (PVDF) membrane. They increased the stability of the CTAB by immobilizing it on a carbon support using harsh chemicals and conditions. In our work, the CTAB-containing membrane was prepared in a single step, but it was made long-term stable through strong electrostatic interaction between positively charged quaternary ammonium group in CTAB and negatively charged sulfonic acid group in PSF-SPES (Scheme 3.1).

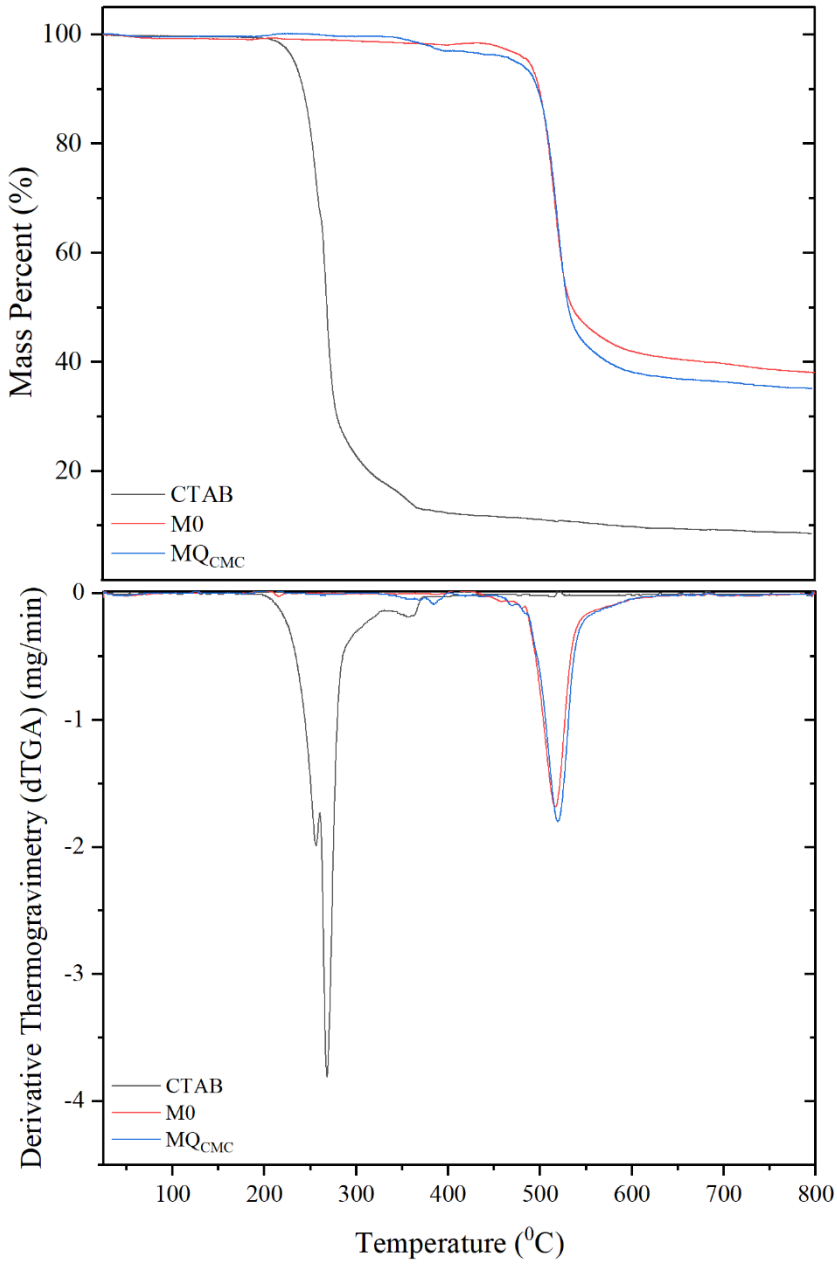

Figure 3.10. TGA and dTG analysis of pure CTAB, M0 and MQ_{CMC} membranes as a function of temperature.

The strength of the electrostatic binding of the CTAB to SPES was evaluated by storing the membranes in 1 M NaCl solution up to 1 month and by filtering the 1 M NaCl through the membrane. As shown in Figure 3.12, the MQ_{CMC} membranes at the end of static storage in NaCl solution or dynamic filtration of NaCl solution showed the same antibacterial activity as compared to their fresh counterparts. The results proved strong electrostatic interaction between the CTAB and SPES since at high salt concentrations in solution, the screening effect of salt ions can easily destroy weak electrostatic bond.

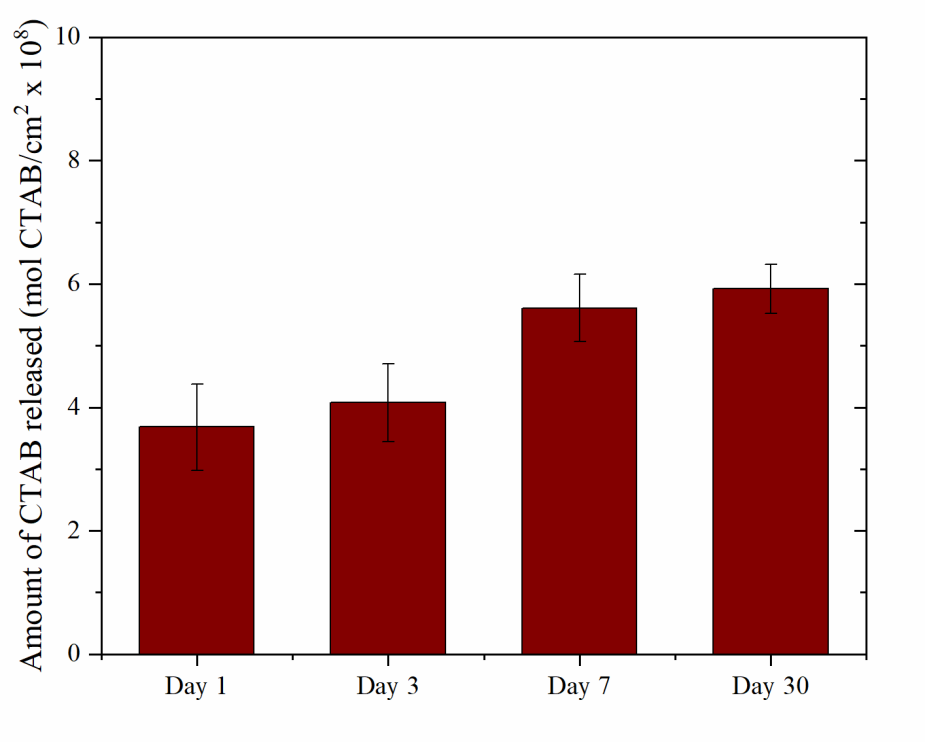

Figure 3.11. CTAB release from the MQ_{CMC} membrane as a function of time.

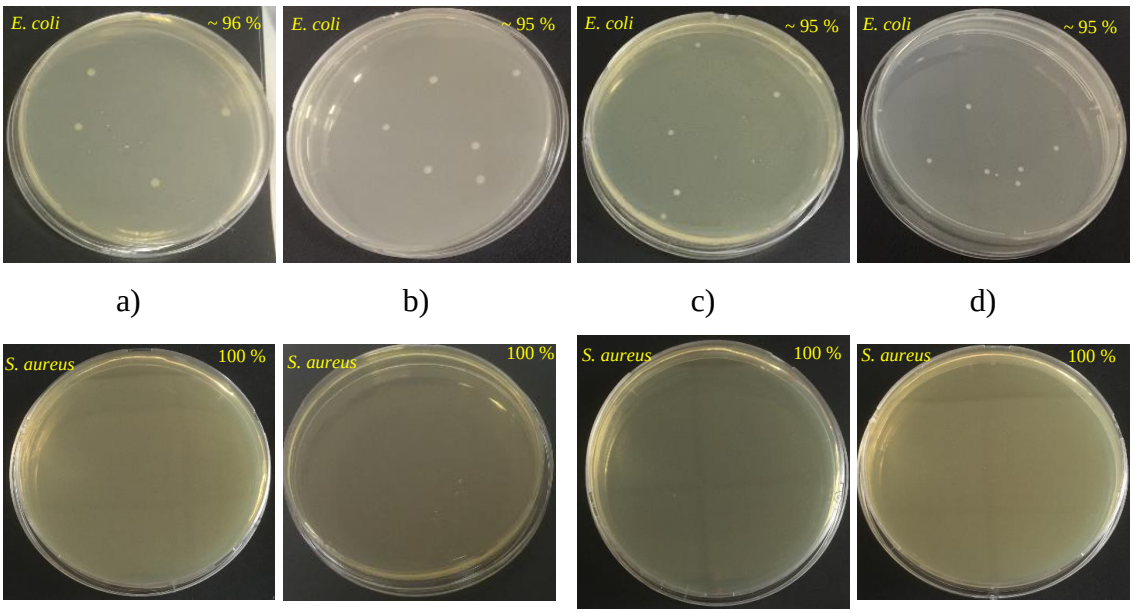

Figure 3.12. Bactericidal rates of the (a,e) fresh MQ_{CMC} membrane (b,f) the MQ_{CMC} membrane exposed to 1 M NaCl for two weeks (c,g) the MQ_{CMC} membrane exposed to 1 M NaCl for 1 month (d,h) the MQ_{CMC} membrane after filtration of 1 L of 1 M NaCl solution.

3.3.5. Antibiofouling Assessment

The antibiofouling properties of the pristine (M0) and MQ_{CMC} membranes were evaluated using dead-end cell filtration system with two model bacteria suspensions. The initial water flux of the membranes was adjusted to the similar value by controlling transmembrane pressure difference (TMP). As shown in Figures 3.13 and 3.14, the initial flux of the pristine membrane decreased sharply since the bacteria instantaneously deposited on the membrane surface. Following the initial stage, the flux continued to decrease linearly indicating the growth of the biofilm thickness over time. However, a sharp flux decline was not recorded for the MQ_{CMC} membrane at the initial stage of the filtration. The results in Table 3.5 show that the MQ_{CMC} membrane demonstrated almost 100% flux recoveries following 10 min rinsing with PBS solution after filtration. On the other hand, flux recoveries for the pristine membrane were determined to be 58.3% and 67.4% at the end of *E. coli* and *S. aureus* filtrations. The results indicate that fouling on the surface of the MQ_{CMC} was due to accumulation of dead bacteria, thus, this fouling was reversible and easily removed with simple rinsing. SEM images in Figure 3.15 show that many bacteria attached on the surface of the pristine membrane, by contrast, only a few bacteria were observed on the MQ_{CMC}. Myint et al. (2010) showed that the roughness and hydrophobicity are important surface properties in determining initial cell adhesion, aggregation and colony formation. Among four nanofiltration membranes investigated, the greatest cell deposition was observed for a membrane which had the most hydrophobic and roughest surface. Our results suggest that in the presence of a strong antibacterial agent on the surface, biofilm formation is not influenced by the roughness, hydrophobicity or surface charge. Although the MQ_{CMC} is more hydrophobic and less negatively charged than the pristine membrane, much higher flux recovery recorded for this membrane is due to its excellent antibacterial activity. The CTAB, mostly accumulated on the surface as confirmed by the XPS analysis (Table 3.4), reduced bacterial attachment by inactivating bacteria through contact. Table 3.6 compares the antibiofouling performance of our membrane with that of other ultrafiltration membranes. Previous studies reported a slightly lower flux decline at the end of *E. coli* filtration. However, in these studies a lower bacteria concentration was filtered in a crossflow filtration unit. For comparison, Hou et al. (2017) filtered $4.2x10^4$ CFU/cm^2 *E. coli* and at the end of filtration they recovered only half of the initial flux (FRR: 58%) after 3 times

of washing with water. On the contrary, in our study, the flux recovery was almost 100% although we filtered 100 times more concentrated *E. coli* in a dead-end filtration unit. Compared to a cross flow filtration mode, fouling/biofouling occurs at a higher rate in a dead-end filtration unit.

Table 3.5. Flux recovery ratio and biofouling resistances of the membranes.

Membranes	E. coli				S. aureus			
	R_{rev} (%)	R_{irrev} (%)	R_{total} (%)	FRR (%)	R_{rev} (%)	R_{irrev} (%)	R_{total} (%)	FRR (%)
M0	4.1	41.7	42.2	58.3	7.2	32.6	39.8	67.4
MQ_{CMC}	22.7	2.4	25.1	97.6	18.8	7.3	25.9	92.7

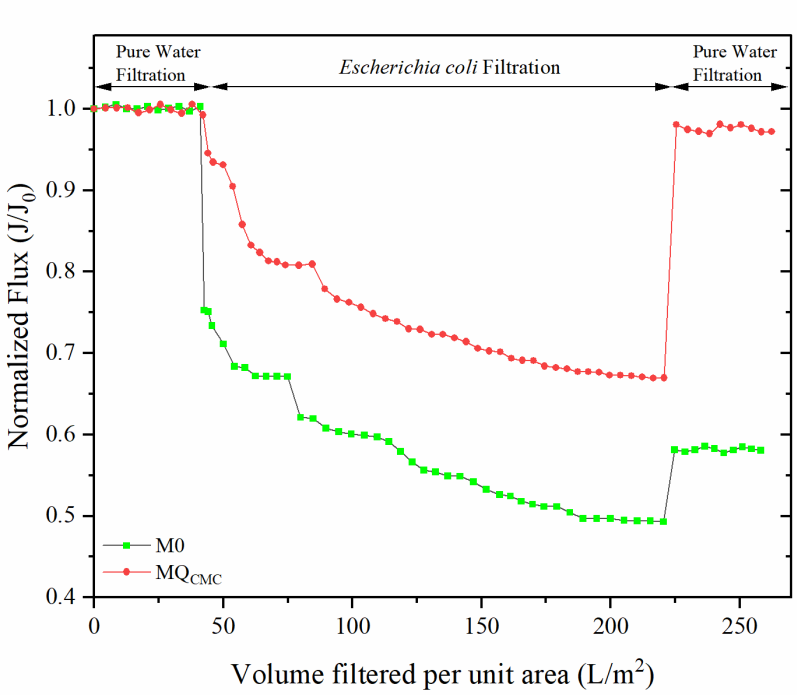

Figure 3.13. Normalized flux of the M0 and MQ_{CMC} membranes as a function of volume filtered per unit area during *E. coli* filtration. Initial water fluxes of M0 and MQ_{CMC} membranes are 185±3.5 and 95±2.3 L/m^2hbar, respectively. Transmembrane pressures (TMP) applied for the filtration with M0 and MQ_{CMC} membranes are 0.5 and 1.0 bar, respectively.

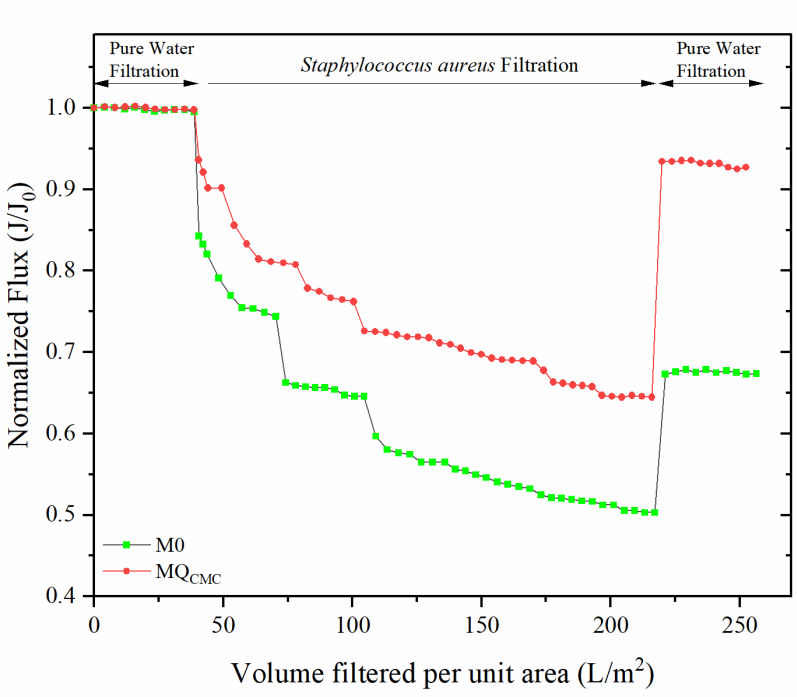

Figure 3.14. Normalized flux of the M0 and MQ_{CMC} membranes as a function of volume filtered per unit area during *S. aureus* filtration. Initial water fluxes of M0 and MQ_{CMC} membranes are 185±3.5 and 95±2.3 L/m^{2}hbar, respectively. Transmembrane pressures (TMP) applied for the filtration with M0 and MQ_{CMC} membranes are 0.5 and 1.0 bar, respectively.

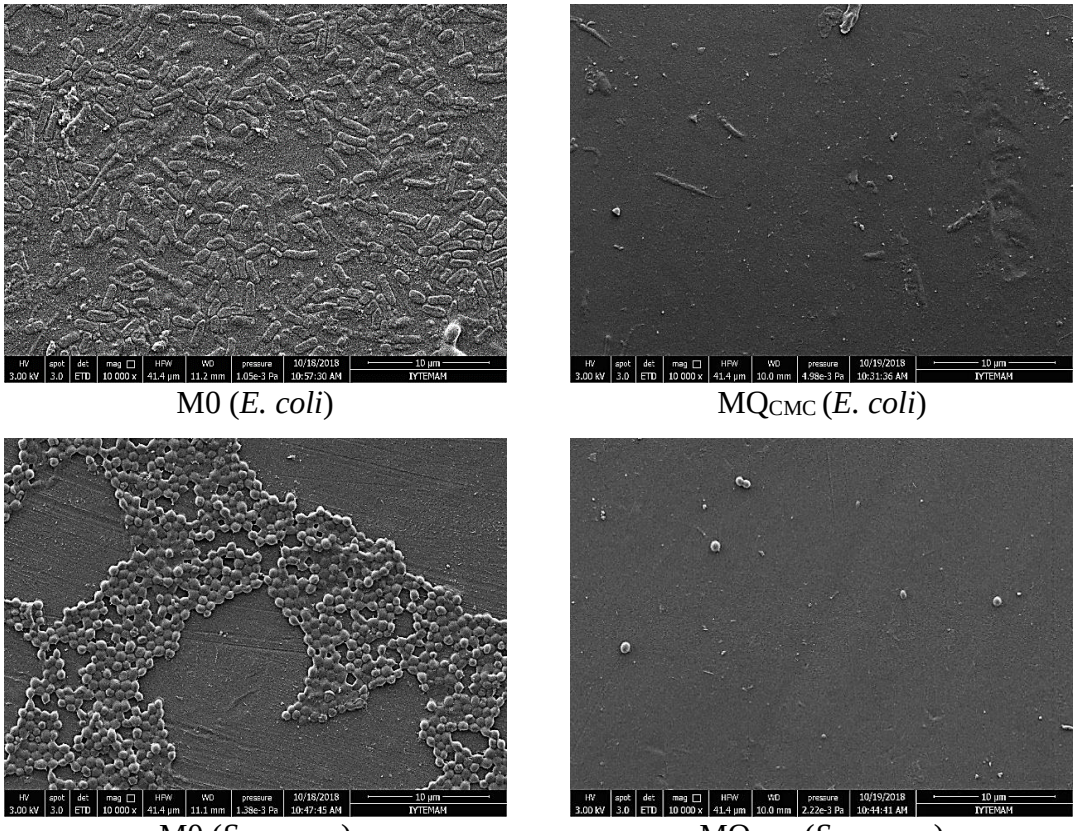

M0 (*E. coli*) MQ_{CMC} (*E. coli*)

M0 (*S. aureus*) MQ_{CMC} (*S. aureus*)

Figure 3.15. SEM images of the M0 and MQ_{CMC} membranes after bacteria filtration.

Table 3.6. Antibiofouling performance of the membranes in the literature.

Membranes	Flow mode	Bacteria concentration (CFU/cm^2)		Flux decline after bacteria filtration (%)		Washing procedure	Flux recovery ratio, FRR (%)		Refs.
		E. coli	S. aureus	E. coli	S. aureus		E. coli	S. aureus	
GO-p-PES	Cross flow	4.8 x 10^5	-	~ 25.0	-	-	-	-	Zhang et al., 2018b
GOQDs-PVDF	Cross flow	~ 1.9 x 10^5	-	24.3	-	-	-	-	Zeng et al., 2016
HPEI-GO/PES	Cross flow	~ 4.5 x 10^4	-	~ 23.0	-	-	-	-	Yu et al., 2013b
PEK-N-Cl	Cross flow	~ 4.2 x 10^4	-	-	-	Pure water (three times)	58.0	-	Hou et al., 2017
MQ	Dead-end	-	~ 2.6 x 10^5	-	~ 50.0	-	-	-	Ping et al., 2019
MQ_{CMC}	Dead-end	~ 9.3 x 10^6	~ 1.2 x 10^7	~ 33.0	~ 36.0	Deionized water (rinsing 10 min)	97.6	92.3	This work

3.4. Conclusion

In this study, a facile approach is proposed for the fabrication of PSF-SPES blend antibacterial ultrafiltration membranes. The method is based on adding a positively charged quaternary ammonium compound, CTAB, in the gelation medium which makes electrostatic interaction with the SPES mostly at the polymer/bath interface. The presence of CTAB in the membranes was verified by ATR-FTIR and XPS measurements. Compared to the pristine membrane, the CTAB-containing membranes displayed lower hydrophilicity, pure water permeability, MWCO and less negative charge. The membrane prepared at the CMC showed the meaningful flux and antibacterial activity simultaneously, consequently, was chosen as the optimum membrane. This membrane had much higher FRR than the pristine membrane following bacteria filtration and rinsing with PBS solution. In addition, the stability of the CTAB in this membrane was proved with leaching experiments and antibacterial activity measurements conducted after storing the membrane in 1 M NaCl up to 1 month and filtering 1 M NaCl solution.

The key advantages of the membrane developed in this study are the single step preparation using commercially available polymers and antibacterial agent without any need for pre-treatment or post treatment of either the membrane or antibacterial agent and its high antibacterial activity. The facile route proposed in this study can be applied using other polymers and antibacterial agents. The prerequisite for the polymer and antibacterial agent is that they should have functional groups such as hydroxyl, carboxyl, amine and sulfonic groups. In addition to CTAB, electrolytes, other surfactants and antibacterial components can also be used in the coagulation bath as long as they are soluble in water. Although the main driving force used in our study to form a stable long-term interaction between the polymer and the antibacterial agent was electrostatic, other type of strong interactions such as covalent bond can also be utilized. It should also be noted that compositions of both casting solution and coagulation bath should be adjusted in such a way that diffusion rates of the polymer and active agent should be comparable so that most of the interaction between them occurs at the interface.

Overall, the successful preparation of an antibacterial membrane through coagulation in CTAB-containing bath opens opportunities for further investigation in water and wastewater treatment. The stability, high antibiofouling properties and ease of manufacturing make our membrane a potential candidate for these applications. Unlike

coating and grafting methods, the facile route proposed in this study can be easily scaled-up to fabricate antibacterial ultrafiltration membranes from commercially available polymers and antibacterial agents without requiring pre- or post-treatment steps.

CHAPTER 4

DEVELOPMENT OF BIOFOULING-RESISTANT ULTRAFILTRATION MEMBRANES WITH RETAINED SIZE SELECTIVITY AND WATER FLUX

4.1. Introduction

Biofouling, caused by the attachment of living microorganisms, such as bacteria and algae, is a serious issue in membrane technology. Unlike other types of foulants, living microorganisms grow rapidly and form a cohesive biofilm on the membrane surface in a short period of time (Madaeni, 1999). In industrial-scale applications, ultrafiltration (UF) and microfiltration (MF) membranes made of polysulfone (PSF), polyethersulfone (PES) and polyvinylidene fluoride (PVDF), are widely used to remove bacteria and algae based on the size exclusion mechanism with low energy requirements (Lovins et al., 2002; Arkhangelsky and Gitis, 2008). These membranes have a high propensity to fouling due to the lack of antibacterial and hydrophilic groups in their structure. The fouling makes the treatment costly due to higher operating pressure, frequent cleaning with harsh chemicals, hence, eventually replacement of the membranes. Surface modification is considered a feasible strategy to increase the fouling resistance of the commercial membranes (Kochkodan and Hilal, 2015). Several research groups used antimicrobial polymers (Munoz-Bonilla and Fernandez-Garcia, 2012), quaternary ammonium compounds (QAC) (Kaur and Liu, 2016), and zwitterionic polymers (Guo et al., 2020) to create antibacterial and antifouling surfaces via surface-initiating polymerization (Krishnamoorthy et al., 2014), grafting (Yang et al 2010), mussel-inspired chemistry (Faure et al., 2013) and layer-by-layer assembling (Chen et al., 2015). Among the techniques mentioned, in the last decades, mussel-inspired polydopamine has attracted great interest in membrane modification due to its material-independent surface functionalizing capability, and presence of catechol and amine groups that make the surface hydrophilic and enable further modifications (Lee et al., 2007). A pure polydopamine (PDA) layer increased fouling resistance against organic foulants, such as oil emulsions (McCloskey et al., 2012) and bovine serum albumin (BSA) (McCloskey et

al., 2010), but, demonstrated limited antibacterial activity to Gram-positive and Gram-negative bacteria (Chang et al., 2016; Kolewe et al., 2018). Therefore, many researchers used the bio-inspired "glue" to co-deposit it with additional antifouling molecules, such as zwitterions (Chang et al., 2016; Yao et al., 2019), reduced graphene oxide-copper nanocomposites (Zhu et al., 2017) to produce (bio)fouling resistant membranes and hydrogels (Kolewe et al., 2018) using a one-step process. Although the prepared membranes demonstrated enhanced hydrophilicity and good antibacterial activity, significant flux decline observed due to the penetration of monomers into the porous support is still a significant challenge (Yao et al., 2019). To mitigate the solution intrusion phenomenon, an interlayer from cellulose nanocrystals (CNC) (Wang et al., 2017d), carbon nanotube (Zhou et al., 2018), polydopamine wrapped carbon nanotube (Zhu et al., 2016c) and cadmium hydroxide ($Cd(OH)_2$) nanowire (Karan et al., 2015) were applied on the porous MF and UF supports before interfacial polymerization. Both the $Cd(OH)_2$ nanowires and the carbon nanotubes are toxic to the environment. Although the CNC is nontoxic, its production is not environmentally friendly due to highly concentric acid solution needed for the hydrolysis of cellulose. Recently, Dobosz et al. (2019) developed a method to modify the surface of ultrafiltration membranes. The method shortened as PolyPrev (the polymer prevention system) is based on creating an inert physical barrier by backfilling the pores from the porous side of the membrane with N_2 gas. This strategy enabled pure PDA modified UF membranes to retain the same flux and pore size as the unmodified membranes. The membrane functionalized with PDA alone was almost completely covered with *E coli* after 24 h incubation. The co-deposition of polyMPC with PDA significantly reduced the number of *E coli* attached to the surface. However, the enhanced biofouling resistance was obtained at the expense of the significant reduction in support's flux. The polyMPC membranes prepared in the presence and in the absence of N_2 backflow exhibited a statistically equivalent pure water flux. The benefit of backflow disappeared due to use of high molecular weight polyMPC resulting in a thick selective layer. It is still thus necessary to develop new surface modification protocols to create a biofouling resistant layer as thin as possible without sacrificing the permeability of the support.

Different from traditional polymer or nanoparticle based agents, in this study, we propose to co-deposit a low molecular weight surfactant, cetyltrimethylammonium bromide (CTAB, MW: 365 Da), with polydopamine. CTAB was chosen mainly due to its small size, commercial availability, low cost and strong antibacterial activity against

Gram-positive and Gram-negative bacteria. Also, it can be directly added into the dopamine solution without requiring any functionalization. The effect of the CTAB concentration on the biofouling resistance of the coated membranes was investigated via dynamic Gram-positive (*S. aureus*) and Gram-negative (*E. coli*) bacteria suspensions filtration. We hypothesize that the co-deposition of a low molecular weight, strong antibacterial agent with dopamine under N_2 backflow can produce a thin coating without changing the flux. To the best of our knowledge, this study is the first that developed biofouling resistant UF PES membrane through a one-step co-deposition of CTAB with dopamine.

4.2. Materials and Method

4.2.1. Materials

Dopamine hydrochloride, tris hydrochloride buffer and sodium hydroxide were purchased from Sigma-Aldrich. Cetyltrimethylammonium bromide (CTAB, MW: 365 Da) was supplied from Alfa Aesar and used as an antibacterial agent. Phosphate Buffered Saline (PBS), used for the preparation of bacteria suspensions and rinsing the membrane after bacteria filtration, sodium chloride (NaCl), used for testing long-term stability of the membrane, and isopropyl alcohol (IPA), used for membrane treatment were obtained from Sigma-Aldrich. Sodium hydroxide (NaOH) and hydrochloric acid (HCl) with 37% purity used for pH adjustment were purchased from Sigma Aldrich and Merck, respectively. Gram-negative (*Escherichia coli*, ATCC 25922) and Gram-positive (*Staphylococcus aureus*, RSKK 1009) bacteria were used in the preparation of model suspensions for antibiofouling tests. The commercial polyethersulfone (PES) ultrafiltration support membrane (NADIR® PM UP150) with a reported nominal molecular-weight limit of 150 kDa was supplied by MicroDyne Nadir. Deionized water with a conductivity of 0.05 μS/cm was used for the experiments. All chemicals were used as received without further purification.

4.2.2. Modification of Membranes

4.2.2.1. Modification of Membranes with Polydopamine

Before using commercial membrane coupons as support, they were pretreated by immersing first into 25% (v/v) IPA solution for 1 h, followed by overnight storage in deionized water. The pre-treated membrane coupons were placed in a custom-designed coating device (Scheme 4.1) that limits coating to only one side (active side) of the membrane. Next, the reaction solution (50 mL), consisting of dopamine hydrochloride (2 mg/mL) dissolved in Tris-HCl buffer solution (10 mM, pH 8.5) at room (25 ^{o}C) temperature, was poured on the active side of the membrane and stirred gently at 100 rpm. In the conventional polymerization system, there was no nitrogen (N_2) backflow (Scheme 4.1a). In contrast, in the PolyPrev polymerization system, the N_2 was continuously fed at 0.3 bar during the polymerization to prevent the diffusion of the molecules into the pores (Scheme 4.1b). The polymerization was carried out at room (25 ^{o}C) temperature for 1 h. The membranes modified by the conventional and PolyPrev polymerization systems were labelled as PES_PDA$_{\text{Conv Poly}}$ and PES_PDA$_{\text{PolyPrev Poly}}$, respectively.

4.2.2.2. Modification of Membranes with Co-deposition

The co-deposition reaction solution was prepared by dissolving CTAB in the dopamine solution at room (25 ^{o}C) temperature. The CTAB concentration was adjust to 10^{-4} M (low critical micelle concentration (CTAB$_{LCMC}$)), 10^{-3} M (critical micelle concentration (CTAB$_{CMC}$)), 10^{-2} M (high critical micelle concentration (CTAB$_{HCMC}$)) and resulting membranes were coded as PES_PDA+CTAB$_{LCMC}$, PES_PDA+CTAB$_{CMC}$, PES_PDA+CTAB$_{HCMC}$, respectively. All membranes were co-deposited by applying a 100 rpm shaking rate at room (25 ^{o}C) temperature for 1 h in the presence of nitrogen backflow (0.3 bar). The support membrane was exposed to the same pretreatment protocol explained in Section 2.2.1.

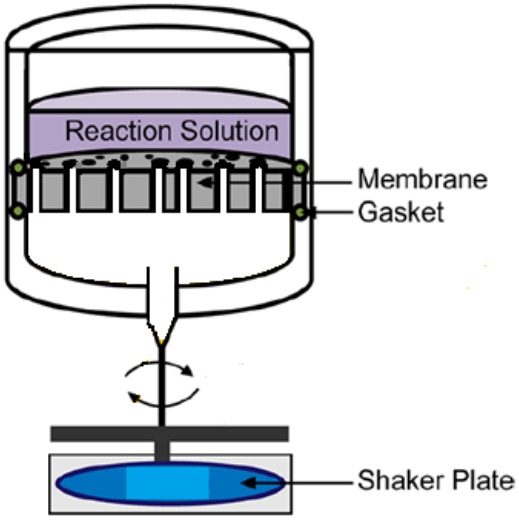

a)

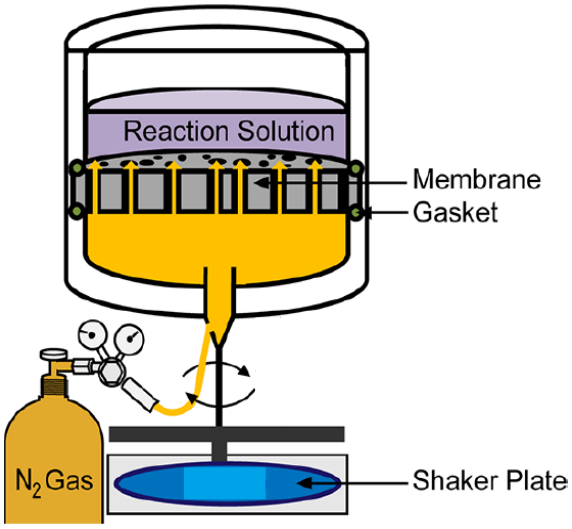

b)

Scheme 4.1. a) Conventional polymerization system, b) PolyPrev polymerization system (Reprinted with permission from Dobosz et al (2019), Copyright (2019) American Chemical Society).

4.2.3. Membrane Filtration Performance

Pure water permeability of the support and modified membranes was determined using a 200 mL dead-end stirred cell (Millipore, Amicon Stirred Cell UFSC20001) with an effective area of 28.7 cm^2. Before any filtration test, first, membrane coupons were compacted at 1 bar using pure water until the flux was stable. Next, pure water was filtered at 0.5 bar and collected permeate volume was recorded for specific time intervals. The volumetric flux was calculated from the slope of the permeate volume vs. time graph and converted to hydraulic pure water permeability (PWP) using following equation:

$$PWP = \frac{\Delta V}{A \Delta t \Delta P} \quad (1)$$

where ΔV is the volume of permeated water (L), A (m^2) is the membrane area, Δt (h) is the permeation time and ΔP (bar) is the transmembrane pressure difference applied through the membrane (n=3 where n is the number of repeated experiments).

4.2.4. Membrane Characterization

The structure and elemental composition of the membranes were determined using X-ray photoelectron spectra (XPS) (Thermo Scientific) at the emission angles of 0° (n=3). The surface zeta potential measurement (NanoPlus Micromeritics Instrument) of the membranes was carried out with the 10^{-2} M NaCl electrolyte solution (n=3). The pH of the electrolyte solution was adjusted using HCl acid and NaOH. The membrane size used in the measurements was 16 mm x 37 mm. The surface hydrophilicity of the membranes was determined with the contact angle measurements (Attension Optical Tensiometer) using a 5 μL deionized water droplet (n=5). The surface morphology of the membranes was characterized using a scanning electron microscope (SEM) (FEI Quanta 250 FEG). Gold nanoparticles were coated on the membrane surface with a Magnetron Sputter Coating Instrument before taking SEM images The surface roughness of the membranes (arithmetic mean (Ra) and root-mean-square (Rq)) was determined using an atomic force microscope (AFM) (MMSPM Nanoscope 8, Bruker). 5 × 5 μm^2 sample area was scanned at a rate of 1 Hz using tapping mode in the air at room temperature by the TAP150 model tip (Bruker) (n=3). Before XPS, SEM, AFM, and contact angle

measurements, all membrane coupons were dried in a vacuum oven overnight at room (25 ^{o}C) temperature. The thickness of the pure PDA and co-deposited layers was measured using a reflectometer system (Mprobe-Vis20) with a spectral range of 400-1100 nm. To this end, crystalline silicon wafers (c-Si) were immersed in the pure PDA and co-deposition solution for 24 h and 72 h, and the coating was carried out at a 100 rpm shaking rate (n=3). (*n* is the number of repeated experiments)

4.2.5. Analysis of Antibiofouling Performance

Bacteria antibiofouling tests were conducted as previously reported (Cihanoğlu and Altinkaya, 2020). The biofouling potential of the support and modified membranes were determined by dynamic filtration of model *E. coli* and *S. aureus* bacteria suspensions in a dead-end cell filtration system with a cell volume of 50 mL and an effective surface area of 13.4 cm^2 (Millipore, Amicon Stirred Cell 8050). Before bacteria filtration, membrane coupons were sterilized with UV light for 20 min (10 min per 13.4 cm^2 surface area). *E. coli* and *S. aureus* bacteria suspensions were prepared in PBS (pH 7.4) to reach concentrations of $1.75x10^8$ and $2.1x10^8$ CFU/mL, respectively. 250 mL bacteria suspensions were filtered through support and modified membranes where the initial fluxes of the membranes were adjusted to the same values. Following filtration, the membrane coupons were rinsed with PBS for 10 min and water flux was re-measured to calculate the flux recovery ratio (FRR).

$$FRR(\%) = \left(\frac{J_R}{J_W}\right) x100 \qquad (2)$$

where J_W is the pure water flux of the clean membrane, and J_R is the pure water flux of the washed membrane. The experiments were carried out at room (25 ^{o}C) temperature.

4.2.6. Stability Test

The co-deposited membrane demonstrated the highest biofouling resistance was chosen for the stability test. To this end, the membrane was stored in a 1 M NaCl solution for 3 months under the static condition at 25 ^{o}C. The surface zeta potential of the stored membrane was measured to compare with the zeta potential of the fresh membrane.

4.3. Results and Discussion

4.3.1. Performance and Characteristics of PDA Coated Membranes

It is known in the literature that the conventional dopamine polymerization on the porous supports results in a serious flux reduction due to the solution intrusion phenomenon causing pore narrowing (Kasemset et al., 2017). To prevent the diffusion of dopamine and the CTAB into pores, we created an inert physical barrier inside the pores with continuous backflow of nitrogen gas (N_2) during polymerization (Scheme 4.1). The commercial PES UF membrane with a tradename of PM UP150 (Germany) was chosen as a support since its commonly used for membrane bioreactor (MBR) applications, thus, improving its biofouling resistance is critical to reduce the cost of treatment. We found that the membrane modified with the conventional polymerization had a lower flux than the unmodified membrane while the coating formed with N_2 flow did not decrease the permeability of the PES support (Figure 4.1a). Figures 4.1b and 4.1c show digital images were taken from the dense side of the membrane (front-side) which was in contact with dopamine solution and from the porous side of the support (backside). The backside of the membrane modified with N_2 backflow remained white (Figure 4.1c), while, in the absence of gas flow it was brown colored (Figure 4.1b) which demonstrated that the polymerization took place also inside the pores. Both the permeability results and the visual images proved that the N_2 gas flow prevented the pore penetration of monomer. The images showed a less intense brown colour on the PES_PDA$_{\text{PolyPrev Poly}}$ membrane corresponding to the lower polymerization rate. This observation can be explained by the reduced dissolved oxygen concentration in the presence of N_2 backflow where the dissolved oxygen and alkaline environment are essential requirements for dopamine polymerization (Dobosz et al., 2019).

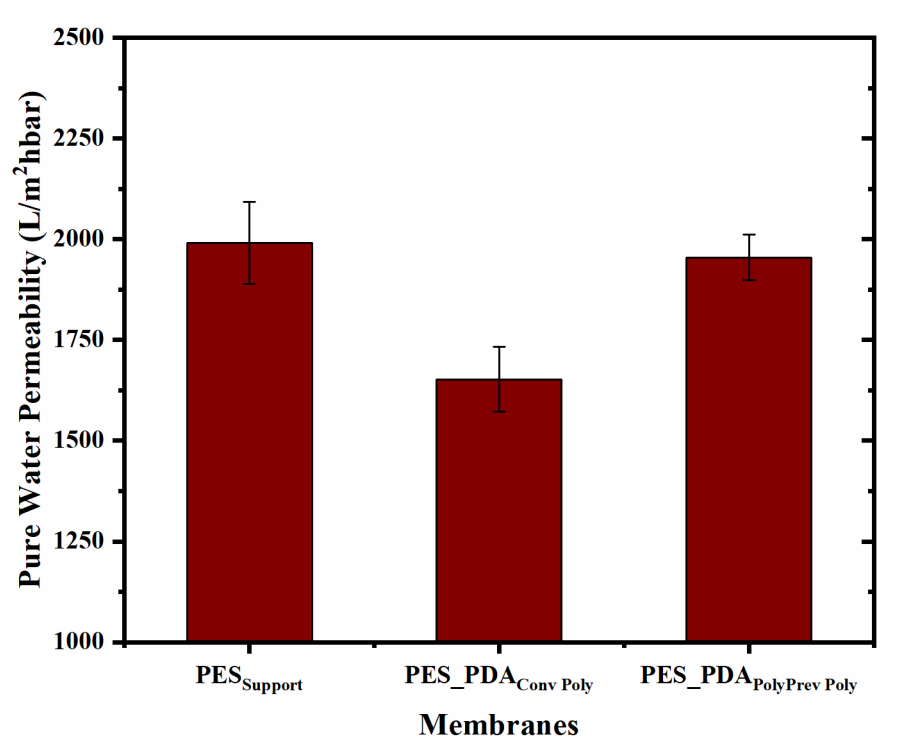

a)

Frontside Backside Backside without O-ring

b)

Frontside Backside Backside without O-ring

c)

Figure 4.1. a) PWP of the membranes. The front and backside images of the b) PES_PDA$_{\text{Conv Poly}}$, c) PES_PDA$_{\text{PolyPrev Poly}}$ membranes.

The surface chemistry of the membranes was analysed by XPS, and the results were given in Table 4.1 and Figure 4.2. Nitrogen and sulfur signals are the characteristic indicators for the PDA and PES, respectively. The nitrogen signal in the unmodified PES membrane comes from the pore former, polyvinyl pyrrolidone, in its structure (Oymaci et al., 2020). The nitrogen atomic percentage increased for both PDA coated membranes, while the sulfur percentage decreased, as expected. The PES_PDA$_{\text{PolyPrev Poly}}$ membrane had a lower N/S ratio which indicated thinner PDA layer formed on the support. This result was found in agreement with the less intense colour observed in the digital image taken from the active side of this membrane (front side) (Figure 4.1c).

Table 4.1. Surface elemental composition (wt%) of support and PDA coated membranes.

Membranes	C (%)	O (%)	S (%)	N (%)	N/S
PES$_{\text{Support}}$	74.17	17.31	6.51	2.01	0.31
PES_PDA$_{\text{Conv Poly}}$	73.73	18.18	4.67	3.42	0.73
PES_PDA$_{\text{PolyPrev Poly}}$	74.43	17.43	5.39	2.75	0.51

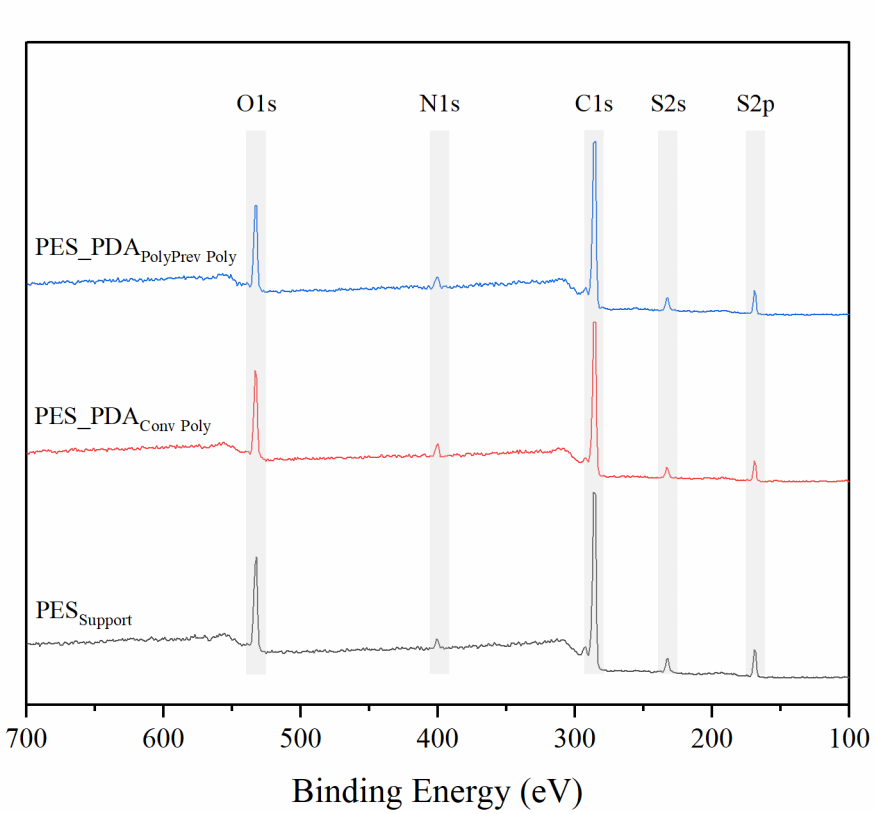

Figure 4.2. General XPS survey of the membranes.

The effect of PDA coating on the surface charge of the support membrane was determined at three different pH values (Figure 4.3). The unmodified PES membrane is negatively charged due to the presence of sulfone groups in its structure (Breite et al., 2016). The protonation of amine groups existing in the PDA structure resulted in a decrease in the negative charge of the support (Liu et al., 2011; Liebscher, 2019). At pH 5.5 and 7.5, the PES_PDA$_{\text{Conv Poly}}$ membrane was more protonated due to presence of more nitrogen atoms on its surface as determined with the XPS analysis (Table 4.1).

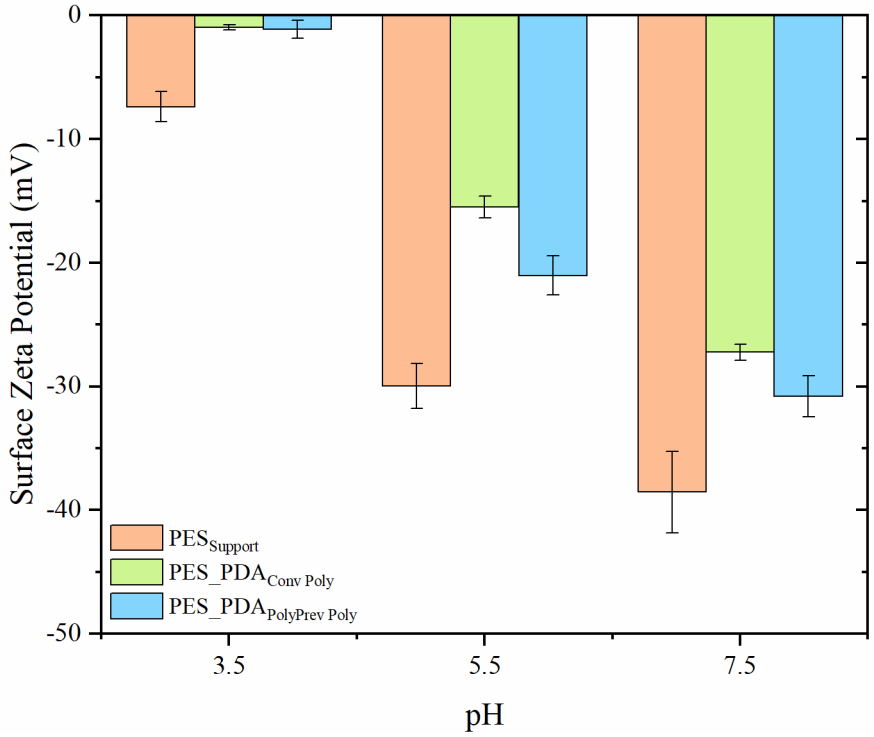

Figure 4.3. Surface Zeta Potential of the support and PDA coated membranes.

The PES support had a water contact angle of 61.4±3.7º, consistent with the literature on other commercial PES UF membranes (Dobosz et al., 2019; Kaner et al., 2015; Weinman et al., 2018). After modification with the PDA layer, water contact angle values decreased. The PDA layer formed with conventional and PolyPrev polymerization systems improved the hydrophilicity of the support at the same level (PES_PDA$_{\text{Conv Poly}}$ membrane: 44.4±2.4º and the PES_PDA$_{\text{PolyPrev Poly}}$ membrane: 46.7±1.9º). The SEM images were taken at two different magnifications (25kX and 100kX) and analyzed to determine surface morphologies and pore size of the membranes (Figure 4.4). The PDA coating without N_2 flow reduced pore diameter from 27.8±4.3 nm to 18.9±1.8 nm. On the other hand, the average pore diameter of the PES_PDA$_{\text{PolyPrev Poly}}$ membrane (26.4±4.1

nm) was statistically the same as the support membrane ($PES_{Support}$) (27.8±4.3 nm). This result also proved the benefit of N_2 backflow in preventing the polymerization in the pores. The surface morphology of the support membrane changed after being coated with PDA. As seen in Figure 4.4, the PDA coating formed with conventional method (no N_2 flow) was made of some aggregates. Depending on the dopamine concentration and reaction temperature, in the conventional dopamine polymerization, formation of aggregates is an inevitable fact (Oymaci et al., 2020). Vecchia et al. (2014) reported that dopamine begins forming oligomers at the beginning of polymerization, and the formed oligomers create seeds for growing PDA aggregates throughout the polymerization. Continuous N_2 backflow during polymerization creates a flow regime between the solid-liquid interface which disturbs aggregate formation on the membrane surface. As a result, no PDA aggregates were observed on the PES_$PDA_{PolyPrev\ Poly}$ membrane. The AFM results given in Figure 4.5 and Table 4.2 showed that the PDA coating increased the surface roughness of the PES membrane. The dopamine polymerization with the N_2 backflow resulted in a slightly higher surface roughness than the conventional polymerization without gas flow.

An ideal surface modification technique should enhance the surface properties such as hydrophilicity without changing the permeability and selectivity of the membrane. In this respect, the results suggest that the protocol based on 1 h dopamine polymerization with N_2 backflow is promising to co-deposit the antibacterial agent. In the following section, the results on the characterization and biofouling resistance of the PES membrane modified with the PDA and CTAB co-deposition under N_2 flow will be presented.

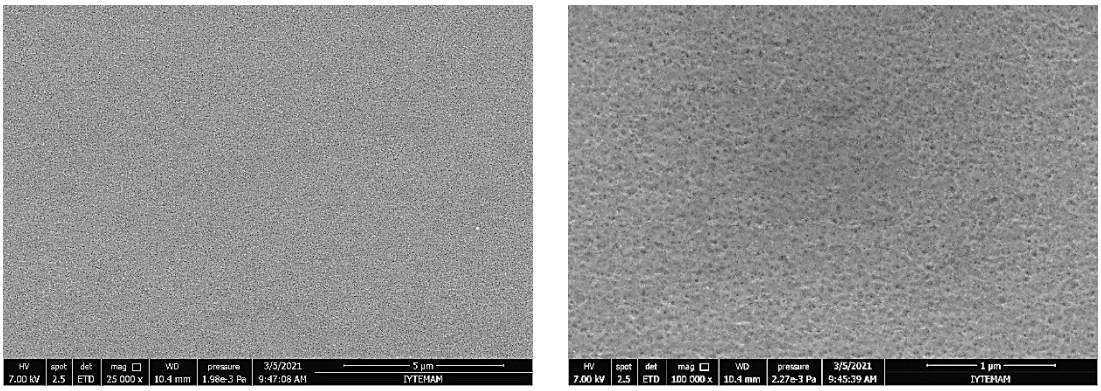

$PES_{Support}$

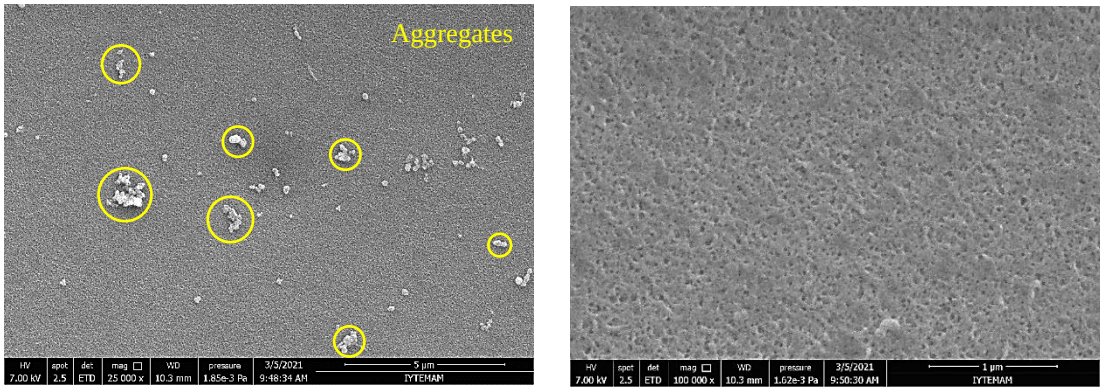

$PES\_PDA_{Conv\ Poly}$

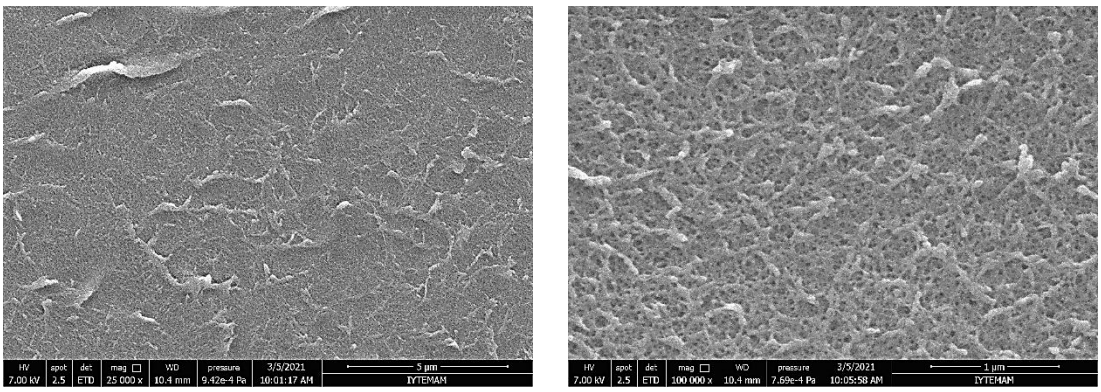

$PES\_PDA_{PolyPrev\ Poly}$

Figure 4.4. Surface SEM images of the support and PDA coated membranes.

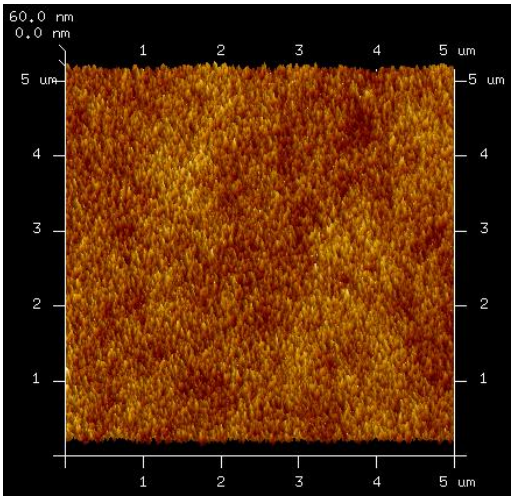

$PES_{Support}$

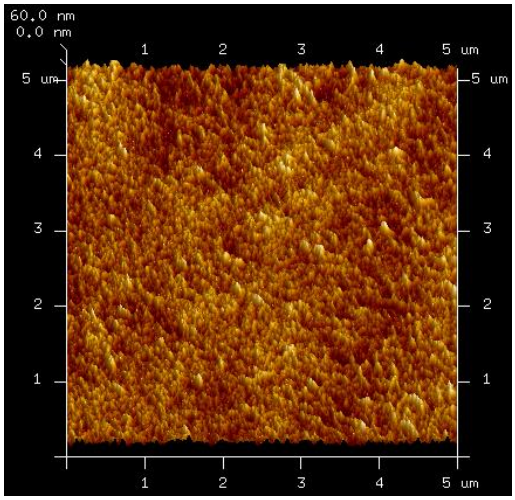

$PES\_PDA_{Conv\ Poly}$

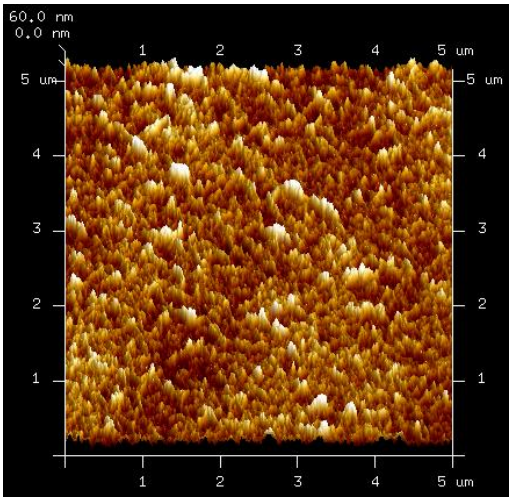

$PES\_PDA_{PolyPrev\ Poly}$

Figure 4.5. AFM images of the support and PDA coated membranes.

Table 4.2. Surface roughness of the support and PDA coated membranes.

Membranes	R_a (nm)	R_q (nm)
$PES_{Support}$	4.36±0.03	5.54±0.05
$PES\_PDA_{Conv\ Poly}$	4.90±0.09	6.17±0.09
$PES\_PDA_{PolyPrev\ Poly}$	5.98±0.26	7.51±0.31

4.3.2. Characterization and Performance of the Co-deposited Membranes Prepared by PolyPrev System

It is reported in the literature that PDA coatings do not show sufficient antibacterial activity against Gram-positive and Gram-negative bacteria (Chang et al., 2016; Kolewe et al., 2018; Yao et al., 2019); therefore, CTAB was co-deposited with dopamine using the PolyPrev system. The surface elemental compositions of the membranes were determined with XPS, and the results were given in Table 4.3. The characteristic indicator signal for both CTAB and dopamine is nitrogen. In addition to N, C and O elements were also detected in the XPS survey spectrum. The N content of the support increased after the introduction of dopamine and dopamine/CTAB layer on the surface. The N1s spectra was analyzed in detail to prove the presence of CTAB in the dopamine layer (Figure 4.6). The characteristics peaks at ~399.6 eV and ~400.2 eV binding energies were attributed to the C-N group and the aromatic C-N and C=N groups, respectively. These two groups are in the structure of dopamine and pore former in the support membrane. On the other hand, the peak at ~402.5 eV belongs to the quaternary ammonium group (Yao et al., 2019; Yang et al., 2015; Han et al., 2018), thus, was observed only in the dopamine layer co-deposited with CTAB. The peak areas under the deconvoluted curves were calculated to quantify the groups in the structure. As shown in Table 4.4, the highest quaternary ammonium amount was found in the PES_PDA+CTAB$_{CMC}$ membrane.

Table 4.3. Surface elemental composition (wt%) of support and co-deposited membranes.

Membranes	C (%)	O (%)	S (%)	N (%)	N/S
PES$_{Support}$	74.17	17.31	6.51	2.01	0.31
PES_PDA$_{PolyPrev\ Poly}$	74.43	17.43	5.39	2.75	0.51
PES_PDA+CTAB$_{LCMC}$	75.57	16.55	4.81	3.07	0.64
PES_PDA+CTAB$_{CMC}$	75.69	16.11	4.58	3.62	0.79
PES_PDA+CTAB$_{HCMC}$	76.16	15.72	5.48	2.64	0.48

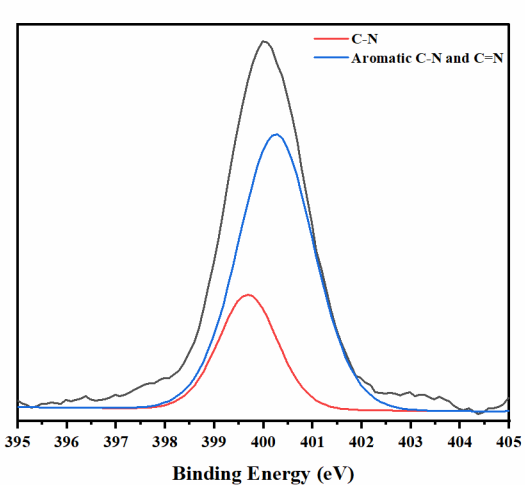

a) $PES_{Support}$

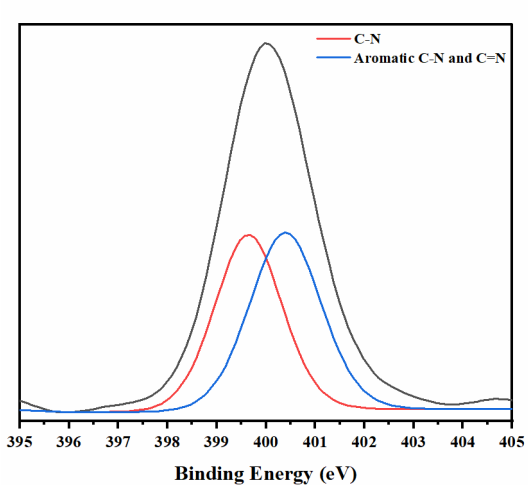

b) $PES\_PDA_{PolyPrev\ Poly}$

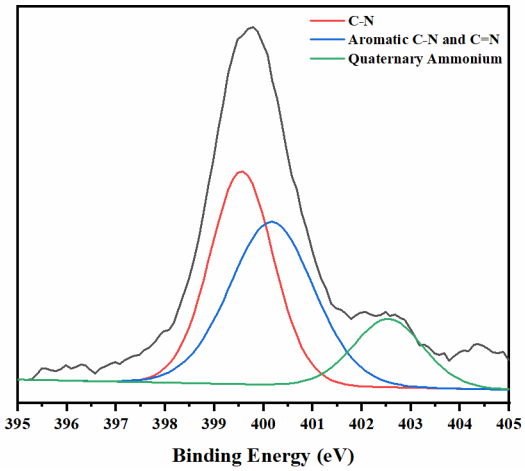

c) $PES\_PDA+CTAB_{LCMC}$

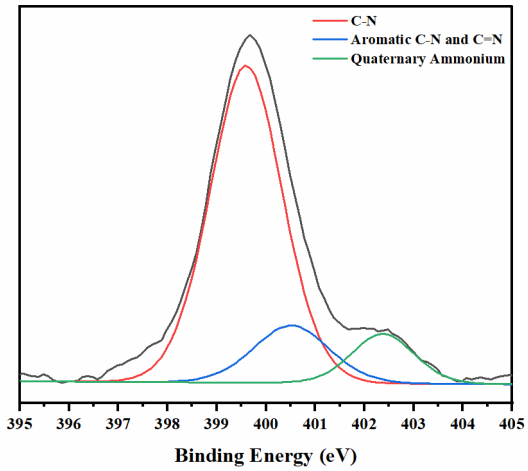

d) $PES\_PDA+CTAB_{CMC}$

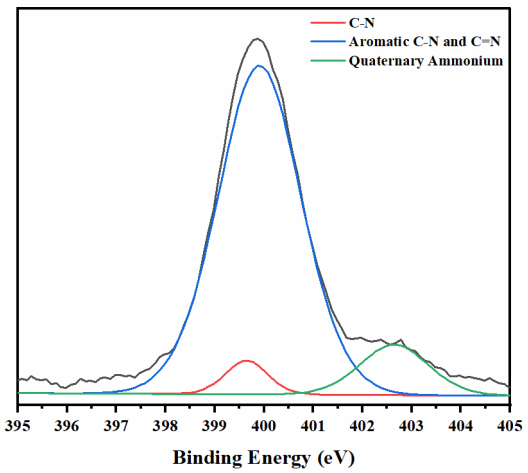

e) $PES\_PDA+CTAB_{HCMC}$

Figure 4.6. High-resolution XPS spectra of N1s region for membranes.

Table 4.4. Peak areas under the deconvolution curves.

Membranes	C-N group at ~399.6 eV	Aromatic C-N and C=N groups at ~400.2 eV	Quaternary Ammonium group at ~402.5 eV
$PES_{Support}$	784.7	2411.9	-
$PES\_PDA_{PolyPrev\ Poly}$	1364.4	1484.9	-
$PES\_PDA+CTAB_{LCMC}$	1133.4	1149.7	399.9
$PES\_PDA+CTAB_{CMC}$	3852.1	725.9	518.9
$PES\_PDA+CTAB_{HCMC}$	85.1	1624.7	206.9

The modified membranes exhibited statistically equivalent PWP to their support membrane as shown in Figure 4.7. The analysis of SEM images showed that the average pore diameter of the co-deposited membranes ($PES\_PDA+CTAB_{LCMC}$ (28.1±3.8 nm), $PES\_PDA+CTAB_{CMC}$ (28.4±4.7 nm), $PES\_PDA+CTAB_{HCMC}$ (27.9±3.5 nm)) was statistically the same as the support membrane ($PES_{Support}$ (27.8±4.3 nm)) (Figure 4.8).

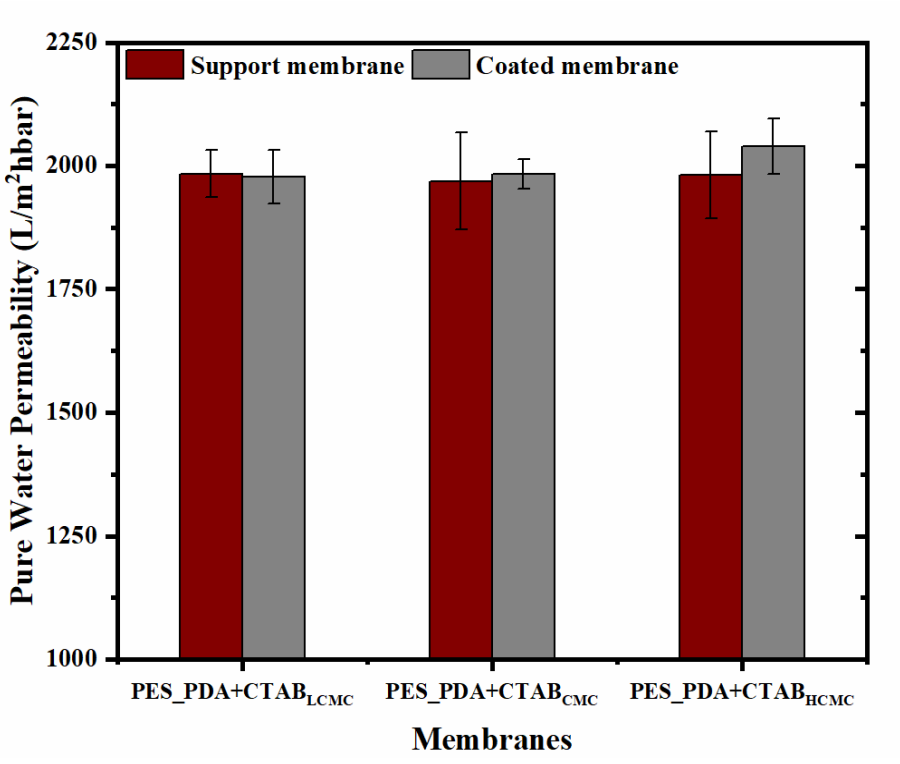

Figure 4.7. PWP of the support and co-deposited membranes as a function of CTAB concentration.

The results suggest that N_2 backflow mitigated the solution intrusion phenomenon and the presence of CTAB did not cause a thick layer formation due to its small size. Dobosz et al. (2019) used the same PolyPrev system in Scheme 4.1 and co-deposited dopamine with the polyMPC (MW:30 kDa) on the PES support (MWCO:100 kDa). Even though the pore penetration was prevented, large sized polymer caused a thick dopamine layer formation and reduced the PWP of the support from 413±6.3 L/m^{2}hbar. to 232±6.4 L/m^{2}hbar.

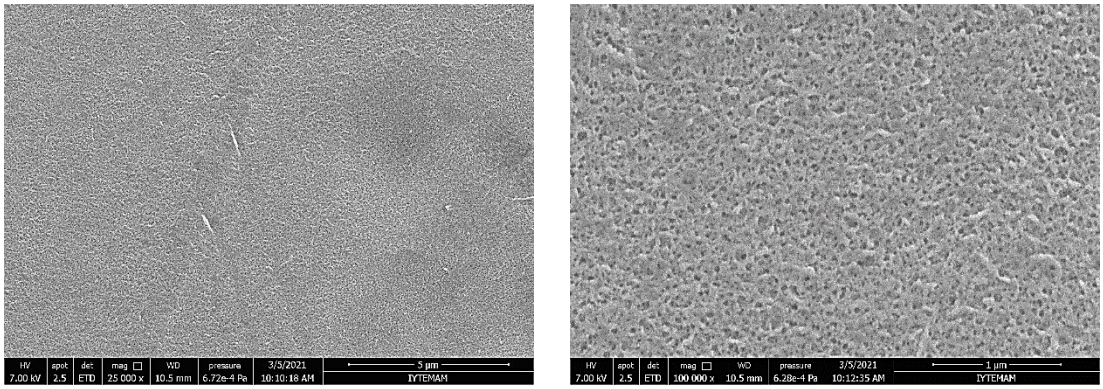

PES_PDA+CTAB$_{LCMC}$

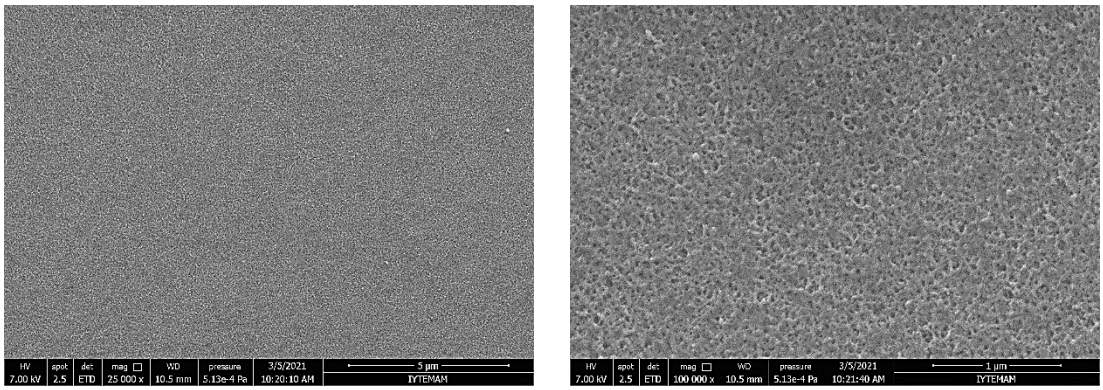

PES_PDA+CTAB$_{CMC}$

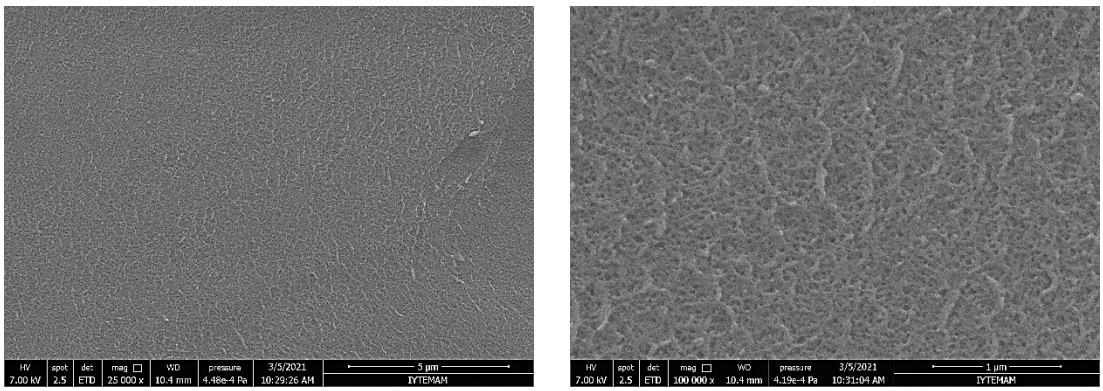

PES_PDA+CTAB$_{HCMC}$

Figure 4.8. Surface SEM images of the co-deposited membranes.

AFM images and surface roughness of the co-deposited membranes were shown in Figure 4.9 and in Table 4.5. The roughness of support slightly increased upon co-deposition of dopamine with CTAB at below (LCMC) and above (HCMC) its micelle concentrations, however, it did not change at the CMC (Table 4.2).

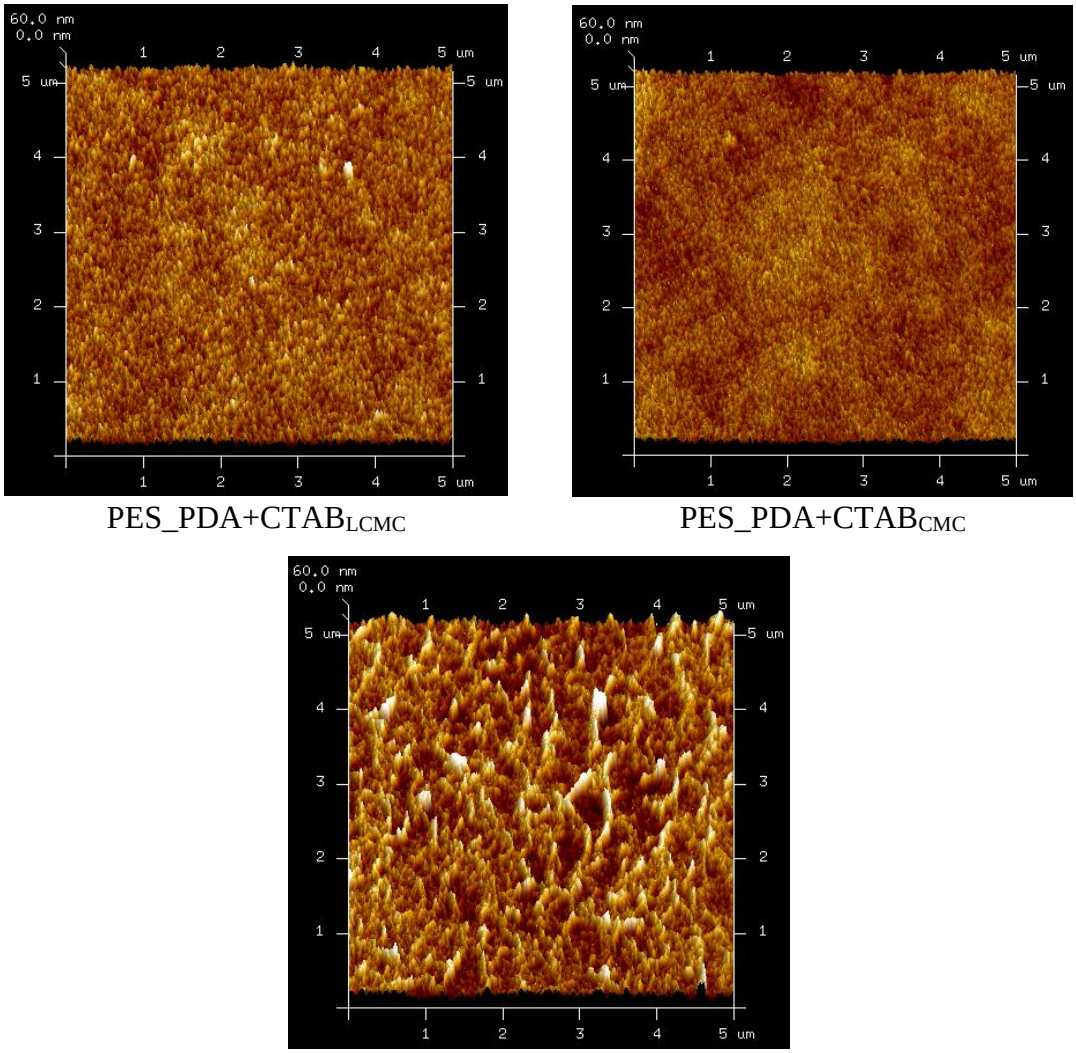

PES_PDA+CTAB$_{LCMC}$ PES_PDA+CTAB$_{CMC}$

PES_PDA+CTAB$_{HCMC}$

Figure 4.9. AFM images of the co-deposited membranes.

Table 4.5. Surface roughness of the co-deposited membranes.

Membranes	R_a (nm)	R_q (nm)
PES_PDA+CTAB$_{LCMC}$	5.52±0.01	6.96±0.02
PES_PDA+CTAB$_{CMC}$	4.74±0.38	6.01±0.47
PES_PDA+CTAB$_{HCMC}$	6.32±0.64	7.94±0.75

The surface hydrophilicity of the PDA coated membrane decreased after co-deposition with CTAB (65.3±1.1º, 67.7±1.4º, 63.9±1.8º for the PES_PDA+CTAB$_{LCMC}$, PES_PDA+CTAB$_{CMC}$, PES_PDA+CTAB$_{HCMC}$ membranes, respectively), consistent with the literature (Cihanoğlu and Altinkaya, 2020). This is an expected result because the hydrophilic quaternary ammonium head group in the structure of CTAB interacts with the catechol group in the PDA, and the hydrophobic tail in the CTAB structure becomes free. This free tail makes the surface of the co-deposited membranes more hydrophobic than pure PDA-coated membranes. Figure 4. 10 shows that all the co-deposited membranes were more protonated than the membrane functionalized with PDA alone (PES_PDA$_{PolyPrev\ Poly}$) due to the positively charged quaternary ammonium head group on the surface. The surface charge gave indirect information about to what extent CTAB was loaded on the surface. The PES_PDA+CTAB$_{CMC}$ membrane had the lowest negative charge at pH 5.5 and 7.5 and the highest positive charge at pH 3.5. Both this result and XPS analysis data (Table 4.4) demonstrated that the highest CTAB loading in the dopamine layer was achieved at the CMC of the CTAB.

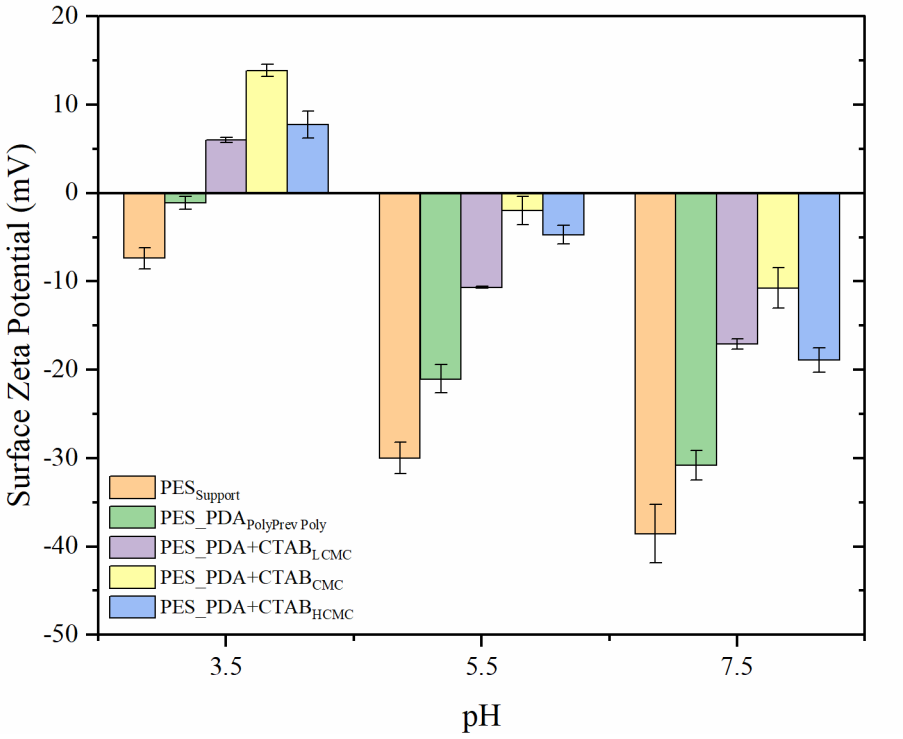

Figure 4.10. Surface Zeta Potential of the membranes.

To understand why CTAB loading decreased above the CMC, we evaluated the dopamine polymerization in bulk phase. For this purpose, the sample was taken from the dopamine solution poured on the membrane surface and the absorbance was measured at

420 nm (Du et al., 2014). As shown in Figure 11, in the presence of CTAB , the absorbance was found higher which indicated that CTAB acts as a template in the liquid phase for the growth of PDA (Ponzio et al., 2014). The competition as to whether polymerization will occur predominantly in the bulk liquid phase or at the solid-liquid interface is determined by the number of templates in the liquid phase (Arzillo et al., 2012; Zhang et al., 2012; Zhang et al., 2013b; Lv et al., 2018; Qiu et al., 2015; Liu et al., 2014; Zhang et al., 2017c; Chassepot and Ball, 2014; Ponzio et al., 2014). Among three concentrations investigated, the CTAB molecules have the highest surface area above the CMC leading to the highest polymerization rate in the bulk phase (Scheme 4.2) (Coppola et al., 2004). Consistent with this argument, even after 72 h polymerization above the CMC of CTAB, no deposited layer was detected on the silicon wafer (Table 4.6). Both the absorbance and thickness measurements showed that the rate of bulk polymerization increased with the increased CTAB concentration. Based on these results, it can be concluded that the lowest positive charge at neutral pH (Figure 4.10) and the lowest quaternary ammonium group (Table 4.4) observed for the PES_PDA+CTAB$_{HCMC}$ membrane are due to the dominance of bulk polymerization over interfacial polymerization of dopamine when the CTAB in the dopamine solution was above its CMC.

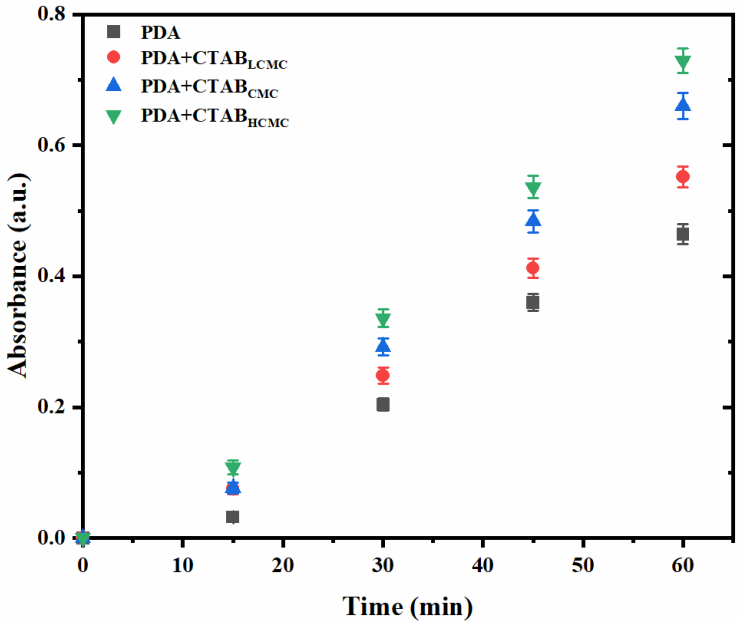

Figure 4.11. The absorbance of PDA as a function of CTAB concentration at the liquid phase.

Table 4.6. The coating thickness on the crystalline silicon wafer.

Membranes	Coating thickness (nm)	
	24 h	72 h
PDA	24.2±1.9	44.0±1.1
PDA+CTAB$_{LCMC}$	21.2±0.9	31.5±0.1
PDA+CTAB$_{CMC}$	18.5±0.5	21.3±1.5
PDA+CTAB$_{HCMC}$	*	*

* The thickness could not be measured.

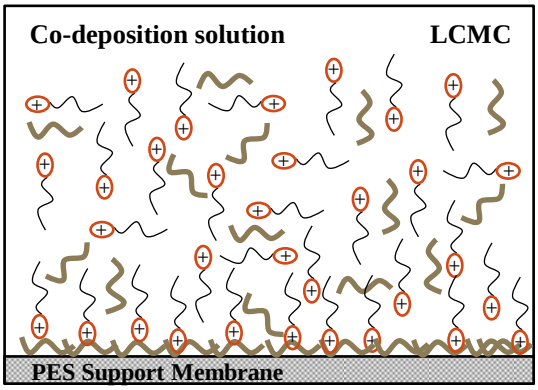

a) PDA+CTAB$_{LCMC}$

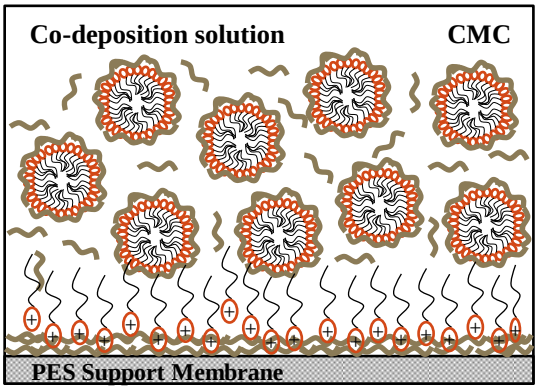

b) PDA+CTAB$_{CMC}$

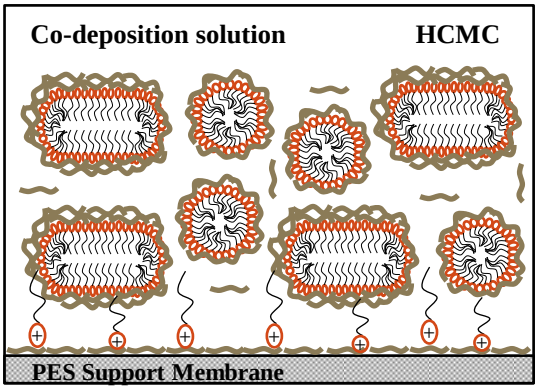

c) PDA+CTAB$_{HCMC}$

Scheme 4.2. The effect of CTAB concentration on the co-deposition rate to membrane surfaces.

4.3.3. Antibiofouling Assessment of Membranes

The antibiofouling behaviour of the support ($PES_{Support}$), PDA coated ($PES\_PDA_{PolyPrev\ Poly}$) and co-deposited ($PES\_PDA+CTAB_{LCMC}$, $PES\_PDA+CTAB_{CMC}$, $PES\_PDA+CTAB_{HCMC}$) membranes were evaluated by dynamic filtration of Gram-positive (*S. aureus*) and Gram-negative (*E. coli*) model bacteria suspensions in the dead-end filtration unit. As shown in Figures 4.12 and 4.13, the $PES_{Support}$ membrane exhibited the highest flux decline and the lowest flux recovery ratio (FRR). Both quantities are used as a measure of the biofouling resistance of a membrane. After coating with the PDA layer, the biofouling resistance of the PES support increased. The improvement can be attributed to the anti-adhesion property through enhanced hydrophilicity and reduced zeta potential of the coated layer. The co-deposition of dopamine with CTAB resulted in lower flux declines during bacteria filtration. Although the presence of CTAB decreased hydrophilic nature of PDA, the higher biofouling resistance of the co-deposited membranes mainly comes from the strong antibacterial activity of CTAB (Kang et al., 2012). The anti-adhesive property of a surface can only reduce the initial bacteria adsorption. On the other hand, the antibacterial surface attacks, disperses or suppresses the activity of attached organisms. Additionally, the lower electrical charge of the CTAB-containing PDA membranes contributed to lower biofouling propensity. The roughness of unmodified and all modified membranes were small enough to prevent penetration of the bacteria into the valleys. Thus, the biofouling tendency of the membranes was not affected by the slight differences in the roughness values (Table 4.5). The antibacterial activity of the CTAB modified membrane surface begins with the electrostatic interaction between positively charged head groups of CTAB and the negatively charged cell wall of bacteria. Next, the long hydrophobic alkyl tail in CTAB further damages the cell wall of bacteria to induce leakage of substances, causing the death of bacteria, thereby inhibited bacterial growth (Zhang et al., 2016d).

Among the co-deposited membranes, the $PES\_PDA+CTAB_{CMC}$ membrane showed the best antibiofouling performance against Gram-positive (*S. aureus*) and Gram-negative (*E. coli*) bacteria as measured with the lowest flux decline and the highest FRR. This observation was directly related with the highest CTAB loading in this membrane (Table 4.4).

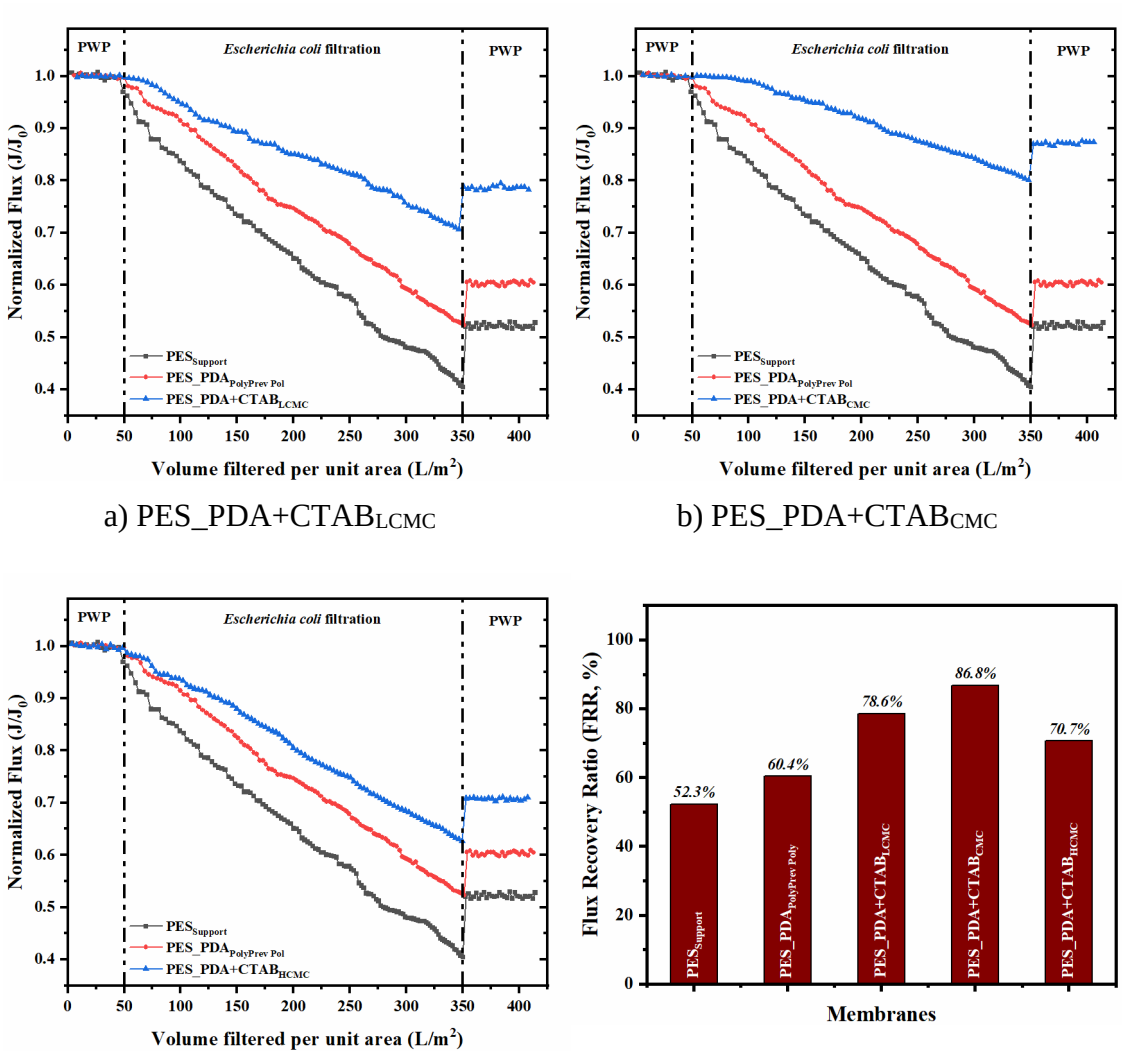

a) PES_PDA+CTAB$_{LCMC}$ b) PES_PDA+CTAB$_{CMC}$

c) PES_PDA+CTAB$_{HCMC}$ d) All membranes

Figure 4.12. The normalized flux and the FRR of support, PDA coated, and co-deposited membranes as a function of volume filtered per unit area during *E. coli* filtration. Transmembrane pressure (TMP) applied to the membranes for the bacteria filtration was 0.3 bar.

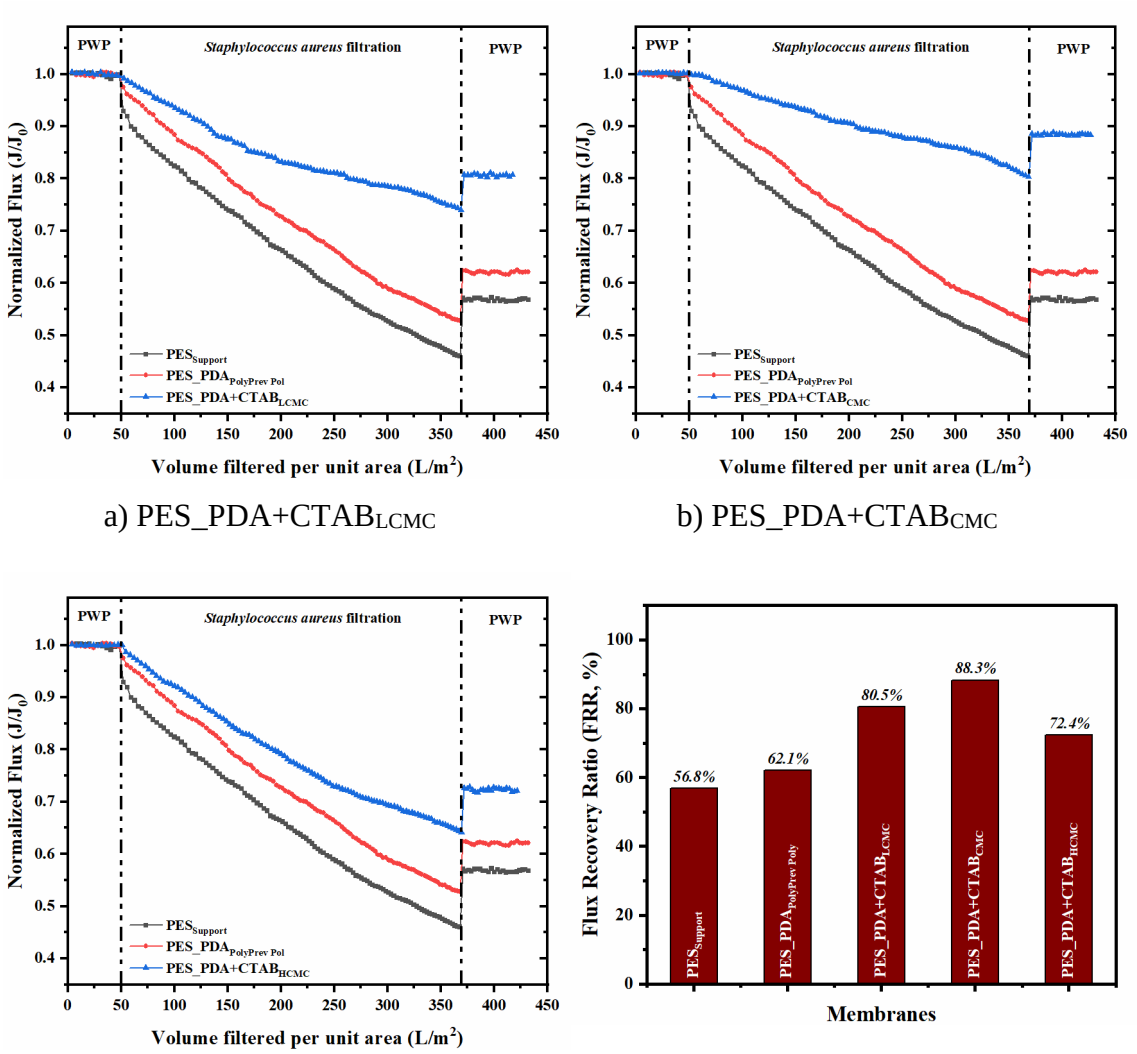

a) PES_PDA+CTAB$_{LCMC}$ b) PES_PDA+CTAB$_{CMC}$

c) PES_PDA+CTAB$_{HCMC}$ d) All membranes

Figure 4.13. The normalized flux and the FRR of support, PDA coated, and co-deposited membranes as a function of volume filtered per unit area during *S. aureus* filtration. Transmembrane pressure (TMP) applied to the membranes for the bacteria filtration was 0.3 bar.

In addition to co-deposition technique, antibacterial groups are incorporated to the membrane surfaces through other surface modification methods. An ideal modification technique should not only impart antibacterial activity to the surface but also should not change the permeability of the support membrane. Table 4.7 compares the performance of different modification methods in terms of flux reduction after surface modification. Although all the methods made the surface resistant to biofouling, they caused significant flux reduction upon modification. In contrast, the method proposed in this study enhanced the biofouling resistance of the PES support without decreasing its flux.

Table 4.7. The flux reduction of the modified membranes in the literature.

Support	Modification Method	Modification Agent	Flux Reduction (%)	Refs.
UF_PES	Co-deposition	PDA+QPEI	74	Yao et al., 2019
UF_PES	UV-graft	Poly(CBOH)	57	Weinman et al., 2018
UF_PES	UV-graft Vacuum filtration	P, GO	47	Zhang et al., 2018b
UF_Chitosan based	Mixed matrix	PEG, MWCNT, BKC	37	Khoerunnisa et al.,2021
UF_PSF	UV-graft	MBHBA	36	Xueli et al., 2013
UF_PES	UV-graft	HMBA	20	Wang et al., 2019
NF_HPAN	Co-deposition	PDA+rGOC	80	Zhu et al., 2017
RO_PA	SI-ATRP	CAA+TMA	~42	Yang et al., 2020a
RO_PA	SI-ATRP	pMEDSAH	~34	Yang et al., 2020b
RO_PA	Modification	PDA, MPC-co-AEMA	~10	Karkhanechi et al., 2014
UF_PES	Co-deposition	PDA+CTAB	No reduction	This work

UF: Ultrafiltration, NF: Nanofiltration, RO: Reverse Osmosis,
PES: Polyethersulfone, PSF: Polysulfone, PA: Polyamide
PDA: Polydopamine, QPEI: Quaternized polyethylenimine
Poly(CBOH): Poly(2-((2-hydroxy-3-(methacryloyloxy)propyl) dimethylammonio)acetate)
P: Zwitterion polyampholyte hydrogel, GO: Graphene oxide nanosheets
PEG: Polyethylene glycol, MWCNT: Multi-walled carbon nanotubes, BKC: Benzalkonium chloride
MBHBA: N-(5-methyl-3-isobutyl-2-hydroxy-benzyl)-acrylamide
HMBA: Hexamethylene bis acetamide
rGOC: Reduced Graphene Oxide-Copper
SI-ATRP: surface-initiated atom transfer radical polymerization
CAA: anionic 2-carboxyethyl acrylate, TMA: cationic [2-(acryloyloxy)ethyl] trimethyl ammonium chloride
pMEDSAH: poly[2-(methacryloyloxy)ethyl-dimethyl-(3-sulfopropyl) ammonium hydroxide]
MPC-co-AEMA: 2-(methacryloyloxy) ethyl phosphorylcholine (MPC) copolymer with 2-aminoethyl methacrylate (AEMA)
CTAB: Cetyltrimethylammonium bromide

4.3.4. Stability of the Membrane

The PES_PDA+CTAB$_{CMC}$ membrane which displayed the best antibiofouling performance during bacteria filtration was chosen to test stability of the CTAB. This membrane was stored in 1 M NaCl solution for 3 months at room temperature (25 ^{o}C). Positively charged quaternary ammonium group (NR_4^+) in CTAB makes electrostatic interaction with the negatively charged polydopamine. The salt ions increase the distance between the charged groups, as a result, the electrostatic interaction decreases. Thus, we used a very high NaCl concentration to weaken the electrostatic binding through charge screening effect. The leached CTAB in water can be determined through measuring N element amount with Total Organic Carbon (TOC) analysis. However, this measurement can be misleading since the N element also comes from the water soluble PVP used as a pore former in the support. As a result, we used surface zeta potential measurements since the presence of CTAB significantly alters the charge of the support and the membrane functionalized with PDA alone. At the end of 3 months of storage, the PES_PDA+CTAB$_{CMC}$ membrane showed zeta potential values equivalent to their fresh counterparts (Table 4.8) indicating strong electrostatic interaction between CTAB and PDA.

The commercial PES UF support membrane chosen in this study is commonly used for membrane bioreactor (MBR) applications. In the case of submerged MBR configuration, the membrane is in direct contact with a high bacteria population. For the best performance, the bacteria in the reactor should be alive to degrade the pollutants. Also, the membrane surface should be resistant to biofouling. In this respect, it is necessary to incorporate antibacterial agents killing bacteria through contact. Otherwise, the antibacterial agent released into the reactor will decrease the bacteria population over time. Additionally, antibiofouling membranes based on contact-killing property is desired since continuous release of antibacterial agent results in a shorter lasting period of the membrane. Our results suggest that the CTAB co-deposited with dopamine enhanced the biofouling resistance of the commercial PES support and remained stable in the deposited layer.

Table 4.8. Surface zeta potential measurements of the membrane before and after exposure to the 1 M NaCl.

Membranes	pH		
	3.5	5.5	7.5
Fresh Membrane	13.8±0.7 mV	-3.1±0.1 mV	-10.7±2.3 mV
Membrane exposed to 1 M NaCl	13.8±1.2 mV	-3.7±0.6 mV	-10.4±3.2 mV

4.4. Conclusions

We have proposed a facile surface modification protocol to enhance the biofouling resistance of the ultrafiltration membranes. The approach is based on co-deposition of dopamine with a low molecular weight, strong antibacterial surfactant, CTAB, under N_2 backflow. The PDA layer alone improved the biofouling resistance of the PES support through enhanced hydrophilicity. However, the presence of CTAB imparted better antibiofouling property to the support through the antibacterial property of the surface. The concentration of CTAB in the dopamine solution was found to have a significant influence on the deposition rate and the biofouling propensity of the membranes. Among three different CTAB concentrations (<CMC, =CMC, >CMC), the lowest flux decline and the highest FRR were observed when the PDA was functionalized with CTAB at the CMC. Above the CMC of CTAB, the bulk polymerization became dominant over interfacial polymerization. Our results demonstrated that the co-deposition protocol proposed in this study can be used to develop biofouling resistant UF membranes without compromising the pore size and the permeability of the support. The CTAB showed its antibacterial activity through contact with bacteria and remained stable in the structure in the long-term storage. This result suggests that the modified membrane has a great potential in submerged MBRs where biofouling resistant membranes showing contact-killing antibacterial activity are urgently needed.

CHAPTER 5

ULTRASOUND-ASSISTED DOPAMINE POLYMERIZATION ON POLYMERIC MEMBRANE SURFACES

5.1. Introduction

Surface modification with mussel-inspired coatings of dopamine have attracted great interest due to catechol (DOPA) and amine (lysine) groups in the dopamine structure forming strong covalent and noncovalent interactions with a broad spectrum of organic and inorganic materials such as polymers, noble metals and ceramics (Lee et al., 2007; Lee et al., 2006). Besides, formed polydopamine (PDA) coatings can be easily post-modified by various molecules such as thiols (Lee et al., 2007), amines (Kang et al., 2012), owing to the presence of functional groups in the PDA structure. Due to their high negative charge density and hydrophilicity, PDA coatings have also been explored for many membrane applications, such as wastewater treatment (Kasemset et al., 2013), battery separators (Ryou et al., 2012), nanofiltration (Li et al., 2015b) and gas separation (Ingole et al., 2015). In all of these applications, superior performance of the membrane, such as high-water flux (Li et al., 2015b), excellent water vapor/N_2 selectivity (Ingole et al., 2015), and high fouling resistance (Miller et al., 2014; Kasemset et al., 2016; McCloskey et al., 2012) was directly, or indirectly related to the PDA layer. Despite the unique properties of PDA coatings, the slow kinetics of dopamine polymerization, which range from several hours to a few days, remains an issue (Lee et al., 2017; Du et al., 2014; Wang et al., 2017a; Wang et al., 2018; Zhang et al., 2016b). This limitation makes the PDA coatings process too time-consuming and restricts their large-scale industrial applications. Different strategies utilizing UV (Du et al., 2014), microwave (Lee et al., 2017), microplasma (Wang et al., 2017a) and chemical oxidizing agents (Wang et al., 2018; Zhang et al., 2016b) have accelerated the polymerization rate to overcome this drawback. However, these techniques have some limitations, such as the degradation of the support due to UV irradiation (Baek et al., 2017), surface contamination of the triggering metal ions (Zhang et al., 2016b), need for chemical oxidizing agents (Wang et

al., 2018), and high energy requirements which can immediately increase temperature up to 100 ^{o}C in a few minutes (Lee et al., 2017). The increased temperature during polymerization can lead to collapsed pores in the support membrane.

In polymer science, ultrasound has been used to degrade synthetic and bio-based polymers for nearly half a century (Paulusse and Sijbesma, 2006) and applied to various polymer synthesis techniques such as sonochemically induced reversible addition fragmentation chain transfer polymerization (Sono-RAFT) (Collins et al.,2019), and sonochemically induced nitroxide-mediated polymerization (Sono-NMP) (McKenzie et al., 2017). In this study, we demonstrated that ultrasound could be used as a trigger to significantly accelerate the polymerization kinetics of dopamine in the bulk phase, and the deposition rate of a PDA film on porous polymeric membranes at room temperature without using any chemical oxidizing agents. We hypothesize that the acceleration with ultrasound is possible through decomposition of water molecules to the reactive oxygen species (ROSs) (Paulusse and Sijbesma, 2006), which are more active than the molecular oxygen (Bayır, 2005) in triggering the oxidation of dopamine. To prove this hypothesis, nitroblue tetrazolium (NBT) assay and radical scavengers were used in the bulk phase polymerization. The PDA coating was successfully formed on the hydrophobic polysulfone (PSF) and relatively hydrophilic, polysulfone-sulfonated polyethersulfone (PSF-SPES) membranes that are commonly used in membrane applications. The effect of the ultrasound triggering on the PDA coating was evaluated using surface free energy, contact angle, XPS, SEM, AFM and ATR-FTIR measurements. In addition, the performance of the PDA-coated membranes was determined by measuring the pure water permeability, the PEG rejection and fouling characteristics using oil/water emulsion as a model foulant. The effect of ultrasound on the structure of the bare membranes was investigated through measuring the PWP and PEG rejection before and after applying ultrasound. Here, for the first time, we demonstrate that ultrasound increases the polymerization kinetics of dopamine on the polymeric membranes. This study not only provides a green and rapid polymerization but also opens a new direction for the applications of ultrasound-assisted based polymerization of dopamine.

5.2 Materials and Method

5.2.1. Materials

Dopamine hydrochloride, Tris-HCl buffer, L-ascorbic acid, Cysteine, nitrotetrazolium blue chloride (NBT) were purchased from Sigma-Aldrich. Polysulfone (PSF) (Mw= 35 kDa) purchased from Sigma-Aldrich, and Sulfonated polyethersulfone (SPES) (Mw= 80 kDa, Sulfonation degree (SD)<30%) kindly donated by Konishi Chemicals, Japan, were used to prepare flat sheet membranes. 1-methyl-2-pyrrolidone (NMP, 99.5%) and N, N-Dimethylacetamide (DMAc, 99%) purchased from Fluka and Sigma-Aldrich, were used to dissolve the polymers. NaOH, HCl, polyethylene glycol (PEG: 35 kDa) and polyethylene oxide (PEO:100 kDa) were purchased from Sigma-Aldrich. The water/paraffin emulsion used to determine the fouling resistance of the membranes was kindly supplied by Işıksan Kimya Corporation and Polyester non-woven fabric (05TH-100) (thickness:161 μm and base weight:100 g/m^2) was purchased from Hirose Paper Mfg. Co. Ltd, Japan, and used as a support layer for manufacturing the membranes. All chemicals were used without further purification and solutions were prepared using deionized (18.2 MΩ cm) water.

5.2.2. Preparation of Flat Sheet Membranes

PSF and PSF-SPES blend membranes were prepared by the non-solvent induced phase inversion technique. The polymers were dried in a vacuum oven at 80 ^{o}C for 24 h to remove moisture. Dried PSF and the PSF:SPES blend (blending ratio is 3:1) were dissolved in NMP and DMAc:NMP mixture (DMAc:NMP ratio of 2:1), respectively by stirring at 100 rpm for 24 h. In order to eliminate air bubbles, solutions rested for 24 h without stirring and then were cast on a clean glass plate and non-woven with the help of an automated film applicator (Sheen Instrument Ltd., model number: 1133N). The initial thickness of the cast membranes was adjusted using a four-sided applicator with a gap size of 200 μm. Following casting, the glass plate was immediately immersed into the coagulation bath including only deionized (18.2 MΩ cm) water at 25 ^{o}C. The polymer concentration in both casting solutions was adjusted to 20 wt.%.

5.2.3. Conventional and Ultrasound-Assisted Polymerization of Dopamine

Dopamine hydrochloride (2 mg/mL) was dissolved in Tris-HCl buffer solution (10 mM, pH 8.5, 25 ^{o}C). For conventional polymerization (Scheme 5.1a), the reaction solution (100 mL) was gently shaken at 70 rpm and room (25 ^{o}C) temperature. For ultrasound-assisted polymerization, an ultrasonic horn (Scheme 5.1b) and an ultrasonic reactor (Scheme 5.1c) operated at 30 W (frequency 20 kHz) and 25 W were used. In both experimental setup, the dopamine solution (100 mL) was not stirred, and the temperature was controlled by a chiller. At specific time intervals, the sample was removed to measure the formed polydopamine intensity using UV-vis spectroscopy. For coating the membranes, the sample coupons were immersed in the dopamine solution for 1 h under the same conditions used for bulk polymerization.

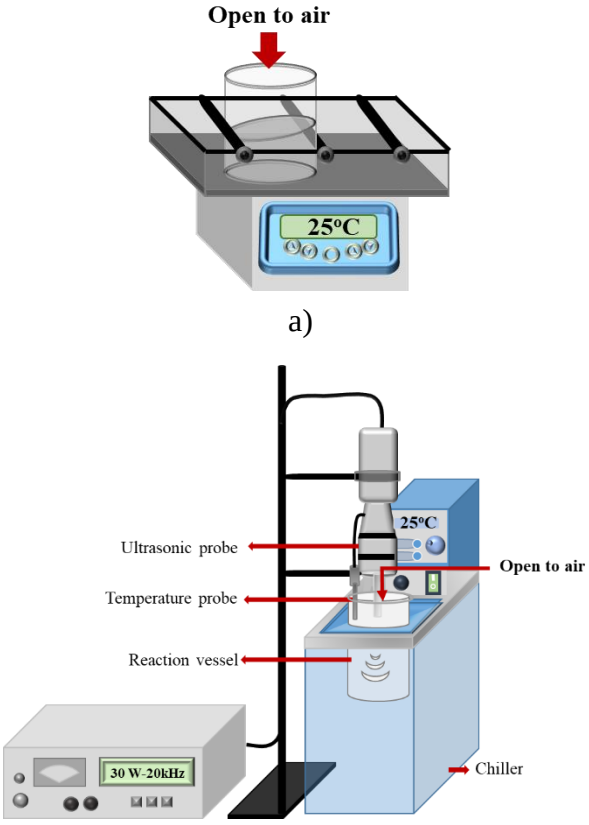

Scheme 5.1. a) conventional polymerization set-up, b) ultrasonic horn polymerization set-up c) ultrasonic reactor polymerization set-up

(Cont. on next page)

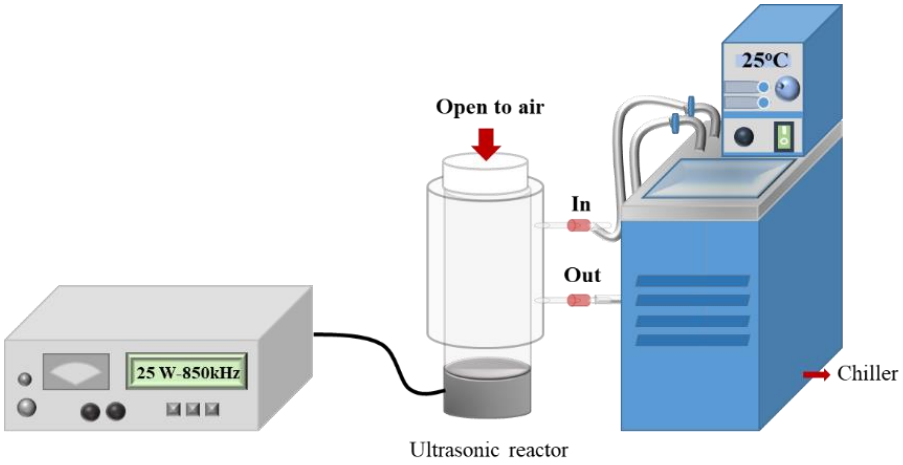

c)

Scheme 5.1. Cont.

5.2.4. Characterization of Membranes

The chemical structure of the bare and modified membranes was determined by Attenuated Total Reflectance Fourier Transformed Infrared Spectrometer (ATR-FTIR), (Perkin Elmer). Spectra were collected at ambient temperature over a scanning range of 4000-650 cm^{-1} with a resolution of 4.0 cm^{-1}. The water contact angle of the membranes was measured (Attension Optical tensiometer) with a 5 µL water droplet (*n*=5). The surface free energy (SFE) calculations based on the OWRK method (Owens, Wendt, Rabel and Kaelble) were carried out using the contact angle measurements of water and diiodomethane. The X-ray photoelectron spectra (XPS, Thermo Scientific) analysis at the emission angle of 0^o was used to determine the elemental composition of the membranes (*n*=3). The surface morphology of the membranes was characterized using a scanning electron microscope (SEM) (FEI Quanta 250 FEG). Before taking the images, the membrane surfaces were coated with gold nanoparticles with a Magnetron Sputter Coating Instrument. The surface roughness of the membranes (arithmetic mean (Ra) and root-mean-square (Rq)) was determined using an atomic force microscope (AFM) (MMSPM Nanoscope 8, Bruker). 5 × 5 μm^2 sample area was scanned at a rate of 1 Hz using tapping mode in the air at room temperature by the TAP150 model tip (Bruker) (*n*=3). Prior to analysis, all the membranes were dried in a vacuum oven (Memmert) at 25 ^oC. (*n* is the number of repeated experiments).

The surface free energy (SFE) values were determined by the OWRK method (Jiang et al., 2011). Equation 5.1 describes the surface tension of the solid (σ_s) with respect to the interfacial tension between solid and liquid (σ_{sl}) and the surface tension of the liquid (σ_l) by the Young equation:

$$\sigma_s = \sigma_{sl} + \sigma_l . cos\theta \tag{5.1}$$

The OWRK method requires contact angle measurements with at least two liquids, one polar (water) and the other nonpolar (diiodomethane) to calculate σ_s and the σ_l from Equation 5.2.

$$\sigma_l = \sigma_l^d + \sigma_l^p, \qquad \sigma_s = \sigma_s^d + \sigma_s^p \tag{5.2}$$

where σ_l^d/σ_s^d and σ_l^p/σ_s^p are the disperse and polar components of the liquid and solid, respectively. The OWRK model uses geometric mean to combine the solid and liquid contributions as follows:

$$\sigma_{sl} = \sigma_s + \sigma_l - 2\left(\sqrt{\sigma_s^d . \sigma_l^d} + \sqrt{\sigma_s^p . \sigma_l^p}\right) \tag{5.3}$$

Substituting this term for σ_{sl} in Young equation (5.1) and solving the unknowns results in a linear expression.

$$y = mx + c \tag{5.4}$$

where

$$y = \frac{1 + cos\theta}{2} . \frac{\sigma_l}{\sqrt{\sigma_l^d}}, \qquad x = \sqrt{\frac{\sigma_l^p}{\sigma_l^d}}, \qquad m = \sqrt{\sigma_s^p}, \qquad c = \sqrt{\sigma_s^d} \tag{5.5}$$

Thus, plotting y versus x enables the calculation of σ_s^p from the slope, and σ_s^d from the intersection with the vertical axis.

5.2.5. Membrane Filtration Performance

The filtration performance of membranes was determined by a 50 mL dead-end stirred cell (Millipore, Amicon Stirred Cell 8050) with an effective area of 13.4 cm^2. Before filtration, membrane coupons were compacted until a constant flux is reached. Next, pure water was filtered at 1 bar and collected permeate volume was recorded for specific time intervals. The volumetric flux was calculated from the slope of the permeate volume vs. time graph and converted to hydraulic pure water permeability (PWP) using following equation:

$$PWP = \frac{\Delta V}{A \Delta t \Delta P} \tag{5.6}$$

where ΔV is the volume of permeated water (L), A (m^2) is the membrane area, Δt (h) is the permeation time and ΔP (bar) is the transmembrane pressure difference applied through the membrane. To determine the rejection characteristics of the membranes, 1 g/L aqueous solutions of 35 kDa PEG and 100 kDa PEO were filtered at 1 bar. The concentrations of the permeate, retentate and feed solutions were measured by Rudolph-J357 Automatic Refractometer. The solute rejection (%) was calculated using the equation:

$$R(\%) = \left(1 - \frac{C_p}{\frac{C_f + C_r}{2}}\right) x100 \tag{5.7}$$

where C_p, C_r and C_f are the concentrations of permeate, retentate and feed solution, respectively. To eliminate concentration polarization, the solution was stirred at 300 rpm. The fouling behaviour of the membranes was evaluated by filtering of water/paraffin emulsion at 1 bar. Following filtration, the membrane coupons were rinsed with pure water for 30 min and water flux was re-measured to calculate the flux recovery ratio (FRR).

$$FRR(\%) = \left(\frac{J_R}{J_W}\right) x100 \tag{5.8}$$

where J_W and J_R are the pure water fluxes of the clean and the washed membranes. The experiments were carried out at room (25 ^{o}C) temperature. (n=3 where n is the number of repeated experiments).

The hydraulic resistance of the porous bare and PDA coated membranes is defined as follows (McCloskey et al., 2010):

$$R_i = \frac{\Delta p}{\mu J_i} \tag{5.9}$$

where Δp is the transmembrane pressure, μ is the viscosity of the feed solution, J_i is the steady-state water flux and R_i is the hydraulic resistance of the membrane.

Equation 5.9 can be employed for coated membranes to quantify the effect of PDA coating on membrane flux. The coating layer adds resistance to the membrane's overall hydraulic resistance, and it can be expressed as:

$$J_{PDA} = \frac{\Delta p}{\mu(R_0 + R_{PDA})} \tag{5.10}$$

where J_{PDA} is the pure water flux of PDA coated membrane, R_0 is the hydraulic resistance of bare membrane, R_{PDA} is the hydraulic resistance of the PDA coated membrane. By combining equations 5.9 and 5.10, R_{PDA} can be calculated as follows:

$$R_{PDA} = \frac{\Delta p}{\mu}\left(\frac{1}{J_{PDA}} - \frac{1}{J_0}\right) \tag{5.11}$$

where J_0 is the steady-state pure water flux of bare membrane.

5.2.6. Stability of Coating Layer

The chemical stability of the PDA-coating layer on membranes was evaluated in a strong acidic and alkaline environment. To this end, coated membranes with 1.5 cm x 1.5 cm sizes were immersed in 5 mL 0.1 M NaOH and 0.1 M HCl for 24 h. Next, the leached PDA in solution was quantified by measuring the absorbance of the solution at 420 nm with UV-vis spectroscopy (Du et al., 2014).

5.3. Results and Discussion

5.3.1. Bulk Phase Polymerization

Figure 5.1 shows the qualitative colour change and quantified UV/Vis absorbance of the dopamine solution (2 mg mL^{-1}, 10 mM Tris-HCl, pH=8.5) as a function of reaction time. The colour of the solution turned darker brown within 15 min in ultrasound-assisted polymerization, while very little change was observed even after 60 min in conventional polymerization (Figure 5.1a). In ultrasound-assisted polymerization technique, the absorbance of the characteristic peak at 420 nm, attributed to the polydopamine, increased from 0 to 2.31±0.16 after 60 min, which was much higher than the peak observed using conventional polymerization as shown in Figure 5.1b. To demonstrate the effectiveness and controllability of the ultrasound system, the solution was exposed to the ultrasound-assisted polymerization for 30 min (ON) and then to the conventional polymerization for 30 min (OFF), and this cycle was repeated three times. The result in Figure 5.1c shows that the absorbance intensity of the PDA increased sharply when the ultrasound was applied. On the contrary, the change was insignificant during the conventional polymerization which demonstrates that the ultrasound accelerated the polymerization kinetics of dopamine in bulk phase.

a)

Figure 5.1. a) Colour change of the dopamine solution as a function of time. b) Time-dependence of absorbance at 420 nm. c) Absorbance changes by turning ON (30 min) and OFF (30 min) of the ultrasound.

(Cont. on next page)

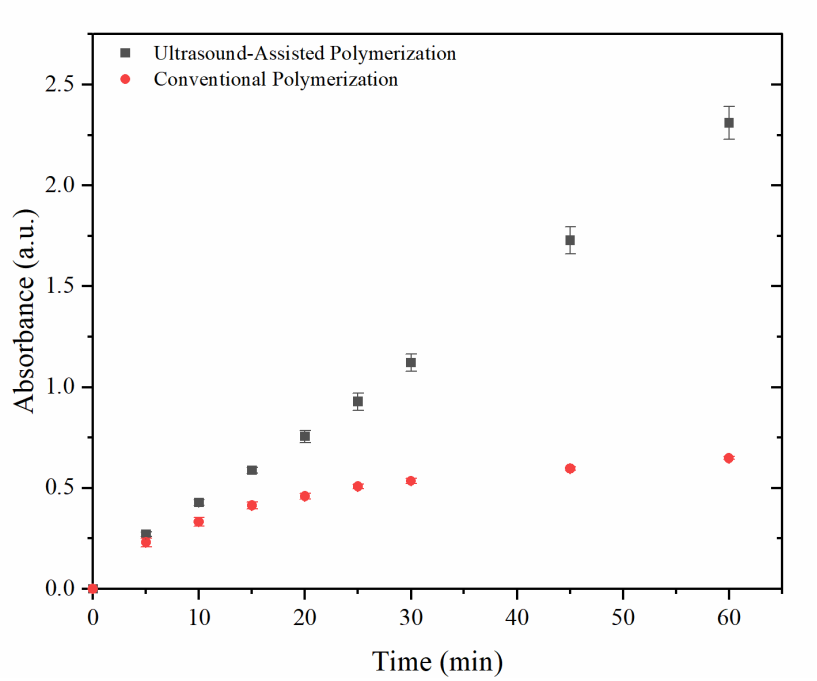

b)

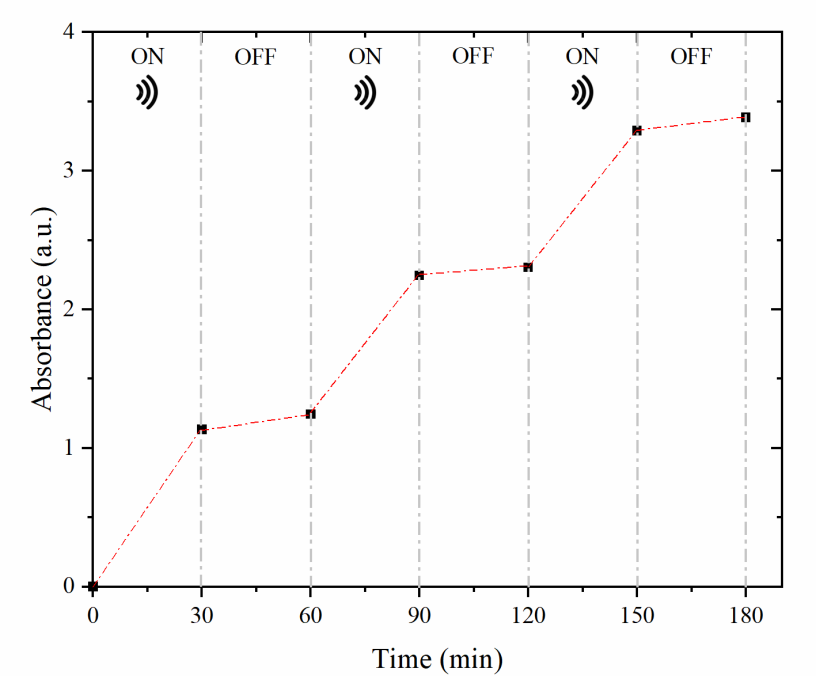

c)

Figure 5.1. Cont.

Figure 5.2 shows that the rate of dopamine polymerization was lower at a high ultrasound frequency (850 kHz, 25 W) than at a lower frequency (20 kHz, 30 W). At high frequency, considerable amount of ROSs and intermediate the product H_2O_2 (McKenzie et al., 2019) are generated. Although ROSs accelerate the oxidative self-polymerization

kinetics of dopamine (Lee et al., 2017; Du et al., 2014; Zhang et al., 2016), high H_2O_2 concentration suppresses the polymerization kinetics by degrading the polydopamine formed (Zhang et al., 2016b; Wang et al., 2016). Based on the results in Figure 5.2, low-frequency (20 kHz) ultrasound was applied for further investigations.

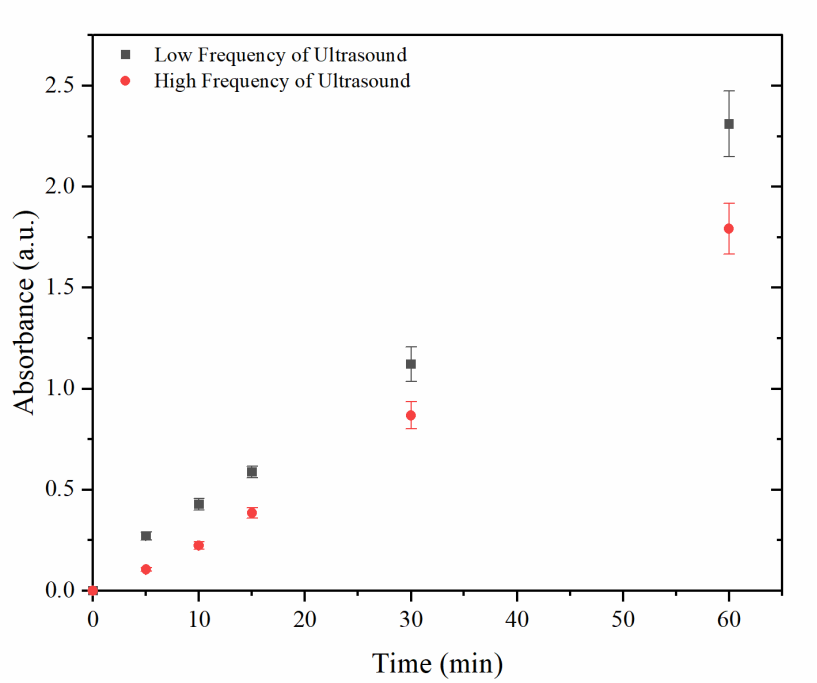

Figure 5.2. Effect of ultrasound frequency on the absorbance of dopamine solution.

Conventionally, the nitroblue tetrazolium (NBT) assay is used to determine the production of superoxide anion (O_2^-). The dissolved molecular oxygen in the dopamine solution is reduced by ultrasound to a superoxide anion, accelerating the polymerization rate of dopamine (Matsuoka et al., 2016; Brandes and Janiszewski, 2005; Auclair et al., 1978). To this end, the NBT (0.82 mg/mL) assay was used to determine to what extent the ultrasound-assisted polymerization accelerated the oxidation state of dopamine. When NBT is added to the dopamine solution, it is reduced to a light absorbing molecule (at 560 nm), blue NBT formazan, during the polymerization of dopamine. Figure 5.3 shows that the colour change during conventional polymerization was lower, and the results suggest that ultrasound greatly accelerates the oxidation state of dopamine due to increasing ROSs production rate in the presence of ultrasound. To prevent the generation of radicals, two different very strong reductants and radical scavengers, ascorbic acid (2 mg/mL), and cysteine (2 mg/mL) (Niki et al., 1991; Dinis et al., 1994), were added into dopamine solution. As shown in Figure 5.4, no polymerization took place in the presence of both scavengers, even after 60 min ultrasound. This result indicates that the ROSs

generated during the ultrasound-assisted polymerization process were quenched by radical scavengers and increasing the radical generation rate is the key mechanism for the observed accelerated polymerization.

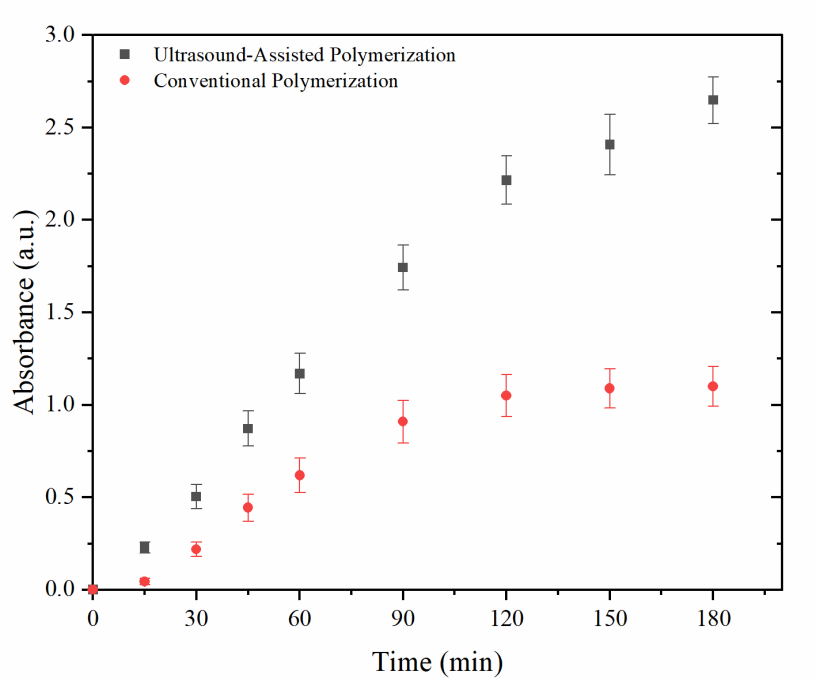

Figure 5.3. Absorbance of blue NBT formazan at 560 nm as function of time.

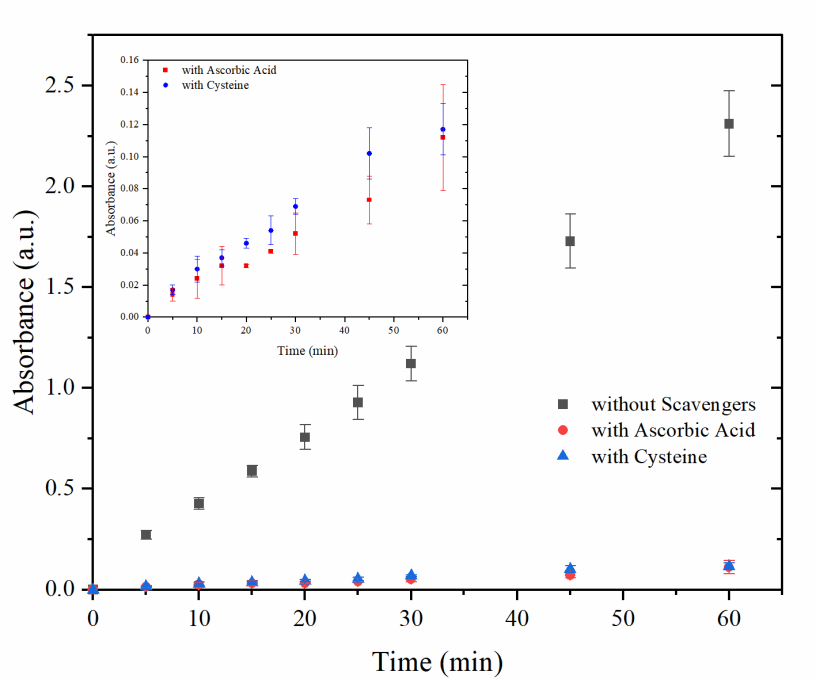

Figure 5.4. Effect of scavengers on the absorbance of dopamine solution.

5.3.2. Polymerization on Membrane Surfaces

In literature, the rate of dopamine deposition was generally quantified with the spectroscopic ellipsometry (Lee et al., 2017; Du et al., 2014; Wang et al., 2017a; Wang et al., 2018; Zhang et al., 2016b). However, this technique is limited to inorganic samples with smooth surfaces and cannot be applied to the polymeric membranes prepared by phase inversion. To compare the PDA deposition rates by conventional and ultrasound assisted polymerization techniques, we characterized the coatings using ATR-FTIR spectroscopy, contact angle, surface free energy and XPS measurements. Besides, the surface morphology changes in the membranes after coating were characterized by AFM and SEM analysis. In the spectrum of the PDA coated membranes, three IR band intensities belonging to the ν(N-H) and ν(O-H) peaks at 3300 cm^{-1} and ν_{ring}(C=C) peaks at 1623 cm^{-1} were observed, which indicated the presence of dopamine on the membrane surfaces (Figure 5.5). The area under the ν(N-H) and ν(O-H) peaks was found larger in the case of ultrasound assisted polymerization which demonstrated that the kinetics of PDA deposition process was accelerated using ultrasound as a trigger (Table 5.1).

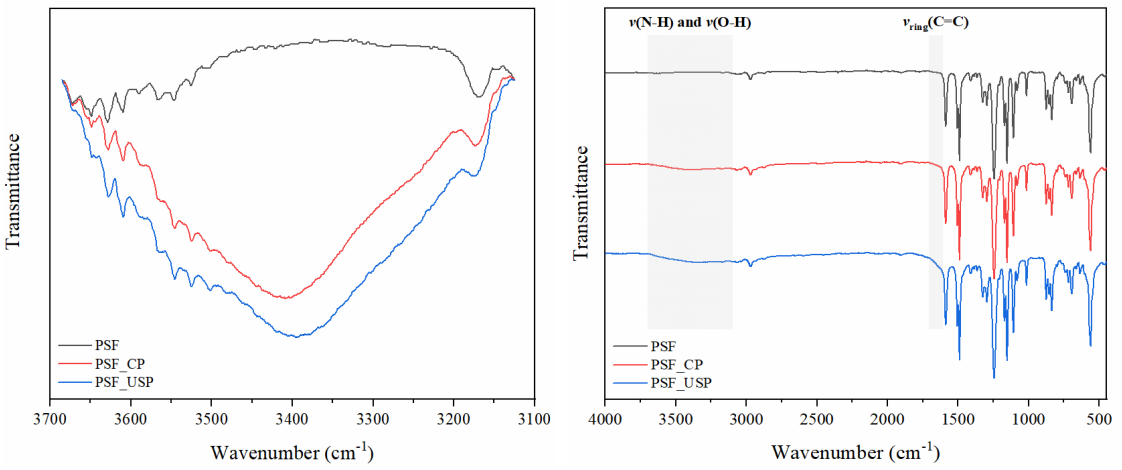

a)

Figure 5.5. ATR-FTIR spectra of the bare and modified a) PSF and b) PSF-SPES membranes (CP: Conventional Polymerization, USP: Ultrasound-Assisted Polymerization).

(Cont. on next page)

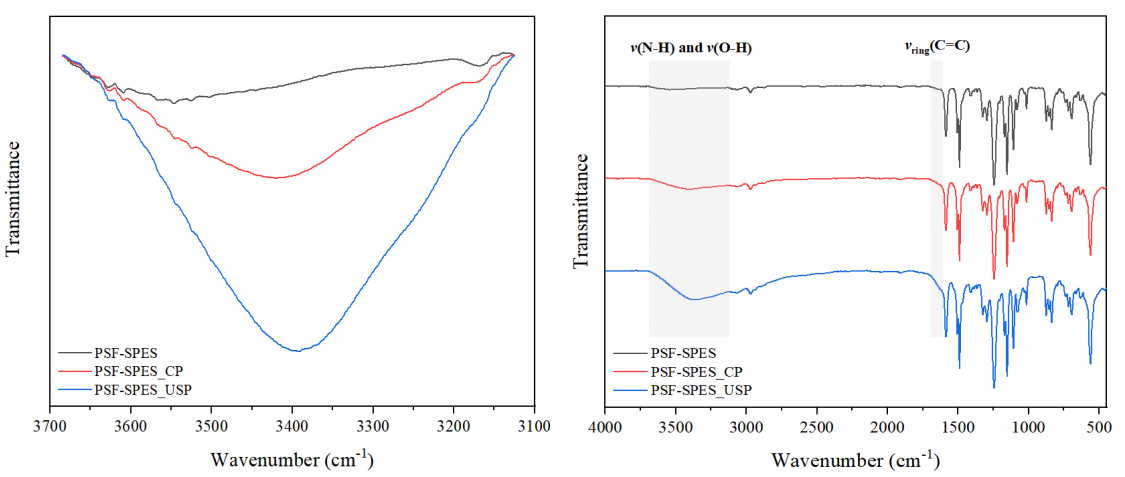

b)

Figure 5.5. Cont.

Table 5.1. Peak area of the bare and PDA coated membranes.

Membranes	Peak Area		
	v(N-H) and *v*(O-H) peaks at 3300 cm^{-1}		
	Bare	Conventional Polymerization	Ultrasound-Assisted Polymerization
PSF	41.1	400.5	515.2
PSF-SPES	345.7	2030.1	3918.4

Table 5.2 lists the water contact angles of the bare and PDA coated membranes. Hydrophilicity of both membranes increased upon PDA coating as a result of hydrophilic groups such as -OH, -COOH and $-NH_2$ in the polydopamine layer. On the other hand, a more hydrophilic surface was obtained on both supports by ultrasound assisted polymerization. The surface free energies (SFE) of the PDA coated membranes are summarized in Table 5.3 and compared with those determined for the uncoated membranes (Table 5.4). The PDA coating obtained in the presence of an ultrasonic horn resulted in a larger increase in the SFE's of both membranes. Mostly, the polar component (σ_s^p) of the SFE was increased since the PDA has polar functional groups, such as OH and NH (Jiang et al., 2011). The increase in the polar component was more pronounced when the PDA was deposited on the hydrophobic PSF support. XPS analysis quantitatively determined the chemical composition of the unmodified and PDA modified membranes. The general survey given in Figure 5.6 shows that unmodified membranes possessed characteristic peaks of C 1s, O 1s, S 2s and S 2p, while the modified ones have

an additional N 1s peak. Sulfur element comes from the PSF and SPES. The nitrogen peak detected only in the modified membranes confirmed the presence of the PDA layer on both supports. To illustrate the effect of ultrasound on the PDA deposition rates, we considered the N/S ratios of the membranes coated by two techniques. Compared with the conventional polymerization technique, the PDA coating with ultrasound assisted polymerization resulted in larger N/S ratio (Table 5.5). AFM images and surface roughness of the PSF and PSF-SPES membranes were given in Figure 5.7 and Table 5.6, respectively. The PDA coating on both membranes increased the surface roughness. However, the membranes coated in the presence of ultrasound had lower roughness values. Ultrasound creates a vibration that prevents aggregate formation on the membrane surfaces during the coating, thus, enabling to produce smoother surfaces. The effect of ultrasound was found more prominent on the roughness of the coated PSF-SPES membrane. The surface morphology of the PSF membranes did not change significantly after coating with the PDA layer as shown in Figure 5.8. However, PDA aggregates were observed on the relatively rough PSF-SPES membrane when coated with conventional polymerization without ultrasound.

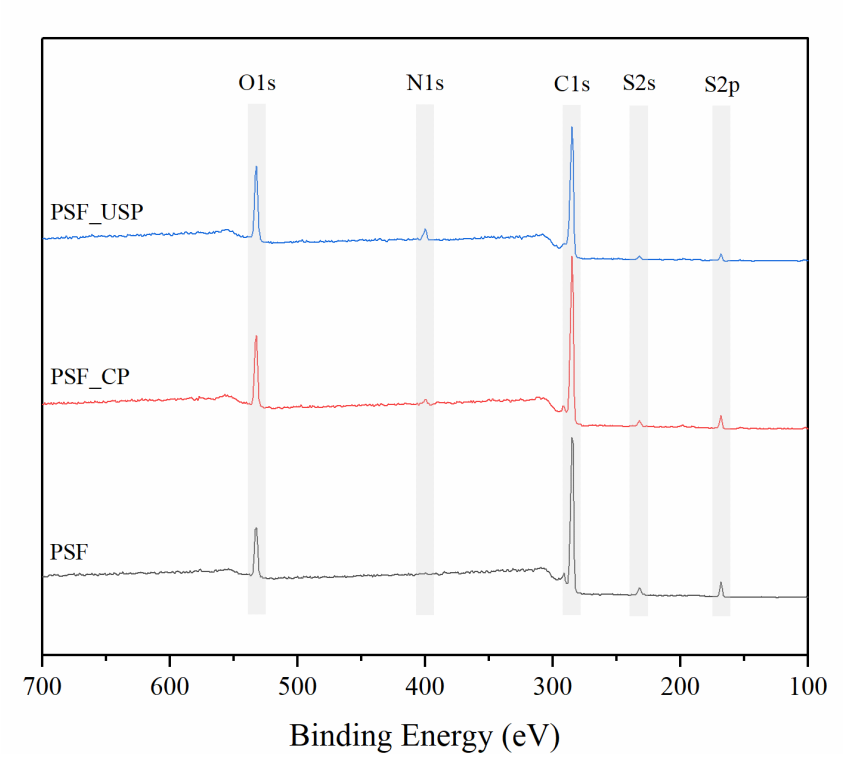

a)

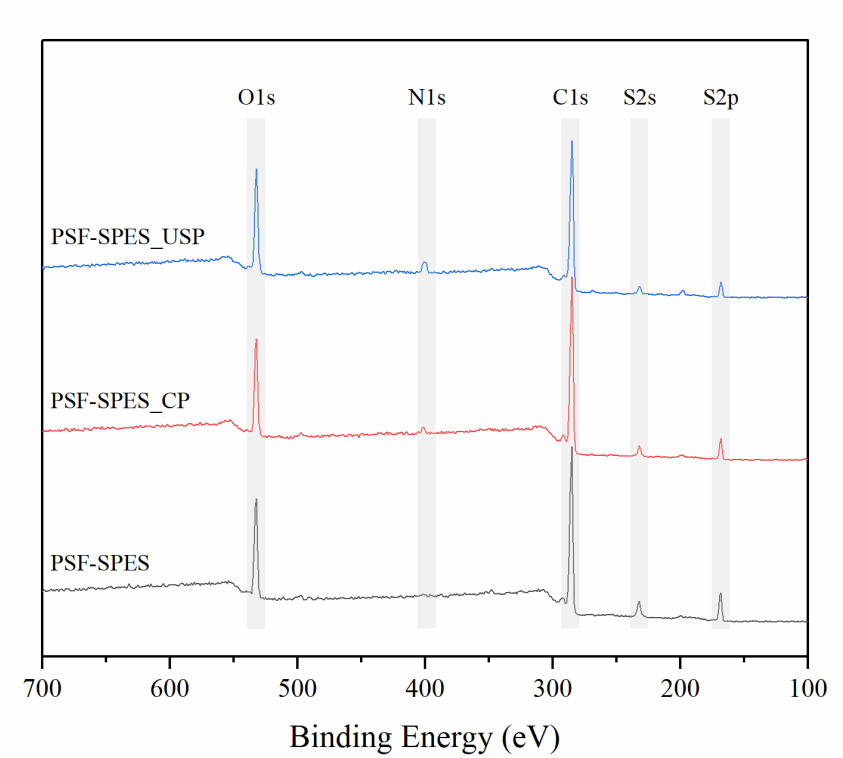

b)

Figure 5.6. The general survey of the bare and modified a) PSF and b) PSF-SPES membranes (CP: Conventional Polymerization, USP: Ultrasound-Assisted Polymerization).

Table 5.2. Contact angles of the bare and PDA coated membranes.

Membranes	Contact Angle (°)			The change in Contact Angle (%)	
	Bare	Conventional Polymerization	Ultrasound-Assisted Polymerization	$(\theta_0-\theta_{CP})/\theta_0$	$(\theta_0-\theta_{USP})/\theta_0$
PSF	97.4±0.2	76.9±0.6	69.9±0.6	21.0	28.2
PSF-SPES	72.9±0.8	58.9±0.8	46.8±0.1	19.1	35.9

θ_0: The contact angle of bare membrane.
θ_{CP}: The contact angle of the PDA coated membrane by conventional polymerization.
θ_{USP}: The contact angle of the PDA coated membrane by ultrasound-assisted polymerization.

Table 5.3. Surface free energy and its components of the PDA coated membranes.

Membranes	Coating technique	Contact Angle (°)		Surface free energy components (mN/m)			$(\sigma_s^p-\sigma_{so}^p)/\sigma_{so}^p$	$(\sigma_s-\sigma_{so})/\sigma_{so}$
		Water	Diiodomethane	σ_s	σ_s^d	σ_s^p		
PSF	CP	76.9±0.6	32.2±0.4	47.1	43.3	3.8	250.9	0.080
	USP	69.9±0.6	31.7±0.4	49.9	43.5	6.4	427.5	0.146
PSF-SPES	CP	58.9±0.8	29.6±0.3	55.7	44.4	11.3	1.2	0.130
	USP	46.8±0.1	31.3±0.5	61.9	43.7	18.2	2.6	0.255

σ_{so}: The total surface free energies of the modified membranes.
σ_{so}^d and σ_{so}^p: Dispersive and polar components of the surface free energies of the modified membranes.
$(\sigma_s-\sigma_{so})/\sigma_{so}$ describes the change in σ_s of the PDA coated membranes in comparison to that of the bare one.
A high value of $(\sigma_s-\sigma_{so})/\sigma_{so}$ means that the total surface free energy of the membranes after the PDA coating increases.

Table 5.4. Surface free energy and its components of the bare membranes.

Membranes	Contact Angle (°)		Surface free energy components(mN/m)		
	Water	Diiodomethane	σ_{so}	σ_{so}^{d}	σ_{so}^{p}
PSF	97.4±0.2	31.6±0.5	43.6	43.5	0.015
PSF-SPES	72.9±0.8	29.8±0.4	49.3	44.3	5.048

σ_{so}: The total surface free energies of the bare membranes.
σ_{so}^{d} and σ_{so}^{p}: Dispersive and polar components of the surface free energies of the bare membranes.

Table 5.5. XPS analysis of the bare and PDA coated membranes.

Membranes	Coating technique	S%	C%	O%	N%	N/S	C/O
PSF	*	3.86	82.74	13.4	-	-	6.17
	CP	3.00	76.82	16.14	4.04	1.35	4.76
	USP	1.82	74.83	19.11	4.24	2.33	3.92
PSF-SPES	*	7.86	71.12	21.02	-	-	3.38
	CP	4.91	73.61	19.53	1.95	0.40	3.77
	USP	3.73	69.03	21.88	5.36	1.44	3.15

* Bare membrane. CP: Conventional polymerization, USP: Ultrasound-assisted polymerization.

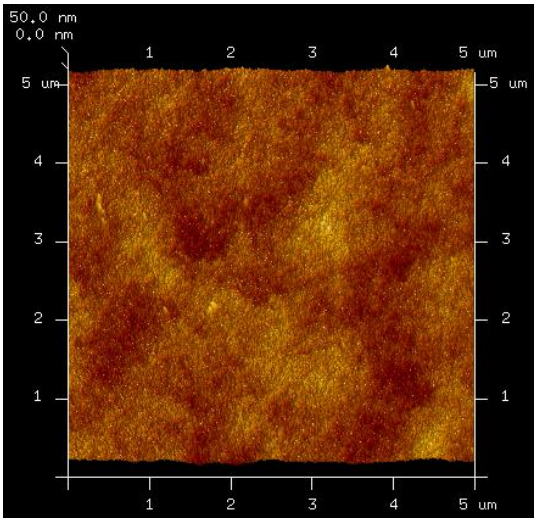

PSF

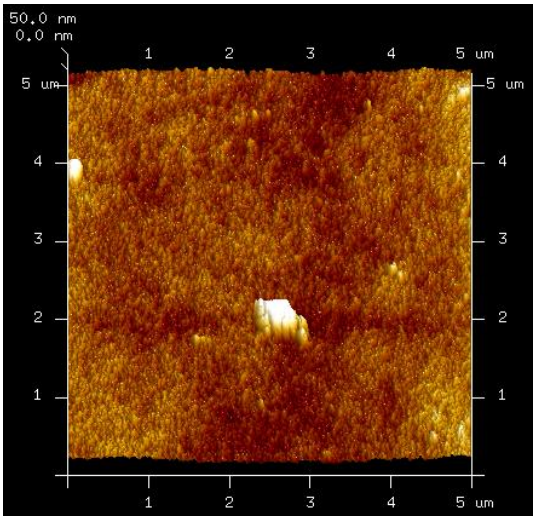

PSF-SPES

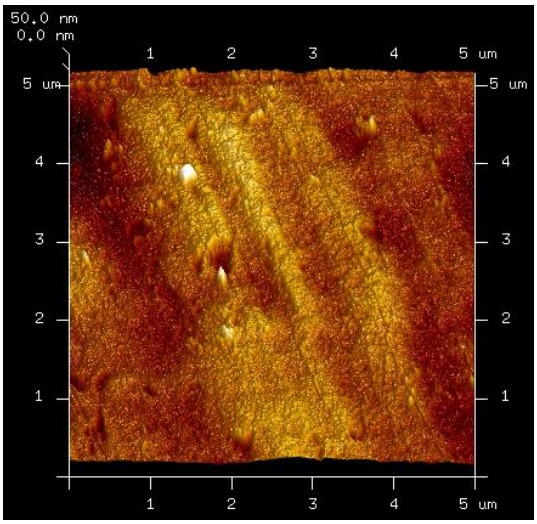

PSF_CP

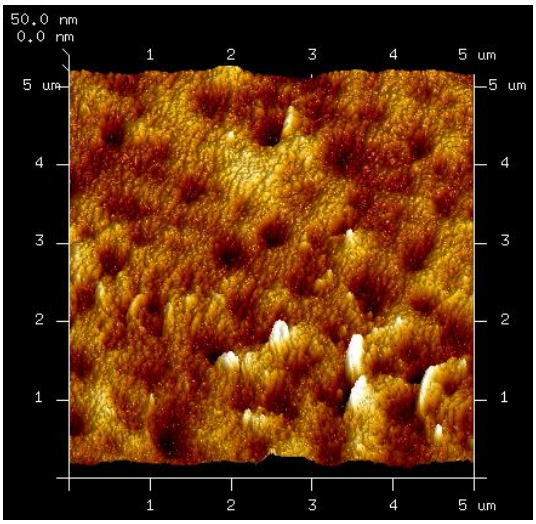

PSF-SPES_CP

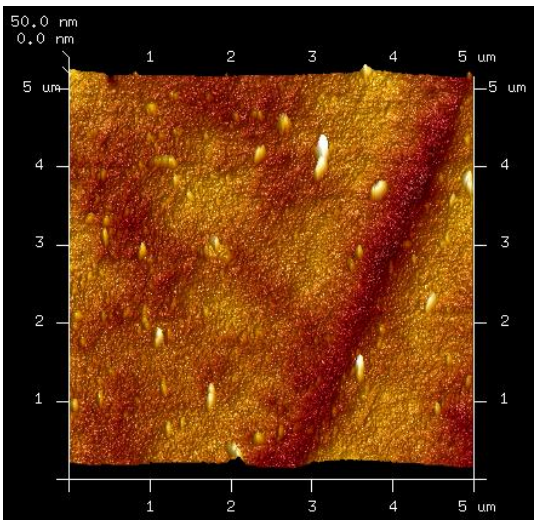

PSF_USP

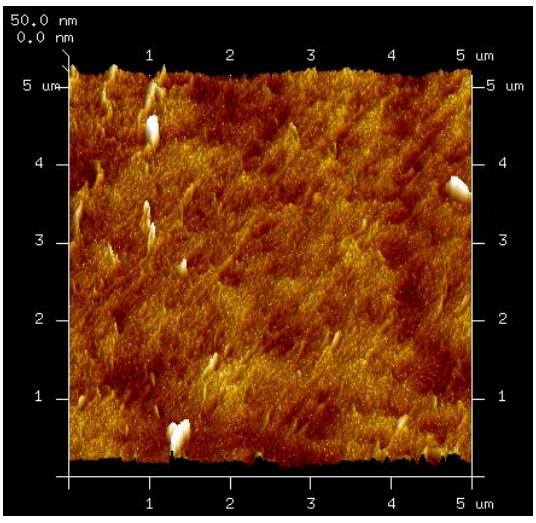

PSF-SPES_USP

Figure 5.7. AFM images of the bare and PDA coated membranes.

Table 5.6. Surface roughness of the bare and PDA coated membranes.

Membranes	R_a (nm)	R_q (nm)
PSF	2.53±0.16	3.15±0.19
PSF_CP	5.41±1.45	7.22±2.01
PSF_USP	3.70±0.76	4.67±0.98
PSF-SPES	3.34±0.01	4.26±0.24
PSF-SPES_CP	8.52±3.18	12.01±4.89
PSF-SPES_USP	4.03±0.45	5.23±0.70

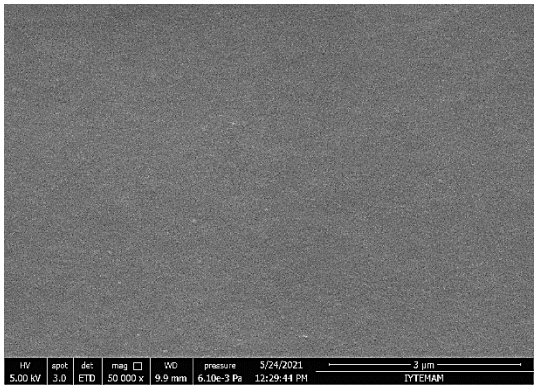

PSF

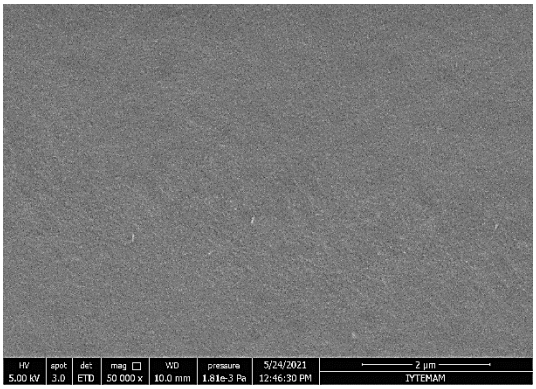

PSF-SPES

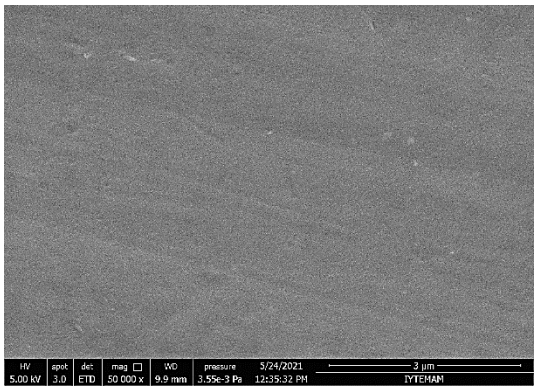

PSF_CP

PSF-SPES_CP

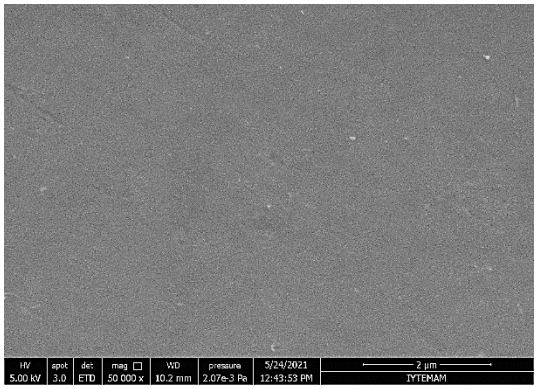

PSF_USP

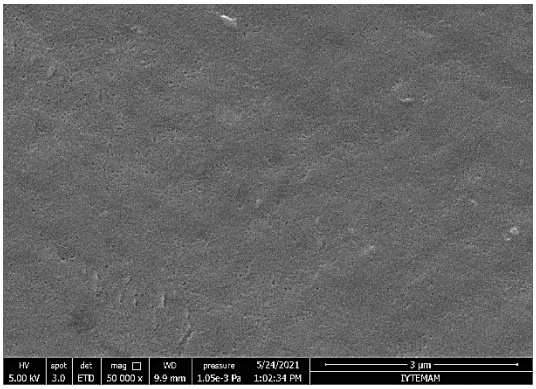

PSF-SPES_USP

Figure 5.8. Surface SEM images of the bare and PDA coated membranes.

5.4. Membrane Filtration Performance

The stability of the membrane structure after ultrasound treatment needs to be checked to verify the applicability of the suggested technique. For this purpose, the pure water permeability (PWP) and PEO 100 kDa rejections before and after ultrasound exposure were measured. As shown in Figure 5.9, the PWP and rejection of both membranes remained constant upon exposure to ultrasound for 1 h. Baek et al. (2017) shortened the PDA coating time on the polyamide reverse osmosis membrane by the use of UV irradiation. However, 30 minute UV irradiation alone caused an increase in NaCl rejection from 1% to ~ 3% indicating the degradation of the polyamide membrane. Similarly, Rupiasih et al (2013) reported the adverse effect of a very short time (2 minute) UV irradiation on the performance of PSF membranes. In this respect, UV irradiation does not seem to be a suitable technique for speeding up the PDA coating. In contrast, the results in Figure 5.9 demonstrated that the ultrasound did not cause any change in the structure of the support membranes within 1 hour PDA coating.

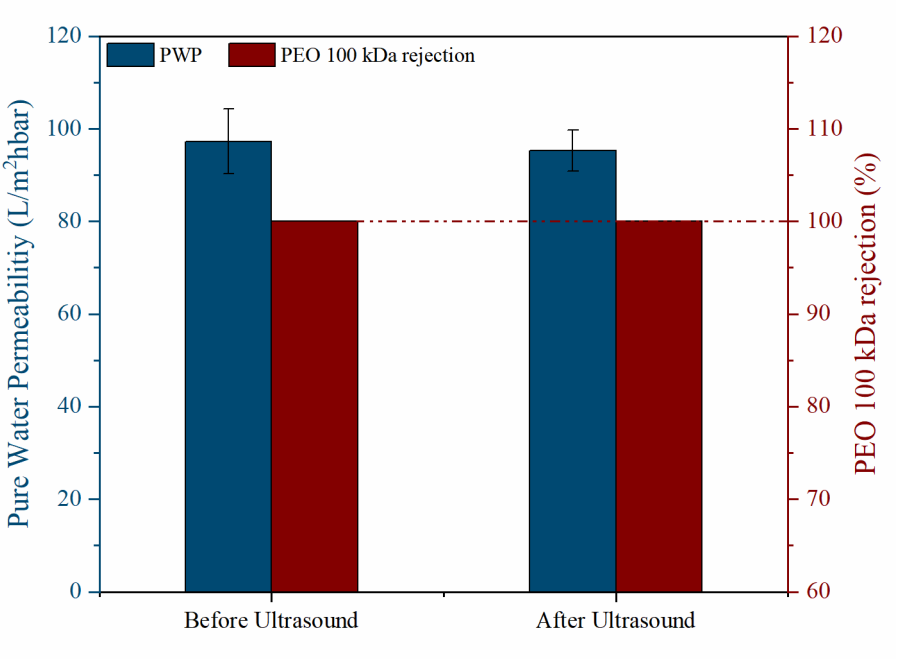

a)

Figure 5.9. Effect of ultrasound on PWP and PEO 100 kDa rejection values of unmodified a) PSF, b) PSF-SPES membranes before and after 1 h ultrasound exposure.

(Cont. on next page)

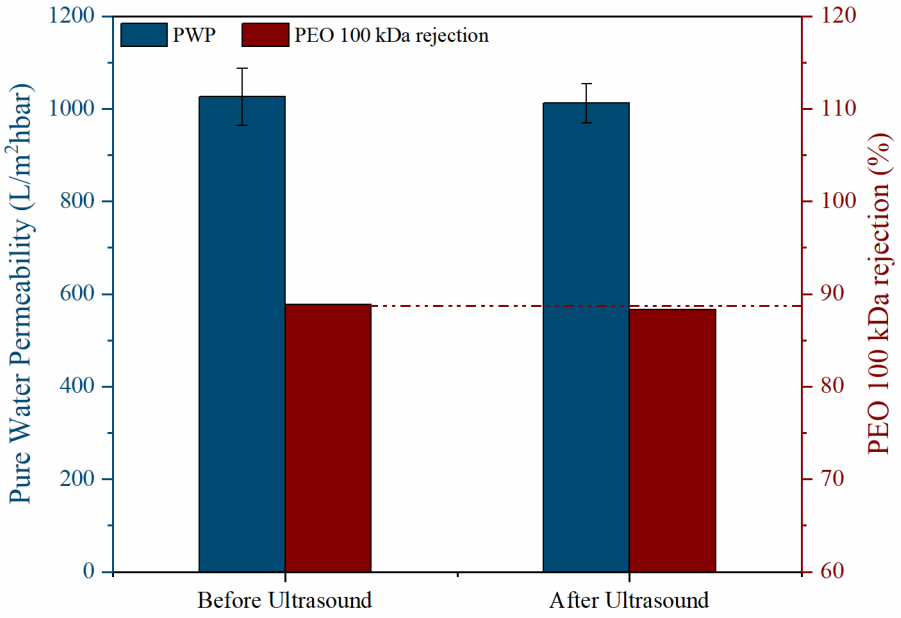

b)

Figure 5.9. Cont.

Figures 5.10 and 5.11 present the change in the PWP and PEG 35 kDa rejection of the membranes upon PDA coating. Dopamine is a small sized molecule and can easily penetrate into the pores. Thus, PDA deposition occurs not only on the surface but also within the membrane pore structure leading to pore constriction and decrease in the permeability and increase in the PEG rejection. The reduction in permeabilities of both membranes when coated with ultrasound was found higher indicating thicker PDA layer formed on the surface and in the pores. This observation was another evidence of enhanced polymerization by the use of ultrasound. The ultrasound was more effective on the coating of the PSF-SPES membrane. The permeability of this membrane decreased by 21.4% and 63.6% when coated with CP and USP techniques. On the other hand, the difference in the water permeabilities of the PSF membranes modified with the two techniques was smaller. This result is in agreement with the FTIR-ATR, contact angle, SFE and XPS analysis results in Tables 5.1-5.3 and 5.5. The PDA coating influenced the pure water permeabilities differently in each membrane. The modification had a larger influence on the PSF membrane due to its smaller pore size. As shown in Table 5.7, the PDA hydraulic resistance on the PSF membrane was significantly higher than the coated PSF-SPES's resistance. Similarly, McCloskey et al., (2010; 2012) reported that after 1 h PDA deposition, the permeability of the PVDF membrane with a nominal pore size of

0.22 µm did not change while the smaller pore sized PSF membrane (18 nm) displayed significant permeability decline.

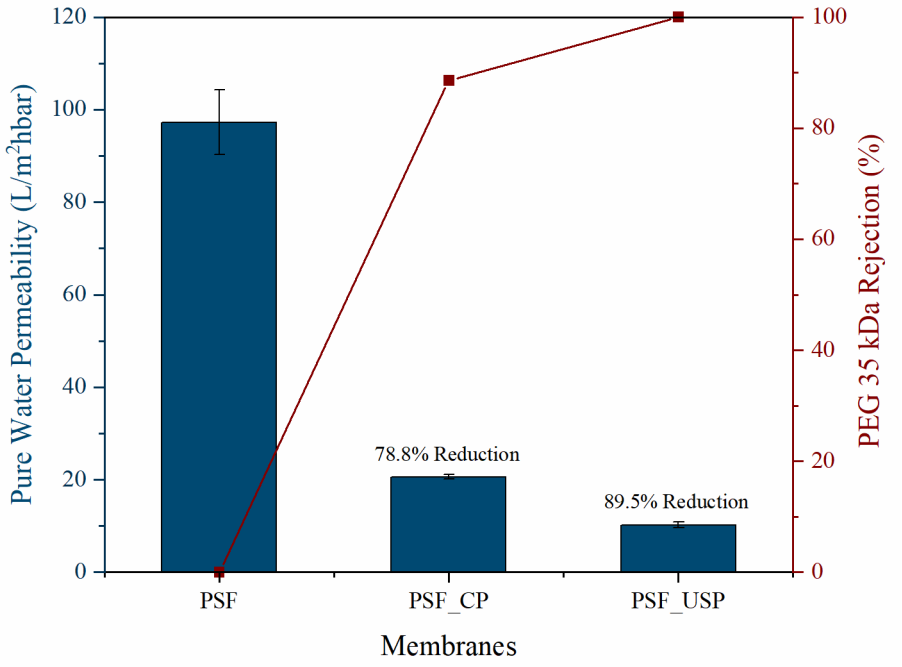

Figure 5.10. The PWP and PEG 35 kDa rejection of the unmodified and PDA coated PSF membranes.

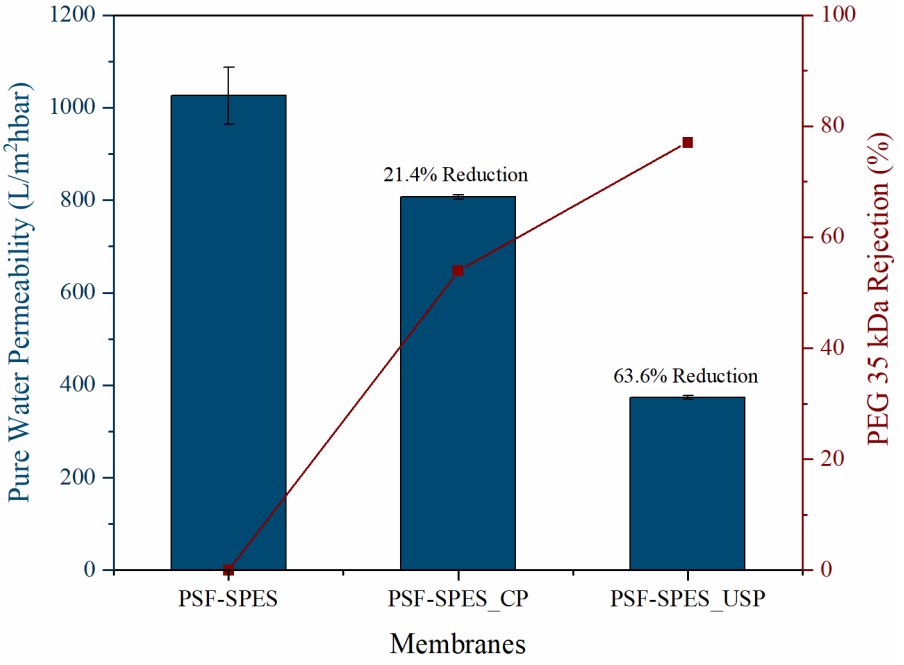

Figure 5.11. The PWP and PEG 35 kDa rejection of the unmodified and PDA coated PSF-SPES membranes.

Table 5.7. Influence of PDA deposition on membrane hydraulic resistance.

Membranes	Hydraulic Resistance x 10^{-10} (m^{-1})	
	PSF	PSF-SPES
Bare	415.7	39.4
PDA coated membranes with CP	1547.8	10.7
PDA coated membranes with USP	3549.9	69.1

The antifouling behavior of the bare and PDA coated membranes was evaluated with dynamic filtration of water/paraffin emulsion. The initial water flux of the membranes was adjusted to the similar value by controlling transmembrane pressure difference (TMP). As shown in Figures 5.12 and 5.13, at the beginning of filtration, the flux decreased sharply due to the accumulation of large oil particles on the membrane surface, consistent with the literature (Ju et al., 2008; He et al., 2016; He et al., 2017; Chen et al., 2009). Flux decline through the PSF-SPES membranes was higher than the PSF membrane due to their larger pore sizes. The PDA coating improved the antifouling properties of the both membranes. The membranes coated with ultrasound-assisted polymerization technique showed lower flux reduction than their counterparts modified with conventional polymerization. This observation is directly related with more PDA deposition by the use of an ultrasound leading to a more hydrophilic surface (Table 5.2). The surface roughness of the membranes did not play a role on the fouling tendencies since the size of oil droplets (Figure 5.14) is significantly larger than the roughness of the membranes. The FRR of the PDA coated PSF-SPES membrane increased from 51.7% to 59.3% in the presence of ultrasound. The PSF membranes coated with and without ultrasound did not display a large difference in their FRRs. This result again confirmed that the ultrasound was more effective on the coating of the PSF-SPES membrane.

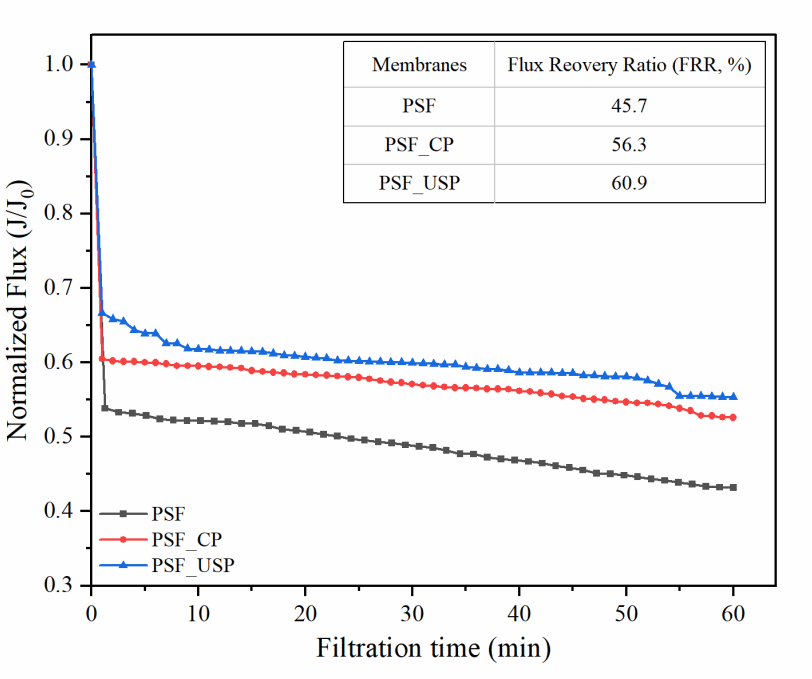

Figure 5.12. Normalized flux of the PSF, PSF_CP, and PSF_USP membranes as a function of time during water/paraffin emulsion filtration. Initial water fluxes of PSF, PSF_CP, and PSF_USP membranes are 19.5±1.4, 20.6±0.5 and 20.4±0.6 L/m^{2}h, respectively.

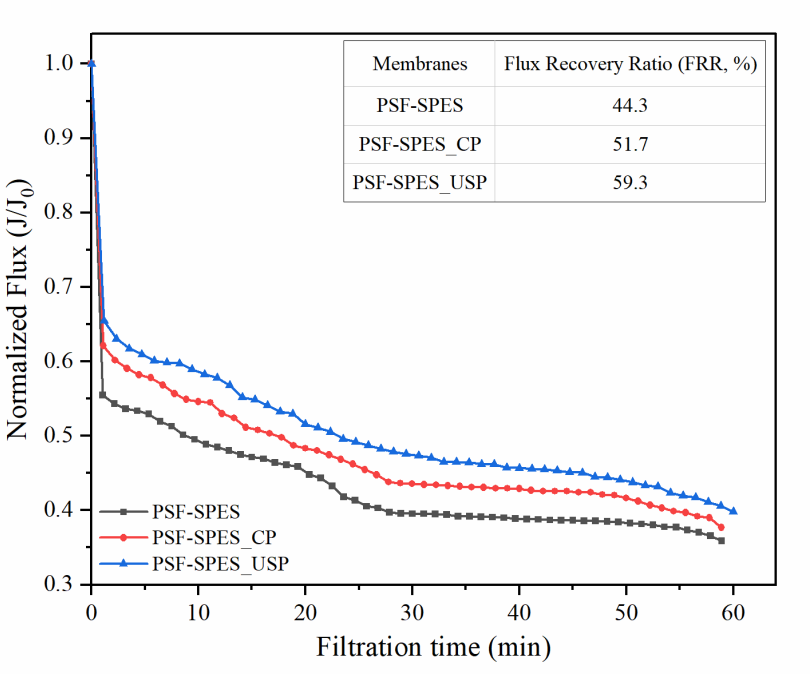

Figure 5.13. Normalized flux of the PSF-SPES, PSF-SPES_CP, and PSF-SPES_USP membranes as a function of time during water/paraffin emulsion filtration. Initial water fluxes of PSF-SPES, PSF-SPES_CP, and PSF-SPES_USP membranes are 410.4±24.8, 403.4±5.1 and 410.4±4.2 L/m^{2}h, respectively.

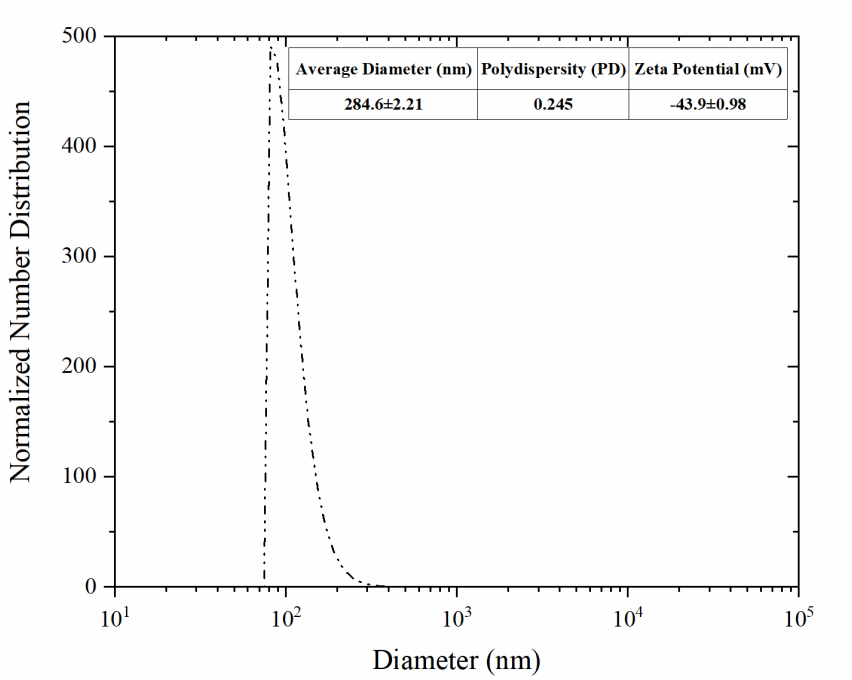

Figure 5.14. Size distribution and zeta potential of water/paraffin emulsion used as synthetic foulant in the experiments.

5.5. Stability of Coating Layer

Recent studies have shown that PDA coatings on different surfaces exhibit strong stability in acidic, neutral, and weak alkaline solutions, but disintegrate in a strongly alkaline condition (Wei et al., 2013; Zhang et al., 2016b; Geng et al., 2020; Yang et al., 2018; Yao et al., 2019; Chang et al., 2016). We also observed a similar behavior, as shown in Figure 5.15, the PDA-coated membranes were more stable in an acidic environment than in alkaline solution. The absorbance measured at 420 nm was used to determine the dissolved PDA in NaOH and HCl solutions. The PSF-SPES membrane modified with ultrasound displayed a significantly lower absorbance value especially in the NaOH solution than its counterpart coated without ultrasound. The XPS analysis results confirmed more PDA deposition on the PSF-SPES membrane in the presence of ultrasound (Table 5.5). Therefore, the results in Figure 5.15 demonstrated that the ultrasound assisted polymerization had also a positive impact on the stability of the PDA coatings especially in NaOH solution. The aggregates were observed on the PSF-SPES membrane modified with conventional polymerization. The lower stability of the PDA layer on the PSF-SPES membrane formed with conventional polymerization could be due to the deposition of PDA as aggregates (Figure 5.8). In addition, the ultrasound may have

changed the mechanism of PDA deposition in such a way that the bonding between the PDA and the substrate surface is stronger. In literature, there is still not an acceptable polymerization mechanism for the PDA (Dreyer et al., 2013). Nevertheless, further studies are needed to investigate the effect of ultrasound on the deposition mechanism and the binding strength.

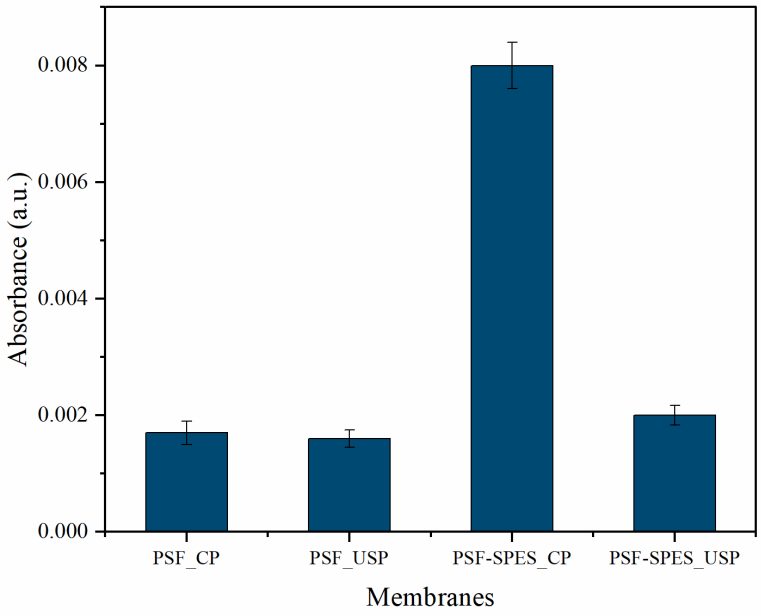

a)

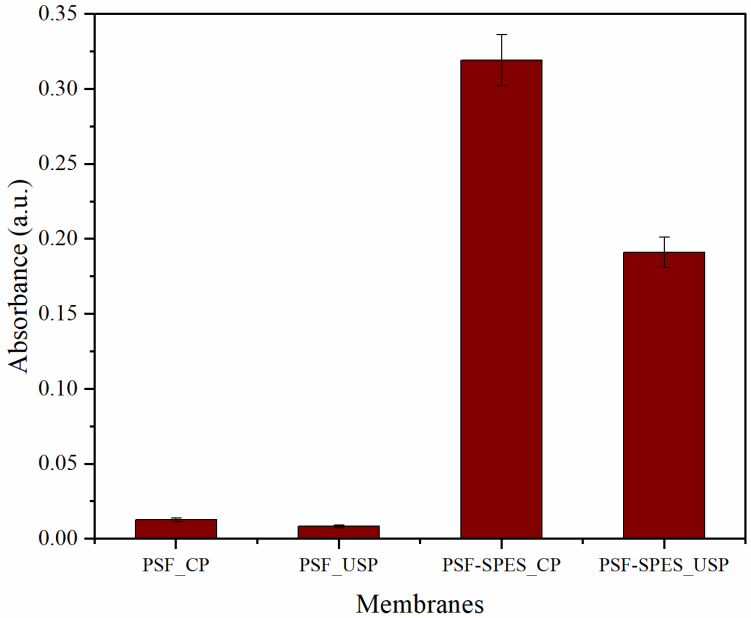

b)

Figure 5.15. UV-visible spectra of the eluent of PDA coated membranes immersed in strongly acidic and alkaline solutions: a) 0.1 M HCl, b) 0.1 M NaOH solutions. The immersion time is 24 h.

5.6. Conclusion

In conclusion, we report for the first time that the slow-kinetics of dopamine polymerization on polymeric membrane surfaces can be accelerated by ultrasound triggering. The bulk polymerization studies proved that the acceleration occurs through the decomposition of water molecules to the ROSs. All the surface characterization results, and oily water filtration studies demonstrated that the kinetics of PDA coating on both membranes was enhanced. The structures of the bare membranes were not adversely affected by the ultrasound exposure. The PDA deposition improved oil/water fouling resistance of the membranes. On the other hand, the membranes modified with ultrasound had higher fouling resistance and chemical stability than their counterparts coated without ultrasound. The ultrasound was found to have more prominent effect on the PSF-SPES support. This finding can be explained by more hydrophilic nature of the PSF-SPES leading to more contact between the dopamine solution and the membrane surface during the polymerization. The ultrasound-assisted polymerization does not require any chemical oxidizing agents and can be applied at room temperature on various polymeric membranes without changing the bulk structures. Most importantly, the method can be applied at large industrial scales which makes it convenient for the modification of large membrane areas. We anticipate that an environmentally friendly ultrasound-assisted polymerization could enhance the efficiency of the PDA coating on membranes for large scale applications by shortening the coating time.

CHAPTER 6

CONCLUSION

This thesis study aimed to manufacture fouling resistant polymeric NF and UF membranes using unique approaches that enable easy production and industrial scalability. The approaches used in the manufacturing of the polymeric membranes and their advantages are summarised as follows:

In Chapter 2, PAI based positively charged flat sheet NF membrane was prepared in a single step. The positive surface charge was provided by the PEI dissolved in the coagulation bath. During phase inversion, PEI made in situ chemical crosslinking with PAI at the polymer/coagulation bath interface. The highest positive charge density was obtained at alkaline pH in the coagulation bath. The membrane had high divalent ions selectivity high PWP and good stability in acidic solution. In addition, the fouling test results carried out under the dynamic filtration of BSA demonstrated that the membrane had good fouling resistance and flux recovery ratio.

In Chapter 3, PSF-SPES blend membranes were prepared with the phase inversion technique. Strong bactericidal agent, cetyltrimethylammonium bromide, was dissolved in the coagulation bath and incorporated into the membrane through the electrostatic interaction between the positively charged quaternary ammonium group (NR_4^+) in CTAB and the negatively charged sulfonic acid (SO_3^-) group in SPES. Among three CTAB concentrations investigated, the highest antibacterial activity against Gram-positive (*S. aureus*) and Gram-negative (*E. coli*) bacteria was observed at the critical micelle concentration. The stability of CTAB in the membrane structure was proved with leaching experiments and antibacterial activity measurements conducted after storing the membrane in 1M NaCl up to 1 month and filtering 1M NaCl solution. Leaching experiments that continued up to 30 days demonstrated that 96% of the CTAB remained in this membrane. Furthermore, at the end of 1 month of storage in 1M NaCl solution, no change was observed in the antibacterial activity of this membrane compared to the fresh membrane.

In Chapter 4, a new co-deposition strategy was used to impart the anti-biofouling behavior onto the commercial PES UF membrane without changing the size selectivity and PWP of the support membrane. To this end, three different CTAB concentrations (<CMC, =CMC and >CMC) were co-deposited with dopamine in the presence of nitrogen (N_2) gas backflow. The PWP and pore size of the support membrane did not change with co-deposition, confirming the benefit of N_2 backflow in mitigating the solution intrusion phenomenon. Among three different CTAB concentrations used in dopamine solution, the membrane functionalized with dopamine and CTAB at its critical micelle concentration exhibited the best antibiofouling activity against Gram-positive (*S. aureus*) and Gram-negative (*E. coli*) bacteria. The CTAB in the structure of this membrane remained stable when stored in 1 M NaCl for 3 months. These findings demonstrated the potential of the co-deposition approach used in this study to modify commercial ultrafiltration membranes without compromising their pore size and flux.

In Chapter 5, ultrasound was used as green, controllable, and facile pathway to accelerate the polymerization kinetics of dopamine. It was found that the ultrasound dramatically accelerated the slow kinetics of dopamine in the bulk phase and increased the deposition rate of the PDA coating on the surface of the PSF and PSF-SPES membranes. The PDA coated membranes prepared by ultrasound-assisted polymerization had more surface free energy, higher hydrophilicity, better fouling resistance against water/paraffin emulsion, higher flux recovery ratio and higher stability in strong acid and alkaline solution than their counterparts modified without ultrasound.

In conclusion, all the membrane preparation protocols proposed in this thesis study can be adapted for large-scale production. In addition, they contribute to the green membrane production efforts by eliminating the need for pore formers, pre-treatment/post-treatment of the support membranes, antibacterial agent and minimizing the leaching risk from the membranes.

REFERENCES

Arkhangelsky, E., Gitis, V., 2008. Effect of transmembrane pressure on rejection of viruses by ultrafiltration membranes. Sep. Purif. Technol. 62, 619-628.

Arsuaga, J.M., Sotto, A., Rosario, G., Martínez, A., Molina, S., Teli, S.B., Abajo, J., 2013. Influence of the type, size, and distribution of metal oxide particles on the properties of nanocomposite ultrafiltration membranes. J. Membr. Sci. 428, 131-141.

Arzillo, M., Mangiapia, G., Pezzella, A., Heenan, R.K., Radulescu, A., Paduano, L., d'Ischia, M., 2012. Eumelanin buildup on the nanoscale: Aggregate growth/assembly and visible absorption development in biomimetic 5,6-dihydroxyindole polymerization. Biomacromolecules 13, 2379-2390.

Ba, C., Langer, J., Economy, J., 2009. Chemical modification of P84 copolyimide membranes by polyethyleneimine for nanofiltration. J. Membr. Sci. 327, 49-58.

Baek, Y., Freeman, B.D., Zydney, A.L., Yoon, J., 2017. A facile surface modification for antifouling reverse osmosis membranes using polydopamine under UV irradiation. Ind. Eng. Chem. Res. 56, 19, 5756-5760.

Bai, X., Zhang, Y., Wang, H., Zhang, H., Liu, J., 2013. Study on the modification of positively charged composite nanofiltration membrane by TiO_2 nanoparticles. Desalination 313, 57-65.

Baker, S.M., Leach, K.A., Devereaux, C.E., Gragson, D.E., 2000. Controlled patterning of diblock copolymers by monolayer Langmuir-Blodgett deposition. Macromolecules 33, 5432-5436.

Baker, R.W., 2012. Membrane Technology and Applications, 3rd ed., John Wiley & Sons, Ltd., New York, NY.

Banerjee, I., Pangule, R.C., Kane, R.S., 2011. Antifouling coatings: recent developments in the design of surfaces that prevent fouling by proteins, bacteria, and marine organisms. Adv. Mater. 23, 690-718.

Barclay, T.G., Hegab, H.M., Clarke, S.R., Markovic, M.G., 2017. Versatile surface modification using polydopamine and related polycatecholamines: Chemistry, structure, and applications. Adv. Mater. Interfaces 4, 1601192.

Bayır, H., 2005. Reactive oxygen species. Crit. Care Med. 33, S498.

Belfort, G., Davis, R.H., Zydney, A.L., 1994. The behavior of suspensions and macromolecular solutions in crossflow microfiltration. J. Membr. Sci. 96 (1-2), 1-58.

Birkner, M., Ulbricht, M., 2015. Ultrafiltration membranes with markedly different pH- and ion-responsivity by photografted zwitterionic polysulfobetain or polycarbobetain. J. Membr. Sci. 494, 57-67.

Boributh, S., Chanachai, A., Jiraratananon, R., 2009. Modification of PVDF membrane by chitosan solution for reducing protein fouling. J. Membr. Sci. 342, 97-104.

Bowen, W.R., Mohammad, A.W., Hilal, N., 1997. Characterization of nanofiltration membranes for predictive purposes - use of salts, uncharged solutes and atomic force microscopy. J. Membr. Sci. 126, 91-105.

Breite, D., Went, M., Prager A., Schulze, A., 2016. The critical zeta potential of polymer membranes: How electrolytes impact membrane foulings. RSC Adv. 6, 98180-98189.

Cao, X., Tang, M., Liu, F., Nie, Y., Zhao, C., 2010. Immobilization of silver nanoparticles onto sulfonated polyethersulfone membranes as antibacterial materials. Colloid Surfaces B 81, 555-562.

Castrillón, S.R.-V., Lu, X., Shaffer, D.L., Elimelech, M., 2014. Amine enrichment and poly(ethylene glycol)(PEG) surface modification of thin-film composite forward osmosis membranes for organic fouling control. J. Membr. Sci. 450 (2014) 331-339.

Chang, C.C., Kolewe, K.W., Li, Y., Kosif, I., Freeman, B.D., Carter, K. R., Schiffman, J.D., Emrick, T., 2016. Underwater superoleophobic surfaces prepared from polymer zwitterion/ dopamine composite coatings. Adv. Mater. Interfaces 3, 1500521.

Chassepot, A., Ball, V., 2014. Human serum albumin and other proteins as templating agents for the synthesis of nanosized dopamine-eumelanin. J. Colloid Interface Sci. 414, 97-102.

Chen, D.; Wu, M.; Li, B.; Ren, K.; Cheng, Z.; Ji, J.; Li, Y., Sun, J., 2015. Layer-by-layer-assembled healable antifouling films. Adv. Mater. 27 (39), 5882-5888.

Chen, W., McCarthy, T.J., 1997. Layer-by-layer deposition: A tool for polymer surface modification. Macromolecules 30, 78-86.

Chen, Y., Zhang, Y., Zhang, H., Liu, J., Song, C., 2013. Biofouling control of halloysite nanotubes-decorated polyethersulfone ultrafiltration membrane modified with chitosan-silver nanoparticles. Chem. Eng. J. 228, 12-20.

Cheng, S., Oatley, D.L., Williams, P.M., Wright, C.J., 2012. Characterisation and application of a novel positively charged nanofiltration membrane for the treatment of textile industry wastewaters. Water Res. 46, 33-42.

Chiang, Y.C., Hsub, Y.Z., Ruaan, R.C., Chuang, C.J., Tung, K.L., 2009. Nanofiltration membranes synthesized from hyperbranched polyethyleneimine. J. Membr. Sci. 326, 19-26.

Cihanoğlu, A., Altinkaya, S.A., 2018. A facile approach for preparation of positively charged nanofiltration membranes by in-situ crosslinking between polyamide-imide and polyethylenimine. Sep. Purif. Technol. 207, 353-362.

Cihanoğlu, A., Altinkaya, S.A., 2020. A facile route to the preparation of antibacterial polysulfone-sulfonated polyethersulfone ultrafiltration membranes using a cationic surfactant cetyltrimethylammonium bromide. J. Membr. Sci. 594, 117438

Collins, J., McKenzie, T.G., Nothling, M.D., Allison-Logan, S., Ashokkumar, M., Qiao, G.G., 2019. Sonochemically initiated RAFT polymerization in organic solvents. Macromolecules 52, 185-195.

Coppola, L., Gianferri, R., Nicotera, I., Oliviero, C., Ranieri, G.A., 2004. Structural changes in CTAB/H_2O mixtures using a rheological approach. Phys. Chem. Chem. Phys. 6, 2364-2372.

Cornelissen, E.R., Vrouwenvelder, J.S., Heijman, S.G.J., Viallefont, X.D., Kooij, D.V.D., Wessels, L.P., 2007. Periodic air/water cleaning for control of biofouling in spiral wound membrane elements. J. Membr. Sci. 287, 94-101.

Cui, Y., Yao, Z.K., Zheng, K., Du, S.Y., Zhu, B.K., Zhu, L.P., Du, C.H., 2015. Positively charged nanofiltration membrane formed by quaternization and cross-liking of blend PVC/P(DMA-co-MMA) precursors. J. Membr. Sci. 492, 187-196.

Dinis, T.C.P., Madeira, V.M.C., Almeida, L.M., 1994. Action of phenolic derivatives (acetaminophen, salicylate, and 5-aminosalicylate) as inhibitors of membrane lipid peroxidation and as peroxyl radical scavengers. Arch. Biochem. Biophys. 315, 161-169.

Dobosz, K.M., Kuo-LeBlanc, C.A., Emrick, T., Schiffman, J.D., 2019. Antifouling ultrafiltration membranes with retained pore size by controlled deposition of zwitterionic polymers and poly(ethylene glycol). Langmuir 35 (5), 1872-1881.

Dreyer, D.R., Miller, D.J., Freeman, B.D., Paul, D.R., Bielawski, C.W., 2013. Perspectives on poly(dopamine). Chem. Sci. 4, 3796-3802.

Du, X., Li, L., Li, J., Yang, C., Frenkel, N., Welle, A., Heissler, S., Nefedov, A., Grunze, M., Levkin, P.A., 2014. UV-triggered dopamine polymerization: Control of polymerization, surface coating, and photopatterning. Adv. Mater. 26, 8029-8033.

Elimelech, M., Zhu, X., Childress, A.E. Hong, S., 1997. Role of membrane surface morphology in colloidal fouling of cellulose acetate and composite aromatic polyamide reverse osmosis membranes. J. Membr. Sci. 127 (1), 101-109.

Fang, W., Shi, L., Wang, R., 2013. Interfacially polymerized composite nanofiltration hollow fiber membranes for low-pressure water softening. J. Membr. Sci. 430, 129-139.

Faure, E., Falentin-Daudré, C., Jérôme, C., Lyskawa, J., Fournier, D., Woisel, P., Detrembleur, C., 2013. Catechols as versatile platforms in polymer chemistry. Prog. Polym. Sci. 38 (1), 236-270.

Fei, P., Liao, L., Meng, J., Cheng, B., Hu, X., Song, J., 2018. Non-leaching antibacterial cellulose triacetate reverse osmosis membrane via covalent immobilization of quaternary ammonium cations. Carbohyd. Polym. 181, 1102-1111.

Feng, Y., Lin, X., Li, H., He, L., Sridhar, T., Suresh, A.K., Bellare, J., Wang, H., 2014. Synthesis and characterization of Chitosan-grafted BPPO ultrafiltration composite membranes with enhanced antifouling and antibacterial properties. Ind. Eng. Chem. Res. 53, 14974-14981.

Gao, J., Sun, S.P., Zhu, W.P., Chung, T.S., 2014. Polyethyleneimine (PEI) cross-linked P84 nanofiltration (NF) hollow fiber membranes for Pb^{2+} removal. J. Membr. Sci. 452, 300-310.

Gherasim, C.V., Luelf, T., Roth, H., Wessling, M., 2016. Dual-charged hollow fiber membranes for low-pressure nanofiltration based on polyelectrolyte complexes: one-step fabrication with tailored functionalities. ACS Appl. Mater. Interfaces 8, 19145-19157.

Gilbertson, L.M., Albalghiti, E.M., Fishman, Z.S., Perreault, F., Corredor, C., Posner, J.D., Elimelech, M., Pfefferle, L.D., Zimmerman, J.B., 2016. Shape-dependent surface reactivity and antimicrobial activity of nano-cupric oxide. Environ. Sci. Technol. 50 (7), 3975-3984.

Goh, K., Setiawan, L., Wei, L., Si, R., Fane, A.G., Wang, R., Chen, Y., 2015. Graphene oxide as effective selective barriers on a hollow fiber membrane for water treatment process. J. Membr. Sci. 474, 244-253.

Guillen, G.R., Pan, Y., Li, M., Hoek, E.M.V., 2011. Preparation and characterization of membranes formed by nonsolvent induced phase separatıon: a review. Ind. Eng. Chem. Res. 50 (7), 3798-3817.

Guo, H., Wang, Z., Liu, Y., Huo, P., Gu, J., Zhao, F., 2020. Synthesis and characterization of novel zwitterionic poly(aryl ether oxadiazole) ultrafiltration membrane with good antifouling and antibacterial properties. J. Membr. Sci. 611, 118337.

Hadidi, M., Zydney, A.L., 2014. Fouling behavior of zwitterionic membranes: Impact of electrostatic and hydrophobic interactions. J. Membr. Sci. 452, 97-103.

Han, L., Xiang, L., Zhang, J., Chen, J., Liu, J., Yan, B., Zeng, H., 2018. Biomimetic Lubrication and surface interactions of dopamine-assisted zwitterionic polyelectrolyte coatings. Langmuir 34, 11593-11601.

Hester, J.F., Banerjee, P., Mayes, A.M., 1999. Preparation of protein-resistant surfaces on poly(vinylidene fluoride) membranes via surface segregation. Macromolecules 32, 1643-1650.

Hoek, E.M.V., Bhattacharjee, S., Elimelech, M., 2003. Effect of membrane surface roughness on colloid-membrane DLVO interactions. Langmuir 19, 11, 4836-4847.

Hoek, E.M.V., Ghosh, A.K. , Huang, X., Liong, M., Zink, J.I., 2011. Physical–chemical properties, separation performance, and fouling resistance of mixed-matrix ultrafiltration membranes. Desalination 283, 89-99.

Hoek, E.M.V., Hong, S., Elimelech, M., 2001. Influence of membrane surface properties on initial rate of colloidal fouling of reverse osmosis and nanofiltration membranes. J. Membr. Sci. 188 (1), 115-128.

Hoek, E.M.V., Tarabara, V.V., 2013. Encyclopedia of membrane science and technology, John Wiley & Sons Canada, Limited, Hoboken, NJ.

Hong, S., Elimelech, M., 1997. Chemical and physical aspects of natural organic matter (NOM) fouling of nanofiltration membranes. J. Membr. Sci. 132 (2), 159-181.

Hou, S., Dong, X., Zhu, J., Zheng, J., Bi, W., Li, S., Zhang, S., 2017. Preparation and characterization of an antibacterial ultrafiltration membrane with N-Chloramine functional groups. J. Colloid Interf. Sci. 496, 391-400.

Hu, X., Lin, X., Zhao, H., Chen, Z., Yang, J., Li, F., Liu, C., Tian, F., 2016. Surface functionalization of polyethersulfone membrane with quaternary ammonium salts for contact-active antibacterial and anti-biofouling properties. Materials 9, 376.

Huang, Y.W., Wang, Z.M., Yan, X., Chen, J., Guo, Y.J., Lang, W.Z., 2017. Versatile polyvinylidene fluoride hybrid ultrafiltration membranes with superior antifouling, antibacterial and self-cleaning properties for water treatment. J. Colloid Interf. Sci. 505, 38-48.

Ingole, P.G., Choi, W.K., Baek, I.H., Lee, H.K., 2015. Highly selective thin film composite hollow fiber membranes for mixed vapor/gas separation. RSC Adv. 5, 78950.

Ji, Y., An, Q., Zhao, Q., Chen, H., Gao, C., 2011. Preparation of novel positively charged copolymer membranes for nanofiltration. J. Membr. Sci. 376, 254-265.

Jiang, J., Zhu, L., Zhu, L., Zhu, B., Xu, Y., 2011. Surface characteristics of a self-polymerized dopamine coating deposited on hydrophobic polymer films. Langmuir 27, 14180-14187.

Jiang, S., Cao, Z., 2010. Ultralow-fouling, functionalizable, and hydrolyzable zwitterionic materials and their derivatives for biological applications. Adv. Mater. 22, 920-932.

Kakihana, Y., Cheng, L., Fang, L.F., Wang, S.Y., Jeon, S., Saeki, D., Rajabzadeh, S., Matsuyama, H., 2017. Preparation of positively charged PVDF membranes with improved antibacterial activity by blending modification: effect of change in membrane surface material properties. Colloid Surfaces A 533, 133-139.

Kaner, P., Johnson, D.J., Seker, E., Hilal, N., Altinkaya, S.A., 2015. Layer-by-layer surface modification of polyethersulfone membranes using polyelectrolytes and AgCl/TiO_2 xerogels. J. Membr. Sci. 493, 807-819.

Kang, B., Li, Y.D., Liang, J., Yan, X., Chen, J., Lang, W.Z., 2016. Novel PVDF hollow fiber ultrafiltration membranes with antibacterial and antifouling properties by embedding N-Halamine functionalized multiwalled carbon nanotubes (MWNTs). RSC Adv. 6, 1710-1721.

Kang, K., Lee, K.H., Han, Y.M., Gao, H., Xie, S.E., Muller, D.A., Park, J., 2017. Layer-by-layer assembly of two-dimensional materials into wafer-scale heterostructures. Nature 2017, 550, 229-233.

Kang, S., Herzberg, M., Rodrigues, D.F., Elimelech, M., 2008. Antibacterial effects of carbon nanotubes: size does matter. Langmuir 24, 6409-6413.

Kang, S., Pinault, M., Pfefferle, L.D., Elimelech, M., 2007. Single-walled carbon nanotubes exhibit strong antimicrobial activity. Langmuir 23, 8670-8673.

Kang, S.M., Hwang, N.S., Yeom, J., Park, S.Y., Messersmith, P.B., Choi, I.S., Langer, R., Anderson, D.G., Lee, H., 2012. One-step multipurpose surface functionalization by adhesive catecholamine. Adv. Funct. Mater. 22, 2949-2955.

Karan, S., Jiang, Z., Livingston, A.G., 2015. Sub–10 nm polyamide nanofilms with ultrafast solvent transport for molecular separation. Science 348, 1347-1351.

Karkhanechi, H., Takagi, R., Matsuyama, H., 2014. Enhanced antibiofouling of RO membranes via polydopamine coating and polyzwitterion immobilization. Desalination 337, 23-30

Kasemset, S., He, Z., Miller, D.J., Freeman, B.D., Sharma, M.M., 2016. Effect of polydopamine deposition conditions on polysulfone ultrafiltration membrane properties and threshold flux during oil/ water emulsion filtration. Polymer 97, 247-257.

Kasemset, S., Lee, A., Miller, D.J., Freeman, B.D., Sharma, M.M., 2013. Effect of polydopamine deposition conditions on fouling resistance, physical properties, and permeation properties of reverse osmosis membranes in oil/water separation. J. Membr. Sci. 208, 425-426.

Kasemset, S., Wang, L., He, Z., Miller, D.J., Kirschner, A., Freeman, B.D., Sharma, M.M., 2017. Influence of polydopamine deposition conditions on hydraulic permeability, sieving coefficients, pore size and pore size distribution for a polysulfone ultrafiltration membrane. J. Membr. Sci. 522, 100-115.

Kaur, R., Liu, S., 2016. Antibacterial surface design-contact kill. Prog. Surf. Sci. 91, 136-153.

Khan, M.T., Hong, P.Y., Nada, N., Croue, J.P., 2015. Does chlorination of seawater reverse osmosis membranes control biofouling?. Water Res. 78, 84-97.

Khoerunnisa, F., Kulsum, C., Dara, F., Nurhayati, M., Nashrah, N., Fatimah, S., Pratiwi, A., Hendrawan, H., Nasir, M., Ko, Y.G., Ng, E.P., Opaprakasit, P., 2021. Toughened chitosan-based composite membranes with antibiofouling and antibacterial properties via incorporation of benzalkonium chloride. RSC Adv. 11, 16814

Kim, K.J., Fane, A.G., Nystrom, M., Pihlajamaki, A., Bowen, W.R., Mukhtar, H., 1996. Evaluation of electroosmosis and streaming potential for measurement of electric charges of polymeric membranes. J. Membr. Sci. 116, 149-159.

Kim, S., Ozaki, H., Kim, J., 2006. Effect of pH on the rejection of inorganic salts and organic compound using nanofiltration membrane. Korean J. Chem. Eng. 23, 28-33.

Kochkodan, V., Hilal, N.A., 2015. Comprehensive review on surface modified polymer membranes for biofouling mitigation. Desalination 356, 187-207.

Kolewe, K.W., Dobosz, K.M., Emrick, T., Nonnenmann, S.S., Schiffman, J.D., 2018. Fouling resistant hydrogels prepared by the swelling-assisted infusion and polymerization of dopamine. ACS Appl. Bio Mater. 1, 33-41.

Krishnamoorthy, M., Hakobyan, S., Ramstedt, M., Gautrot, J.E., 2014. Surface-initiated polymer brushes in the biomedical field: Applications in membrane science, biosensing, cell culture, regenerative medicine and antibacterial coatings. Chem. Rev. 114 (21), 10976-11026.

Lee, H., Dellatore, S.M., Miller, W.M., Messersmith, P.B., 2007. Mussel-inspired surface chemistry for multifunctional coatings. Science 318 (5849), 426-430.

Lee, M., Lee, S.H., Oh, I.K., Lee, H., 2017. Microwave-accelerated rapid, chemical oxidant-free, material-independent surface chemistry of poly(dopamine). Small 13, 1600443.

Li, M., Lv, Z., Zheng, J., Hu, J., Jiang, C., Ueda, M., Zhang, X., Wang, L., 2017b. Positively charged nanofiltration membrane with dendritic surface for toxic element removal. ACS Sustainable Chem. Eng. 5, 784-792.

Li, Q., Imbrogno, J., Belfort, G., Wang, X.L., 2015a. Making polymeric membranes antifouling via “grafting from” polymerization of zwitterions. J. Appl. Polym. Sci. 132, 41781(1-12).

Li, W., Shi, C., Zhou, A., He, X., Sun, Y., Zhang, J., 2017a. A positively charged composite nanofiltration membrane modified by EDTA for LiCl/$MgCl_2$ separation. Sep. Purif. Technol. 186, 233-242.

Li, Y., Su, Y., Li, J., Zhao, X., Zhang, R., Fan, X., Zhu, J., Ma, Y., Liu, Y., Jiang, Z., 2015b. Preparation of thin film composite nanofiltration membrane with improved structural stability through the mediation of polydopamine. J. Membr. Sci. 476, 10.

Liebscher, J., 2019. Chemistry of polydopamine-scope, variation, and limitation. Eur. J. Org. Chem. 2019, 4976-4994.

Lin, J., Tang, C.Y., Huang, C., Tang, Y.P., Ye, W., Li, J., Shen, J., Van den Broeck, R. Van Impe, J., Volodin, A., Van Haesendonck, C., Sotto, A., Luis, P., Van der Bruggen, B., 2016a. A comprehensive physico-chemical characterization of superhydrophilic loose nanofiltration membranes. J. Membr. Sci. 501, 1-14.

Lin, J., Tang, C.Y., Ye, W., Sun, S.P., Hamdan, S.H., Volodin, A., Van Haesendonck, C., Sotto, A., Luis, P., Van der Bruggen, B., 2015b. Unraveling flux behavior of superhydrophilic loose nanofiltration membranes during textile wastewater treatment. J. Membr. Sci. 493, 690-702.

Lin, J., Ye, W., Baltaru, M.C., Tang, Y.P., Bernstein, N.J., Gao, P., Balta, S., Vlad, M., Volodin, A. Sotto, A., Luis, P., Zydney, A.L., Bruggen, B.V., 2016b. Tight ultrafiltration membranes for enhanced separation of dyes and Na_2SO_4 during textile wastewater treatment. J. Membr. Sci. 514, 217-228.

Lin, J., Ye, W., Zeng, H., Yang, H., Shen, J., Darvishmanesh, S., Luis, P., Sotto, A., Van der Bruggen, B., 2015a. Fractionation of direct dyes and salts in aqueous solution using loose nanofiltration membranes. J. Membr. Sci. 477, 183-193.

Liu, C., Faria, A.F., Ma, J., Elimelech, M., 2017. Mitigation of biofilm development on thin-film composite membranes functionalized with zwitterionic polymers and silver nanoparticles. Environ. Sci. Technol. 51, 182-191.

Liu, Q., Yu, B., Ye, W., Zhou, F., 2011. Highly selective uptake and release of charged molecules by pH-responsive polydopamine microcapsules. Macromol. Biosci. 11, 1227-1234.

Liu, Y., Chang, C.P., Sun, T., 2014. Dopamine-assisted deposition of dextran for nonfouling applications. Langmuir 30, 3118-3126.

Lovins, W.A., Taylor, J.S., Hong, S.K., 2002. Micro-organism rejection by membrane systems. Environ. Eng. Sci. 19, 453-467.

Lv, Y., Yang, S-J., Du, Y., Yang, H-C., Xu, Z-K., 2018. Co-deposition kinetics of polydopamine/polyethyleneimine coatings: Effects of solution composition and substrate surface. Langmuir 34, 13123-13131.

Ma, Y., Dai, J., Wu, L., Fang, G., Guo, Z., 2017. Enhanced anti-ultraviolet, anti-fouling and anti-bacterial polyelectrolyte membrane of polystyrene grafted with trimethyl quaternary ammonium salt modified lignin. Polymer 114, 113-121.

Madaeni, S. S., 1999. The application of membrane technology for water disinfection. Wat. Res. 33, 301-308.

Mansouri, J., Harrisson, S., Chen, V., 2010. Strategies for controlling biofouling in membrane filtration systems: challenges and opportunities. J. Mater. Chem. 20, 4567-4586.

Matin, A., Khan, Z., Zaidi, S.M.J., Boyce, M.C., 2011. Biofouling in reverse osmosis membranes for seawater desalination: phenomena and prevention. Desalination 281, 1-16.

Matz, R., 1972. The structure of cellulose acetate membranes. The development of porous structures in anisotropic membranes. Desalination 10 (1), 1-15.

Mauter, M.S., Wang, Y., Okemgbo, K.C., Osuji, C.O, Giannelis, E.P., Elimelech, M., 2011. Antifouling ultrafiltration membranes via post-fabrication grafting of biocidal nanomaterials. ACS Appl. Mater. Inter. 3 (8), 2861-2868.

McCloskey, B.D., Park, H.B., Ju, H., Rowe, B.W., Miller, D.J., Chun, B.J., Kin, K., Freeman, B.D., 2010. Influence of polydopamine deposition conditions on pure water flux and foulant adhesion resistance of reverse osmosis, ultrafiltration, and microfiltration membranes. Polymer 51 (15), 3472-3485.

McCloskey, B.D.; Park, H.B.; Ju, H.; Rowe, B.W.; Miller, D.J., Freeman, B.D., 2012. A bioinspired fouling-resistant surface modification for water purification membranes. J. Membr. Sci. 413, 82-90.

McKenzie, T.G., Colombo, E., Fu, Q., Ashokkumar, M., Qiao, G.G., 2017. Sono-RAFT polymerization in aqueous medium. Angew. Chem. Int. Ed. 56, 12302-12306.

McKenzie, T.G., Karimi, F., Ashokkumar, M., Qiao, G.G., 2019. Ultrasound and sonochemistry for radical polymerization: sound synthesis. Chem. Eur. J. 25, 1-18.

Miller, D.J., Paul, D.R., Freeman, B.D., 2014. An improved method for surface modification of porous water purification membranes. Polymer 55, 1375-1383.

Mulder, M., 1996. Basic principles of membrane technology. Kluwer Academic Publisher.

Mullett, M., Fornarelli, R., Ralph, D., 2014. Nanofiltration of mine water: Impact of feed pH and membrane charge on resource recovery and water discharge. Membranes 4, 163-180.

Munoz-Bonilla, A., Fernandez-Garcia, M., 2012. Polymeric materials with antimicrobial activity. Prog. Polym. Sci. 37, 281-339.

Myint, A.A., Lee, W., Mun, S., Ahn, C.H., Lee, S., Yoon, J., 2010. Influence of membrane surface properties on the behavior of initial bacterial adhesion and biofilm development onto nanofiltration membranes. Biofouling 26, 313-321.

Niki, E., 1991. Action of ascorbic acid as a scavenger of active and stable oxygen radicals. Am. J. Clin. Nutr. 54, 1119-1124.

Oki, T., Kanae, S., 2006. Global hydrological cycles and world water resources. Science 313, 1068-1072.

Olcay, A.N., Polat, M., Polat, H., 2016. Ancillary effects of surfactants on filtration of low molecular weight contaminants through cellulose nitrate membrane filters. Colloids Surf. A 492, 199-206.

Ostuni, E., Chapman, R.G., Holmlin, R.E., Takayama, S., Whitesides, G.M., 2001. A survey of structure-property relationships of surfaces that resist the adsorption of protein. Langmuir 17, 5605-5620.

Oymaci, P., Nijmeijer, K., Borneman, Z., 2020. Development of polydopamine forward osmosis membranes with low reverse salt flux. Membranes 10, 94.

Pal, A., Dey, T.K., Bindal, R.C., 2016. Intrinsic dependence of hydrophilic and electrokinetic features of positively charged thin film composite nanofiltration membranes on molecular weights of poly(ethyleneimine)s. Polymer 93, 99-114.

Paulusse, J.M.J., Sijbesma, R.P., 2006. Ultrasound in polymer chemistry: Revival of an established technique. J. Polym. Sci. A Polym. Chem. 44, 5445-5453.

Peeters, J.M.M., Boom, J.P., Mulder, M.H.V., Strathmann, H., 1998. Retention measurements of nanofiltration membranes with electrolyte solutions. J. Membr. Sci. 145, 199-209.

Perreault, F., Faria, A.F., Nejati, S., Elimelech, M., 2015. Antimicrobial properties of graphene oxide nanosheets: why size matters. ACS Nano 9 (7), 7226-7236.

Perreault, F., Tousley, M.E., Elimelech, M., 2014. Thin-film composite polyamide membranes functionalized with biocidal graphene oxide nanosheets. Environ. Sci. Technol. Lett. 1, 71-76.

Ping, M., Zhang, X., Liu, M., Wu, Z., Wang, Z., 2019.Surface modification of polyvinylidene fluoride membrane by atom-transfer radical-polymerization of quaternary ammonium compound for mitigating biofouling. J. Membr. Sci. 570-57, 286-293.

Prihasto, N., Liu, Q.F., Kim, S.H., 2009. Pre-treatment strategies for seawater desalination by reverse osmosis system. Desalination 249, 308-316.

Ponzio, F., Bertani, P., Ball, V., 2014. Role of surfactants in the control of dopamine-eumelanin particle size and in the inhibition of film deposition at solid-liquid interfaces. J. Colloid Interface Sci. 431, 176-179.

Qiu, C., Setiawan, L., Wang, R., Tang, C.Y., Fane, A.G., 2012. High performance flat sheet forward osmosis membrane with an NF-like selective layer on a woven fabric embedded substrate. Desalination 287, 266-270.

Qiu, W.Z., Yang, H.C., Wan, L.S., Xu, Z.K., 2015. Co-deposition of catechol/polyethyleneimine on porous membranes for efficient decolorization of dye water. J. Mater. Chem. A 3, 14438-14444.

Rana, D., Matsuura, T., 2010. Surface modifications for antifouling membranes. Chem. Rev. 110, 2448-2471.

Razi, F., Sawada, I., Ohmukai, Y., Maruyama, T., Matsuyama, H., 2012. The improvement of antibiofouling efficiency of polyethersulfone membrane by functionalization with zwitterionic monomers. J. Membr. Sci. 401, 292-299.

Rupiasih, N.N., Suyanto, H., Sumadiyasa, M., Wendri, N., 2013. Study of effects of low doses UV radiation on microporous polysulfone membranes in sterilization process. Open J. Org. Polym. Mater. 3, 12-18.

Ryou, M.H., Lee, D.J., Lee, J.N., Lee, Y.M., Park, J.K., Choi, J.W., 2012. Excellent cycle life of lithium-metal anodes in lithium-ion batteries with mussel-inspired polydopamine-coated separators. Adv. Energy Mater. 2, 645.

Ryu, J.H., Messersmith, P.B., Lee, H., 2018. Polydopamine surface chemistry: A decade of discovery. ACS Appl. Mater. Interfaces 10, 7523-7540.

Sathaye, S.D., Patil, K.R., Kulkarni, S.D., Bakre, P.P., Pradhan, S.D., Sarwade, B.D., Shintre, S.N., 2003. Modification of spin coating method and its application to grow thin films of cobalt ferrite. J. Mater. Sci. 38, 29-33.

Setiawan, L., Wang, R., Li, K., Fane, A.G., 2011. Fabrication of novel poly(amide-imide) forward osmosis hollow fiber membranes with a positively charged nanofiltration-like selective layer. J. Membr. Sci. 369, 196-205.

Sun, S.P., Chung, T.S., 2011. Hyperbranched polyethyleneimine induced cross-linking of polyamide-imide nanofiltration hollow fiber membranes for effective removal of ciprofloxacin. Environ. Sci. Technol. 45, 4003-4009.

Szoke, S., Patzay, G., Weiser, L., 2003. Characteristics of thin-film nanofiltration membranes at various pH-values. Desalination 151, 123-129.

Tada, S., Inaba, C., Mizukami, K., Fujishita, S., Gemmei-Ide, M., Kitano, H., Mochizuki, A., Tanaka, M., Matsunaga, T., 2009. Anti-biofouling properties of polymers with a carboxybetaine moiety. Macromol. Biosci. 9, 63-70.

Tekinalp, Ö., Altinkaya, S.A., 2019. Development of high flux nanofiltration membranes through single bilayer polyethyleneimine/alginate deposition. J. Colloid Interf. Sci. 537, 215-227.

Thorsteinsson, T., Másson, M., Kristinsson, K.G., Hjálmarsdóttir, M.A., Hilmarsson, H., Loftsson, T., 2003. Soft antimicrobial agents: Synthesis and activity of labile environmentally friendly long chain quaternary ammonium compounds. J. Med. Chem. 46, 4173-4181.

Tiller, J.C., Liao, C.-J., Lewis, K., Klibanov, A.M., 2001. Designing surfaces that kill bacteria on contact. Proc. Natl. Acad. Sci. 98, 5981-5985.

Tiraferri, A., Vecitis, C.D., Elimelech, M., 2011. Covalent binding of single-walled carbon nanotubes to polyamide membranes for antimicrobial surface properties. ACS Appl. Mater. Inter. 3, 2869-2877.

Ulman, A., 1996. Formation and Structure of Self-Assembled Monolayers. Chem. Rev. 96, 1533-1554.

UNICEF and WHO. 2015. Progress on sanitation and drinking water: 2015 Update and MDG Assessment; UNICEF Publications: Geneva, Switzerland.

United Nations Educational, Scientific and Cultural Organization. 2019. France.

Vatanpour, V., Madaeni, S.S., Moradian, Ro., Zinadini, S., Astinchap, B., 2011. Fabrication and characterization of novel antifouling nanofiltration membrane prepared from oxidized multiwalled carbon nanotube/polyethersulfone nanocomposite. J. Membr. Sci. 375 (1-2), 284-294.

Vecchia, N.F.D., Luchini, A., Napolitano, A., D'Errico, G., Vitiello, G., Szekely, N. K., D'Ischia, M., Paduano, L., 2014. Tris Buffer modulates polydopamine growth, aggregation, and paramagnetic properties. Langmuir 30, 9811-9818.

Wang, H., Zhang, Q., Zhang, S., 2011. Positively charged nanofiltration membrane formed by interfacial polymerization of 3,3'5,5'-biphenyl tetraacyl chloride and piperazine on a poly(acrylonitrile) (PAN) support. J. Membr. Sci. 378, 243-249.

Wang, J., Ma, G., Huang, W., He, Y., 2018. Visible-light initiated polymerization of dopamine in a neutral environment for surface coating and visual protein detection. Polym. Chem. 9, 5242-5247.

Wang, J., Zhu, J., Tsehaye, M.T., Li, J., Dong, G., Yuan, S., Li, X., Zhang, Y., Liu, J., Van der Bruggen, B., 2017b. High flux electroneutral loose nanofiltration membranes based on rapid deposition of polydopamine/polyethyleneimine. J. Mater. Chem. A 5, 14847-14857.

Wang, J.J., Yang, H.C., Wu, M.B., Zhang, X., Xu, Z.K., 2017d. Nanofiltration membranes with cellulose nanocrystals as an interlayer for unprecedented performance. J. Mater. Chem. A 5, 16289-16295.

Wang, K., Lin, X., Jiang, G., Liu, J.Z., Jiang, L., Doherty, C.M., Hill, A.J., Xu, T., Wang, H., 2014. Slow hydrophobic hydration induced polymer ultrafiltration membranes with high water flux. J. Membr. Sci. 471, 27-34.

Wang, Q., Wang, J., Gao, X., Yu, H., Ma, Z., Zhang, Y., Gao, C., 2019. Antibiofouling polysulfone ultrafiltration membranes via surface grafting of capsaicin derivatives. Water Sci. Technol. 79, 1821-1832.

Wang, T., Yang, Y., Zheng, J., Zhang, Q., Zhang, S., 2013. A novel highly permeable positively charged nanofiltration membrane based on a nanoporous hyper-crosslinked polyamide barrier layer. J. Membr. Sci. 448, 180-189.

Wang, X., Jing, S., Liu, Y., Liu, S., Tan, Y., 2017c. Diblock copolymer containing bioinspired borneol and dopamine moieties: synthesis and antibacterial coating applications. Polymer 116, 314-323.

Wang, Z., Xu, C., Lu, Y., Wei, G., Ye, G., Sun, T., Chen, J., 2017a. Microplasma-assisted rapid, chemical oxidant-free and controllable polymerization of dopamine for surface modification. Polym. Chem. 8, 4388-4392.

Wang, Z., Wang, K., Zhang, Y., Jiang, Y., Lu, X., Fang, L., Gan, D., Lv, C., Zhang, H., Qu, S., 2016. Protein-affinitive polydopamine nanoparticles as an efficient surface modification strategy for versatile porous scaffolds enhancing tissue regeneration. Part. Part. Syst. Charact. 33, 89.

Wei, Q., Becherer, T., Angioletti-Uberti, S., Dzubiella, J., Wischke, C., Neffe, A.T., Lendlein, A., Ballauff, M., Haag, R., 2014. Protein interactions with polymer coatings and biomaterials. Angew. Chem. Int. Ed. 53, 8004-8031.

Wei, X., Wang, S., Shi, Y., Xiang, H., Chen, J., Zhu, B., 2014. Characterization of a positively charged composite nanofiltration hollow fiber membrane prepared by a simplified process. Desalination 350, 44-52.

Weinman, S.T., Bass, M., Pandit, S., Herzberg, M., Freger, V., Husson, S.M., 2018. A switchable zwitterionic membrane surface chemistry for biofouling Control, J. Membr. Sci. 548, 490-501.

Wu, C., Wang, Z., Liu, S., Xie, Z., Chen, H., Lu, X., 2018. Simultaneous permeability, selectivity and antibacterial property improvement of PVC ultrafiltration membranes via in-situ quaternization. J. Membr. Sci. 548, 50-58

Wu, D., Huang, Y., Yu, S., Lawless, D., Feng, X., 2014. Thin film composite nanofiltration membranes assembled layer-by-layer via interfacial polymerization from polyethyleneimine and trimesoyl chloride. J. Membr. Sci. 472, 141-153.

Xu, J., Feng, X., Hou, J., Wang, X.., Shan, B., Yu, L., Gao, C., 2013. Preparation and characterization of a novel polysulfone UF membrane using a copolymer with capsaicin-mimic moieties for improved anti-fouling properties. J. Membr. Sci. 446, 171-180.

Xu, J.W., Wang, Y., Yang, Y.F., Ye, X.Y., Yao, K., Ji, J., Xu, Z.K., 2015. Effects of quaternization on the morphological stability and antibacterial activity of electrospun poly(DMAEMA-co-AMA) nanofibers. Colloid Surface B. 133, 148-155.

Xu, S., Wang, P., Sun, Z., Liu, C., Lu, D., Qi, J., Ma, J., 2019. Dual-functionalization of polymeric membranes via cyclodextrin-based host guest assembly for biofouling control. J. Membr. Sci. 569, 124-136.

Xu, Y., Lebrun, R.E., 1999. Investigation of the solute separation by charged nanofiltration membrane: effect of pH, ionic strength and solute type. J. Membr. Sci. 158, 93-104.

Xueli, G., Haizeng, W., Xing, H., Congjie, G., 2013. Surface-modified PSF UF membrane by UV-assisted graft polymerization of capsaicin derivative moiety for foulings and bacterial resistance. J. Membr. Sci. 445, 146-155.

Yang, Y., Qi, P., Ding, Y., Maitz, M. F., Yang, Z., Tu, Q., Xiong, K., Leng, Y., Huang, N., 2015. A biocompatible and functional adhesive amine-rich coating based on dopamine polymerization. J. Mater. Chem. B 3, 72-81.

Yang, Y., Zhang, H., Wang, P., Zheng, Q., Li, J., 2007. The influence of nano-sized TiO_2 filler on the morphologies and properties of PSF UF membrane. J. Membr. Sci. 288, 231-238.

Yang, Y.F.; Li, Y.; Li, Q.L.; Wan, L.S., Xu, Z.K., 2010. Surface hydrophilization of microporous polypropylene membrane by grafting zwitterionic polymer for anti-biofouling. J. Membr. Sci. 362 (1), 255-264.

Yang, Z., Saeki, D., Takagi, R., Matsuyama, H., 2020a. Improved anti-biofouling performance of polyamide reverse osmosis membranes modified with a polyampholyte with effective carboxyl anion and quaternary ammonium cation ratio. J. Membr. Sci. 595, 117529.

Yang, Z., Takagi, R., Zhang, X., Yasui, T., Zhang, L., Matsuyama, H., 2021. Engineering a dual-functional sulfonated polyelectrolyte-silver nanoparticle complex on a polyamide reverse osmosis membrane for robust biofouling mitigation. J. Membr. Sci. 618, 118757.

Yang, Z., Zhang, X., Xie, M., Wu, H-C, Yoshioka, T., Saeki, D., Matsuyama, H., 2020b. Antifouling thin-film composite membranes with multi-defense properties by controllably constructing amphiphilic diblock copolymer brush layer. J. Membr. Sci. 614, 118515.

Yao, L., He, C., Chen, S., Zhao, W., Xie, Y., Sun, S., Nie, S., Zhao, C., 2019. Codeposition of polydopamine and zwitterionic polymer on membrane surface with enhanced stability and antibiofouling property. Langmuir 35, 1430-1439.

Yao, Y., Ba, C., Zhao, S., Zheng, W., Economy, J., 2009. Development of a positively charged nanofiltration membrane for use in organic solvents. J. Membr. Sci. 520, 832-839.

Ye, W., Lin, J., Borrego, R., Chen, D., Sotto, A., Luis, P., Liu, M., Zhao, S., Tang, C.Y., Van der Bruggen, B., 2018. Advanced desalination of dye/NaCl mixtures by a loose nanofiltration membrane for digital ink-jet printing. Sep. Purif. Technol. 197, 27-35.

Yu, H., Zhang, X., Zhang, Y., Liu, J., Zhang, H., 2013a. Development of a hydrophilic PES ultrafiltration membrane containing SiO_2@N-Halamine nanoparticles with both organic antifouling and antibacterial properties. Desalination 326, 69-76.

Yu, L., Deng, J., Wang, H., Liu, J-D., Zhang, Y., 2016. Improved salts transportation of a positively charged loose nanofiltration membrane by introduction of poly(ionic liquid) functionalized hydrotalcite nanosheets. ACS Sustainable Chem. Eng. 4, 3292-3304.

Yu, L., Zhang, Y., Wang, Y., Zhang, H., Liu, J., 2015. High flux, positively charged loose nanofiltration membrane by blending with poly(ionic liquid) brushes grafted silica spheres. J. Hazard. Mater. 287, 373-383.

Yu, L., Zhang, Y., Zhang, B., Liu, J., Zhang, H., Song, C., 2013b. Preparation and characterization of HPEI-GO/PES ultrafiltration membrane with antifouling and antibacterial properties. J. Membr. Sci. 447, 452-462.

Zeng, Z., Yu, D., He, Z., Liu, J., Xiao, F.X., Zhang, Y., Wang, R., Bhattacharyya, D., Tan, T.T.Y., 2016. Graphene oxide quantum dots covalently functionalized PVDF membrane with significantly enhanced bactericidal and antibiofouling performances. Sci. Rep. 6, 20142.

Zhang, C., Ma, M.Q., Chen, T.T., Zhang, H., Hu, D.F., Wu, B.H., Ji, J., Xu, Z.K., 2017c. Dopamine-Triggered one-step polymerization and codeposition of acrylate monomers for functional coatings. ACS Appl. Mater. Interfaces 9, 34356-34366.

Zhang, C., Ou, Y., Lei, W.X., Wan, L.S., Ji, J., Xu, Z.K., 2016b. $CuSO_4/H_2O_2$-induced rapid deposition of polydopamine coatings with high uniformity and enhanced stability. Angew. Chem. Int. Ed. 55, 3054-3057.

Zhang, H.Z., Xu, Z.L., Ding, H., Tang, Y.J., 2017a. Positively charged capillary nanofiltration membrane with high rejection for Mg^{2+} and Ca^{2+} and good separation for Mg^{2+} and Li^{+}. Desalination 420, 158-166.

Zhang, Q., Wang, H., Zhang, S., Dai, L., 2011. Positively charged nanofiltration membrane based on cardo poly(arylene ether sulfone) with pendant tertiary amine groups. J. Membr. Sci. 375, 191-197.

Zhang, R., Liu, Y., He, M., Su, Y., Zhao, X., Elimelech, M., Jiang, Z., 2016a. Antifouling membranes for sustainable water purification: Strategies and mechanisms. Chem. Soc. Rev. 45, 5888.

Zhang, R., Su, Y., Zhao, X., Li, Y., Zhao, J., Jiang, Z., 2014. A novel positively charged composite nanofiltration membrane prepared by bio-inspired adhesion of polydopamine and surface grafting of poly(ethylene imine). J. Membr. Sci. 470, 9-17.

Zhang, S., Lu, F., Tao, L., Liu, N., Gao, C., Feng, L., Wei, Y., 2013a. Bio-inspired anti-oil-fouling chitosan-coated mesh for oil/water separation suitable for broad pH range and hyper-saline environments, ACS Appl. Mater. Inter. 5, 11971-11976.

Zhang, X., Ma, J., Tang, C.Y., Wang, Z., Ng, H.Y., Wu, Z., 2016d. Antibiofouling polyvinylidene fluoride membrane modified by quaternary ammonium compound: direct contact-killing versus induced indirect contact-killing. Environ. Sci. Technol. 50, 5086-5093.

Zhang, X., Wang, Z., Chen, M., Liu, M., Wu, Z., 2016c. Polyvinylidene fluoride membrane blended with quaternary ammonium compound for enhancing anti-biofouling properties: effects of dosage. J. Membr. Sci. 520, 66-75.

Zhang, X., Wang, Z., Chen, M., Ma, J., Chen, S., Wu, Z., 2017b. Membrane biofouling control using polyvinylidene fluoride membrane blended with quaternary ammonium compound assembled on carbon material. J. Membr. Sci. 539, 229-237.

Zhang, X., Wang, Z., Tang, C.Y., Ma, J., Liu, M., Ping, M., Chen, M., Wu, Z., 2018a. Modification of microfiltration membranes by alkoxysilane polycondensation induced quaternary ammonium compounds grafting for biofouling mitigation. J. Membr. Sci. 549, 165-172.

Zhang, Y., Teo, B. M., Postma, A., Ercole, F., Ogaki, R., Zhu, M., Stadler, B., 2013. Highly-branched poly(n-isopropylacrylamide) as a component in poly(dopamine) films. J. Phys. Chem. B 117, 10504-10512.

Zhang, Y., Thingholm, B., Goldie, K.N., Ogaki, R., Stadler, B., 2012. Assembly of poly(dopamine) films mixed with a nonionic polymer. Langmuir 28, 17585-17592.

Zhang, W., Cheng, W., Ziemann, E., Bear, A., Lu, X., Elimelech, M., Bernstein, R., 2018b. Functionalization of ultrafiltration membrane with polyampholyte hydrogel and graphene oxide to achieve dual antifouling and antibacterial properties. J. Membr. Sci. 565, 293-302.

Zhao, F.Y., Ji, Y.L., Weng, X.D., Mi, Y.F., Ye, C.C., An, Q.F., Gao, C.J., 2016. High-flux positively charged nanocomposite nanofiltration membranes filled with poly(dopamine) modified multiwall carbon nanotubes. ACS Appl. Mater. Interfaces 8, 6693-6700.

Zhao, J., Yang, J., Li, Y. Li, D., Wang, Q., Zhang, L., Zhang, Y., Zhang, S., Chen, L., 2020. Improved permeability and biofouling resistance of microfiltration membranes via quaternary ammonium and zwitterion dual-functionalized diblock copolymers. Eur. Polym. 135, 109883.

Zhao, S., Ba, C., Yao, Y., Zheng, W., Economy, J., Wang, P., 2018. Removal of antibiotics using polyethyleneimine cross-linked nanofiltration membranes: Relating membrane performance to surface charge characteristics. Chem. Eng. J. 335, 101-109.

Zheng, Y., Yao, G., Cheng, Q., Yu, S., Liu, M., Gao, C., 2013. Positively charged thin-film composite hollow fiber nanofiltration membrane for the removal of cationic dyes through submerged filtration. Desalination 328, 42-50.

Zhou, Z., Hu, Y., Boo, C., Liu, Z., Li, J., Deng, L., An, X., 2018. High-Performance thin-film composite membrane with an ultrathin spray-coated carbon nanotube interlayer. Environ. Sci. Technol. Lett. 5 (5), 243-248.

Zhu, J., Hou, J., Zhang, Y., Tian, M., He, T., Liu, J., Chen, V., 2018. Polymeric antimicrobial membranes enabled by nanomaterials for water treatment. J. Membr. Sci. 550, 173-197.

Zhu, J., Uliana, A., Wang, J., Yuan, S., Li, J., Tian, M., Simoens, K., Volodin, A., Lin, J., Bernaerts, K., Zhang, Y., Van der Bruggen, B., 2016a. Elevated salt transport of antimicrobial loose nanofiltration membranes enabled by copper nanoparticles via fast bioinspired deposition. J. Mater. Chem. A 4, 13211-13222.

Zhu, J., Wang, J., Uliana, A.A., Tian, M., Zhang, Y., Zhang, Y., Volodin, A., Simoens, K., Yuan, S., Li, J., Lin, J., Bernaerts, K., Bruggen, B.V., 2017. Mussel-inspired architecture of high-flux loose nanofiltration membrane functionalized with antibacterial reduced graphene oxide-copper nanocomposites. ACS Appl. Mater. Interfaces 9, 34, 28990-29001.

Zhu, J., Zhang, Q., Zheng, J., Hou, S., Mao, H., Zhang, S., 2016b. Green fabrication of a positively charged nanofiltration membrane by grafting poly(ethylene imine) onto a poly(arylene ether sulfone) membrane containing tertiary amine groups. J. Membr. Sci. 517, 39-46.

Zhu, M.M., Fang, Y., Chen, Y.C., Lei, Y.Q., Fang, L.F., Zhu, B.K., Matsuyama, H., 2021. Antifouling and antibacterial behavior of membranes containing quaternary ammonium and zwitterionic polymers. J. Colloid Interf. Sci. 584, 225-235.

Zhu, Y., Xie, W., Gao, S., Zhang, F., Zhang, W., Liu, Z., Jin, J., 2016c. Single-walled carbon nanotube film supported nanofiltration membrane with a nearly 10 nm thick polyamide selective layer for high-flux and high-rejection desalination. Small 12, 5034-5041.

Zinadini, S., Zinatizadeh, A.A., Rahimi, M., Vatanpour, V., Zangeneh, H., 2014. Preparation of a novel antifouling mixed matrix PES membrane by embedding graphene oxide nanoplates. J. Membr. Sci. 453, 292-301.

APPENDIX A

PERMISSIONS TO REPRODUCE FIGURES AND TEXTS

All permissions have been taken to reproduce the full text presented in Chapters 2 and 3 and the scheme in Chapter 4 through the Copyright Clearance Center. All documentation of the approvals is listed on the following pages.

Chapter 2

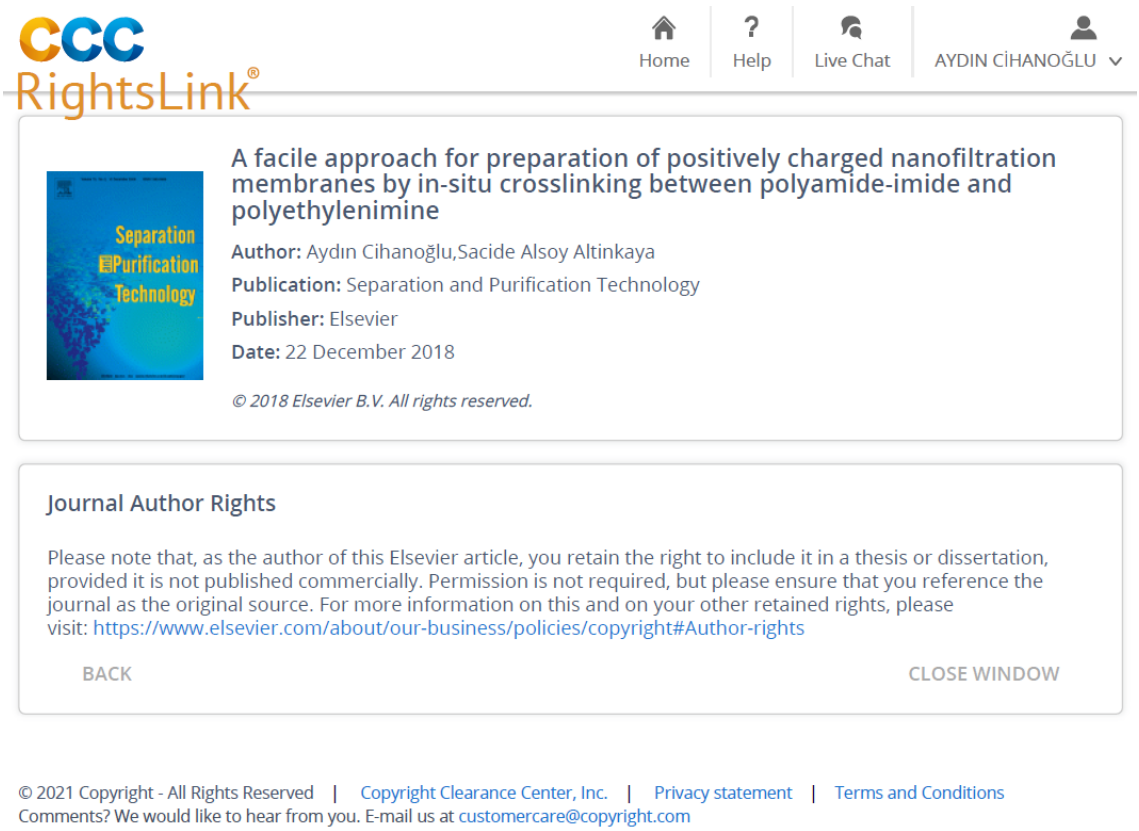

Chapter 3

Chapter 4

Scheme 4.1

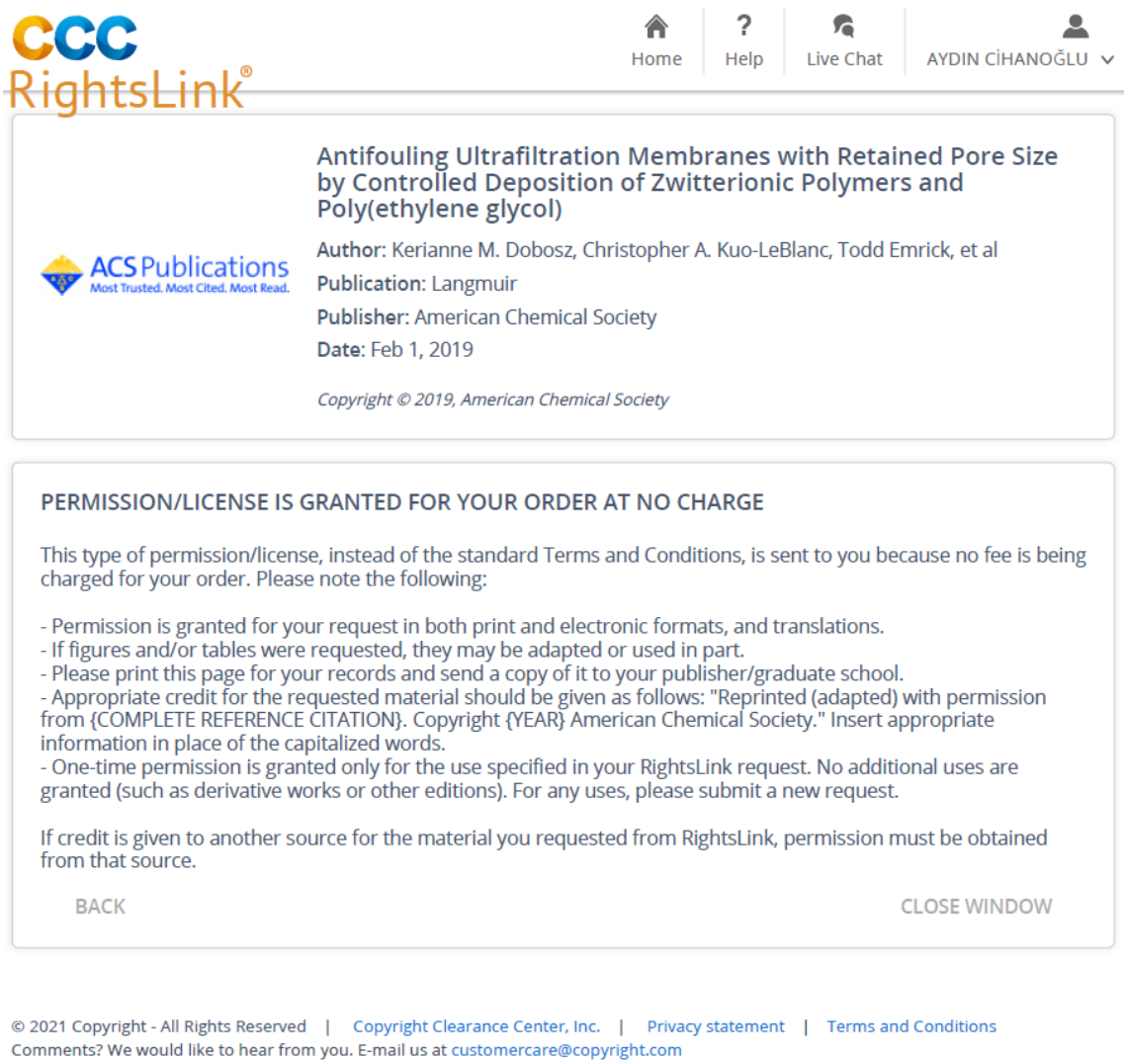

APPENDIX B

SUPPLEMENTARY INFORMATION FOR CHAPTER 3

The sulfonation degree of the sulfonated polyethersulfone (SPES) is almost 30%. It was not possible to produce mechanically strong membranes using pure SPES. The highest mechanical properties were achieved when SPES was blended with polysulfone (PSF) with a PSF:SPES blending ratio of 3:1. The best solvent for dissolving blend polymers was determined by calculating the Hansen solubility parameters (Equations B.1 and B.2). Compared to pure NMP, the blend of solvents NMP and DMAC with a ratio of DMAC/NMP (2:1) was found to have a closer solubility parameter to that of the PSF: SPES. Thus, the PSF:SPES blend was dissolved with a mixture of solvents, DMAC and NMP.

Table B.1. Solubility parameters of solvents and polymers.

Solvent and Polymer	δ_p	δ_d	δ_h	***Solubility Parameter***
NMP	18.00	12.30	7.20	22.96
DMAC	16.80	11.50	10.20	22.77
DMAC/NMP (2:1)	17.20	11.77	9.20	22.78
SPES	18.50	9.70	11.10	23.65
PSF	19.70	8.30	8.30	22.93
PSF/SPES (3:1)	19.40	8.65	9.00	23.07
Water	16.00	15.50	42.30	48.00

$$\delta^2 = \delta_p^2 + \delta_d^2 + \delta_h^2 \qquad (B.1)$$

$$\Delta = \left[\left(\delta_{p,d} - \delta_{s,d}\right)^2 + \left(\delta_{p,p} - \delta_{s,p}\right)^2 + \left(\delta_{p,h} - \delta_{s,h}\right)^2\right]^{1/2} \qquad (B.2)$$

Polymer - Solvent	Δ
Polymer (PSF/SPES (3:1)) – Solvent (Pure NMP)	4.30
Polymer (PSF/SPES (3:1)) – Solvent (DMAC/NMP (2:1))	3.82

VITA

Education

Ph.D.	Chemical Engineering, *İzmir Institute of Technology*, İzmir, Turkey *Thesis*: "Development of Thin Film Composite Antibacterial Membranes" *Advisor*: Prof. Dr. Sacide ALSOY ALTINKAYA - *Co-Advisor*: Prof. Dr. Erol ŞEKER (Head of Department)	2021
M.Sc.	Chemical Engineering, *Ege University*, İzmir, Turkey *Thesis*: "Degradation of Acetic Acid over iron containing ZSM-5 zeolite catalysts by Heterogeneous Fenton - like Oxidation in the absence and presence of ultrasound" *Advisor*: Prof. Dr. Gönül GÜNDÜZ	2014
B.S.	Chemical Engineering, *Selçuk University*, Konya, Turkey *Senior thesis*: "Electrochemical and Spectroelectrochemical investigations of Ethyl Ferrocenylmethyl 3,4-Pyroledicarboxylate - Pyrol Copolymers" *Advisor*: Prof. Dr. Handan KAMIŞ	2010

Academic Experience

Academic Researcher	Chemical Engineering, *University of Massachusetts, Amherst*, Massachusetts, USA *Research Subject*: "Development of antibacterial thin film composite ultrafiltration membranes using a novel approach" *Advisor*: Assoc. Prof. Dr. Jessica D. SCHIFFMAN	2019-2020 (5.5 Months)
Academic Researcher	Chemical Engineering, *Loughborough University*, Leicester, England *Research Subject*: "Novel Fluoropolymer Microcapillary Photoreactor for Intensified Advanced Oxidation Processes" *Advisor*: Prof. Dr. Gianluca LI-PUMA – *Co-Advisor*: Dr. Nuno REIS	2013-2014 (7 Months)
Participant	35th European Membrane Society Summer School, *University of Twente*, Netherlands *Title*: "From Fundamental Concepts Towards Commercialization of Membranes"	June24-29, 2018
Research Assistant	Chemical Engineering, *Uşak University*, Uşak, Turkey	2010-2012 (2 years)

Honors and Awards

- European Membrane Society, Travel Award, The 12th International Congress on Membranes and Membrane Processes (ICOM) (7-11 December 2020)
- The International Research Fellowship (Code:2214-A) for PhD Candidate (1 year) by The Scientific and Technological Research Council of Turkey (TÜBİTAK) (2019-2020).
- The National PhD Scholarship (Code: 2211-E) (4 Years) by The Scientific and Technological Research Council of Turkey (TÜBİTAK) (2014-2018).
- The National M.Sc. Scholarship (Code:2228-A) (2 years) by The Scientific and Technological Research Council of Turkey (TÜBİTAK) (2012-2014).
- The Highest-Ranking (1st) Student of the Chemical Engineering Department, *Selçuk University*, Konya, Turkey, 2010.
- The Honour Student of the Chemical Engineering Department, *Selçuk University*, Konya, Turkey, 2010.

Publications

- **Cihanoğlu A**., Schiffman J.D., Altınkaya S.A., "Preparation of antibacterial ultrafiltration membrane using a novel approach", in preparation to submit to the ACS Applied Materials and Interfaces.

- Metecan A., **Cihanoğlu A**., Altınkaya S.A., "A Positively Charged Loose Nanofiltration Membrane Fabricated Through Complexing of Alginate and Polyethyleneimine with Metal Ions on the Polyamideimide Support for Dye Desalination", *Chemical Engineering Journal*, 2021, 416, 128946.

- **Cihanoğlu A**., Altınkaya S.A., "A Facile Route to The Preparation of Antibacterial Polysulfone-Sulfonated Polyethersulfone Ultrafiltration Membranes using a Cationic Surfactant Cetyltrimethylammonium Bromide", *Journal of Membrane Science*, 2020, 594, 117438.

- **Cihanoğlu A**., Altınkaya S.A., "A Facile Approach for Preparation of Positively Charged Nanofiltration Membranes by In-Situ Crosslinking between Polyamide-Imide and Polyethyleneimine", *Separation and Purification Technology*, 2018, 207, 353-362.

- **Cihanoğlu A**., Gündüz G., Dükkancı M., "Influence of Ultrasound on Heterogeneous Fenton-like Oxidation of Acetic Acid", *Water Science and Technology*, 2017, 76 (10), 2793-2801.

- **Cihanoğlu A**., Gündüz G., Dükkancı M., "Degradation of Acetic Acid by Heterogeneous Fenton-like Oxidation over Iron containing ZSM-5 zeolites", *Applied Catalysis B: Environmental*, 2015, 165, 687-699.

Selected Conferences

- **Cihanoğlu A.**, Schiffman J.D., Altınkaya S.A., "Ultrasound-assisted Dopamine Polymerization: Rapid and Oxidizing Agent Free Polydopamine Coatings on Membrane Surfaces", *The 12th International Congress on Membranes and Membrane Processes (ICOM)*, 7-11 December 2020, Excel London, London, UK. (Virtual Congress). (Oral Presentation)

- Metecan A., **Cihanoğlu A.**, Altınkaya S.A., "Development of High Flux Polyamide-imide Based Positively Charged Nanofiltration Membranes Using Transition Metals for Dye Desalination in Textile Wastewater", *The 12th International Congress on Membranes and Membrane Processes (ICOM)*, 7-11 December 2020, Excel London, London, UK. (Virtual Congress). (Oral Presentation)

- Metecan A., **Cihanoğlu A.**, Altınkaya S.A., "Development of Polyamide-imide Based Positively Charged Nanofiltration Membranes", *6th MEMTEK International Symposium on Membrane Technologies and Applications*, November 18-20, 2019, İstanbul, Turkey. (Oral Presentation)

- **Cihanoğlu A.**, Altınkaya S.A., "One Step Surface Modification of Membranes with Quaternary Ammonium Cations for Improving Antibacterial Activity", *Euromembrane 2018*, July 9-13, 2018, Valencia, Spain. (Poster Presentation)

- **Cihanoğlu A.**, Altınkaya S.A., "The Influence of Solvent Type on the Fouling Behaviour of PSF/SPES Blend Ultrafiltration Membranes during Filtration of Oil-Water Emulsion", *Euromembrane 2018*, July 9-13, 2018, Valencia, Spain. (Poster Presentation)

- **Cihanoğlu A.**, Altınkaya S.A., "Development of Polyamide-imide Based Positively Charged Nanofiltration Membranes by a New Approach", *The 11th International Congress on Membranes and Membrane Processes (ICOM)*, July 29- August 4, 2017, Hilton San Francisco Union Square, San Francisco, California, USA. (Oral Presentation)